DYNAMICAL THEORY OF NEUTRON DIFFRACTION FOR PERFECT CRYSTALS WITH AND WITHOUT STRAIN GRADIENTS

by

Saravanamuthu Maheswaran

B.Sc.(Physics Honours), University of Peradeniya, Sri Lanka, 1981

M.Sc.(Bio Physics), Simon Fraser University, 1985

A THESIS SUBMITTED IN PARTIAL FULFILLMENT OF

THE REQUIREMENTS FOR THE DEGREE OF

DOCTOR OF PHILOSOPHY

in the Department

of

Physics

© Saravanamuthu Maheswaran 1989

SIMON FRASER UNIVERSITY

March 1989

APPROVAL

Name: Saravanamuthu Maheswaran

Degree: Doctor of Philosophy

Title of Thesis: Dynamical Theory of Neutron Diffraction for Perfect Crystals with and without Strain Gradients

Examining Committee:

Chairman: J. F. Cochran

A. S. Arrott

Senior Supervisor

L. E. Ballentine

A. E. Curzon

E. D. Crozier

S. A. Werner

External Examiner

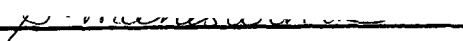Physics Department, University of Missouri, Columbia

Date Approved: March 17, 1989

PARTIAL COPYRIGHT LICENSE

      I hereby grant to Simon Fraser University the right to lend my thesis, project or extended essay (the title of which is shown below) to users of the Simon Fraser University Library, and to make partial or single copies only for such users or in response to a request from the library of any other university, or other educational institution, on its own behalf or for one of its users. I further agree that permission for multiple copying of this work for scholarly purposes may be granted by me or the Dean of Graduate Studies. It is understood that copying or publication of this work for financial gain shall not be allowed without my written permission.

Title of Thesis/Project/Extended Essay

_____

Dynamical Theory of Neutron Diffraction for
_____

Perfect Crystals With and Without Strain Gradients
_____

_____

Author: _____
          (signature)

     S. Maheswaran
          (name)

     29th March 1989.
          (date)

ABSTRACT

The dynamical theory of neutron diffraction is studied for perfect crystals and crystals with strain gradients. In the case of parallel-sided slab crystals, it is customary to distinguish the Bragg case where the beam enters and exits on the same side of the slab and the Laue case where the beam enters on one side and exits on the other. The symmetric Bragg case has the angle of incidence equal to the angle of diffraction with respect to the surface, that is the scattering vector is perpendicular to the surface. In the symmetric Laue case the scattering vector is parallel to the surface. In extreme cases either the incoming or exiting beam is close to being parallel to the surface. Schrödinger's equation for the perfect slab crystal with a periodic potential is solved by two methods which can give similar results. In the first method, which is known as the eikonal approach, a quartic dispersion relation is obtained and solved for all possible internal wave vectors. A given incident plane wave generates four pairs of internal waves. Each pair is coupled together by the periodic potential. Four waves, in addition to the incident wave, appear outside the crystal as a result of the interaction with the crystal slab. All the unknown internal and external amplitudes are found from the boundary conditions. In non-extreme cases, two pairs of internal waves suffice to describe the propagation of neutrons in the crystal. In the second approach, commonly referred to as the Takagi-Taupin method, one assumes that the wave amplitudes are position dependent solutions of coupled differential equations. We have measured the dependence of the diffracted beam intensity as a function of thickness of Si wafers and found good agreement with the theory. The theory has applications in the design of elements for neutron optics, particularly monochromating and analyzing crystals.

In the extreme cases, all four pairs of internal waves are considered. It is shown that three pairs are sufficient to describe adequately the propagation of neutrons inside the crystal in almost all cases. The treatment of perfect crystals given here is unique in the

iv

fullness of the approach and its direct application to a simple and actual experimental geometry.

For practical design considerations it is necessary to introduce elastic strain gradients to improve the efficiency of elements for neutron optics. In the case of homogeneously bent crystals, the solutions of the dynamical problem have been expressed by others in terms of confluent hypergeometric functions. Mathematical obscurities have been eliminated here by expressing the confluent hypergeometric functions in terms of Chebyshev polynomials. The results are in a form suitable for numerical computation of the variation of intensity of neutron scattering with crystal thickness and amplitude of the strain gradient. In the experiments the crystals are bent by loading along two lines at each of two parallel edges. The resulting strain gradients are more complicated than expected. In addition in most of our experiments we have exceeded the limits in which the simple bending theory can be applied. In this situation the displacement field is given by two nonlinear fourth order differential equations. The elasticity theory of bending and the dynamical theory of diffraction can be computationally combined to interpret the experimental results.

Dedicated to my father
for his continual support and encouragement.

ACKNOWLEDGEMENTS

TABLES OF CONTENTS

LIST OF TABLES

Table   **Page**

LIST OF FIGURES

CHAPTER 1

INTRODUCTION

1.1 History

Since the advent of nuclear reactors, the neutron has been extensively used to study condensed matter in general and crystals structures in particular. Thermalized neutrons from reactors have wavelengths comparable to atomic spacings in crystals. Neutron diffraction from crystals supplements x-ray diffraction, particularly in distinguishing among elements on the basis of nuclear cross-sections, which vary strongly from element to element. For example the neutron is strongly scattered by hydrogen. The mass of the neutron is well suited to the study of inelastic scattering, for example from phonons in solids. Because the neutron has a magnetic moment, but no charge, it makes an ideal probe of the magnetic induction on the atomic scale.

The theory of neutron diffraction, like that of x-ray diffraction is well developed in the kinematic and dynamic limits. In the kinematic limit small volumes of matter diffract intensity from beam to beam. In the dynamical theory one adds the amplitudes of the waves scattered from atoms. Dynamical theory is applied to small regions of mosaic crystals to determine the diffracted beam intensities used in the kinematic theory where the lack of correlation from region to region leads to the addition of intensities. Dynamical theory must be used to treat the whole problem of diffraction in crystals with a high degree of correlation over extended volumes. In the study of most crystals it is sufficient to employ kinematic theory, but with the development of commercially available dislocation free silicon wafers (up to 20 cm in diameter and 0.5 −1 mm in thickness) it becomes important to be able to use dynamical theory for large highly correlated crystals. These Si wafers are an order of magnitude too thick for their optimum employment as neutron monochromating crystals. By introducing elastic strain gradients into them it is possible to

increase their ability to reflect neutron beams by an order of magnitude. The main purpose of this study is to increase our understanding of the propagation of neutrons in such crystals. To accomplish this we start with the dynamic theory of perfect crystals. The next step is to calculate diffraction from crystals with uniform elastic strain gradients. The final step is to determine the actual elastic strains in deformed crystals and to apply the dynamical theory with uniform strain gradients to each small region of the crystal with spatially varying strain gradients. The elasticity theory of bent crystals is more complicated than one would gather from most texts on the subject. Rather than one fourth order linear differential equation one is faced with a pair of coupled non linear fourth order differential equations.

The dynamical theory of diffraction is highly developed for the x-ray case, beginning with the historic work of C. G. Darwin, P. P. Ewald and M. V. Laue. The dynamical theory of x-rays is summarized in the books of Zachariasen [1] and James [2] and more recent aspects are included in [3]. Since the first observation of Pendellösung fringe structure in a neutron diffraction experiment, using perfect single crystals of silicon, by C. G. Shull in 1968 [4], interest in the application of the dynamical theory to the neutron case has grown substantially. Excellent reviews exist for the neutron case, such as those of Sears [5] and by Rauch and Petrascheck [6]. The dynamical theory of neutron diffraction is closely related to the corresponding theory for x-ray diffraction. The main difference is that, for neutrons, the coherent wave is weakly absorbed in most materials, whereas, for x-rays, it is very strongly absorbed. This is particularly true for the case of Si crystals. Dynamical theory provides a theoretical frame work for a number of phenomena which are absent in the kinematical theory.

1.2   General review of the dynamical theory for a perfect crystal slab

Consider an incoming plane wave of wave vector $\vec{k_0}$ impinging on a slab of perfect

crystal of thickness t, as shown as in Fig. 1.1. The neutron interaction potential outside the slab is zero. We restrict the problem to the assumption that the external incident wave is oriented very close to satisfying the exact Bragg condition, $(\vec{k_0} + \vec{G})^2 = k_0^2$, for only one particular reciprocal lattice vector (say $\vec{G}$). We write the incoming wave vector as

$$\vec{k_0} = k_{0x}\hat{x} + k_{0z}\hat{z} = -k_0 \sin\psi \; \hat{x} + k_0 \cos\psi \; \hat{z} \qquad (1.1)$$

where ψ is the angle with respect to the surface normal which is along the z direction. The atomic planes make an angle α with respect to the surface normal. The incoming beam makes an angle θ with respect to the atomic planes. From Fig. 1.1, it follows that

$$\psi = \theta - \alpha . \qquad (1.2)$$

The exact Bragg angle is $\theta_B \equiv \sin^{-1}\frac{G}{2k_0}$. The misset angle is $\Delta\theta = \theta - \theta_B$. The reciprocal lattice vector can be written as

$$\vec{G} = G_x \hat{x} + G_z \hat{z} = G\{ \cos\alpha \; \hat{x} - \sin\alpha \; \hat{z} \} \qquad (1.3)$$

In the symmetric Laue diffraction configuration $\vec{G}$ is parallel to the surface, that is $G_z = 0$ and the diffracted beam will exit on the lower surface of the crystal slab. In the symmetric Bragg diffraction configuration $\vec{G}$ is perpendicular to the surface, that is $G_x = 0$, and the diffracted beam will exit on the upper surface of the crystal slab.

Four waves, in addition to the incident wave, appear outside the crystal as a result of the interaction with the crystal slab. Some of these waves are present at the upper surface while the other waves are present at the lower surface of the crystal. As we consider only the elastic scattering, one end of each wave vector lies at the origin A and the other end
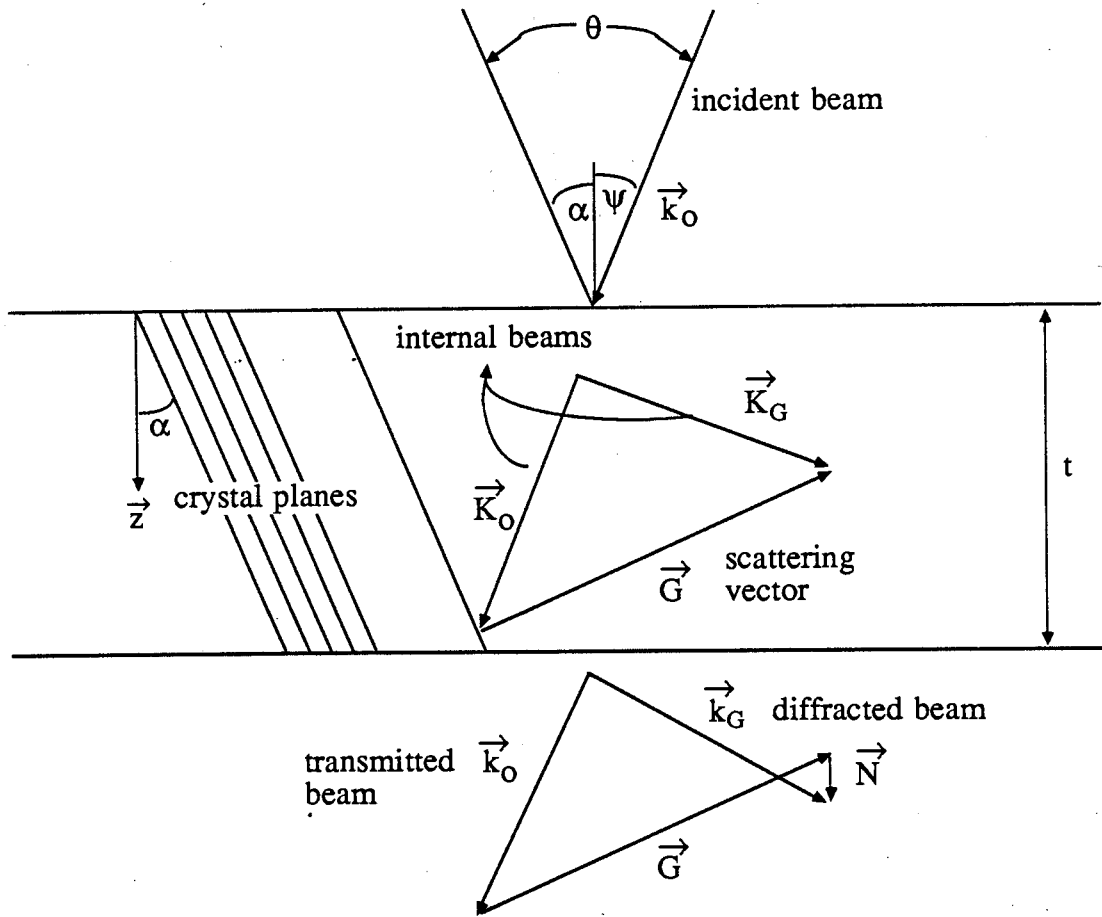
Figure 1.1:- Asymmetric Laue-transmission geometry showing the incident plane
wave of wave vector $\vec{k_O}$, which is Bragg diffracted into the plane wave of
wave vector $\vec{k}_{\vec{G}+\vec{N}}$, nominally called $\vec{k_G}$, by the combined action of the
atomic planes with normal wave vector $\vec{G}$ and the surface with normal wave
vector $\vec{N}$. The internal wave vector $\vec{K_O}$, generally not exactly parallel to the
incident wave vector $\vec{k_O}$ because of refraction at the surface, is coupled to the
internal diffracted wave $\vec{K_G}$ by the periodic potential of wave vector $\vec{G}$ of the
atomic planes. The wave vector $\vec{k_O}$ is incident upon the atomic planes at an
angle called θ which is equal to the Bragg angle θ_B if $\theta = \sin^{-1}\dfrac{G}{2k_O} \equiv \theta_B$.

should lie on the perimeter of the circle with radius k_O (magnitude of the incoming wave vector) and its origin at A in k-space. Furthermore, the end positions are determined by the reciprocal lattice vector and the surface normal because momentum is transferred to the lattice perpendicular to the planes and perpendicular to the surface. These wave vectors are shown in Fig. 1.2. The above mentioned waves are referred to as

– the transmitted wave, $\vec{k_O}$; (same as incoming beam)

– the Bragg diffracted wave, $\vec{k_G}$;

– the mirror reflection of the incoming wave, $\vec{k_m}$;

– the mirror reflection of the Bragg diffracted wave, $\vec{k_{Gm}}$.

According to the law of conservation of energy

$$k_O^2 = k_m^2 = k_G^2 = k_{Gm}^2 \tag{1.4}$$

where $k_O^2 = \vec{k_O} \cdot \vec{k_O}$ and so on.

From Fig. 1.2, we can write

$$k_{mx} = k_{Ox} = -k_O \sin(\theta - \alpha) \tag{1.5a}$$

$$k_{mz} = -k_{Oz} = -k_O \cos(\theta - \alpha) \tag{1.5b}$$

One can calculate the components of $\vec{k_G}$ using the following equation.

$$k_G^2 = (k_{Ox} + G_x)^2 + (k_{Oz} + G_z + \Delta K_z)^2 = k_{Ox}^2 + k_{Oz}^2, \tag{1.6}$$

where ΔK_z is the momentum imparted to the crystal at the surfaces. By solving the eq. (1.6), we will get
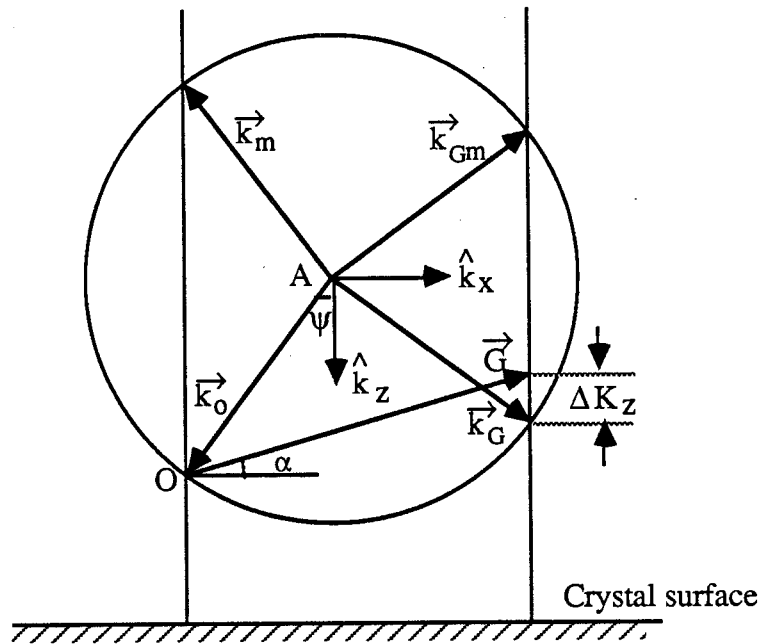
Figure 1.2:- Representation of wave vectors, associated with the external waves present at the upper and lower surfaces of the crystal, in k-space.

$$\Delta K_z = -(k_{oz} + G_z) \pm \sqrt{k_{oz}^2 - (G_x^2 + 2k_{ox}G_x)} \qquad (1.7)$$

and then

$$k_{Gx} = k_{Gmx} = (k_{ox} + G_x) \qquad (1.8a)$$

$$k_{Gz} = (k_{oz} + G_z + \Delta K_z) = \sqrt{k_{oz}^2 - (G_x^2 + 2k_{ox}G_x)} \qquad (1.8b)$$

$$k_{Gmz} = -\sqrt{k_{oz}^2 - (G_x^2 + 2k_{ox}G_x)} \qquad (1.8c)$$

(Note:- For the Bragg geometry the signs of k_{Gz} and k_{Gmz} will interchange.)

In some cases, as shown as in Fig. 1.3, k_{Gz} and k_{Gmz} become purely imaginary, i.e. when the diffracted beam is almost parallel to the crystal surface, for some directions of incident wave (very close to the exact Bragg condition), the Bragg diffracted wave and the mirror reflection of the Bragg diffracted wave become evanescent. The condition for this situation is

$$(k_{ox} + G_x) > k_o \qquad (1.9)$$

Under this condition, both of these evanescent waves are propagated along the surface of the crystal. The amplitudes of the waves, which are propagated along the lower and upper surfaces of the crystal, are damped in the (-ve) and (+ve) z direction respectively in order that the amplitude = 0 at $+\infty$. The calculations are shown in chapter 3.

The amplitudes of the specified external waves are found by matching the waves internal and external to the slab. The external wave vectors select among the many possible internal wave vectors. In particular the components parallel to the surface of the internal wave vectors must match the components parallel to the surface of the external
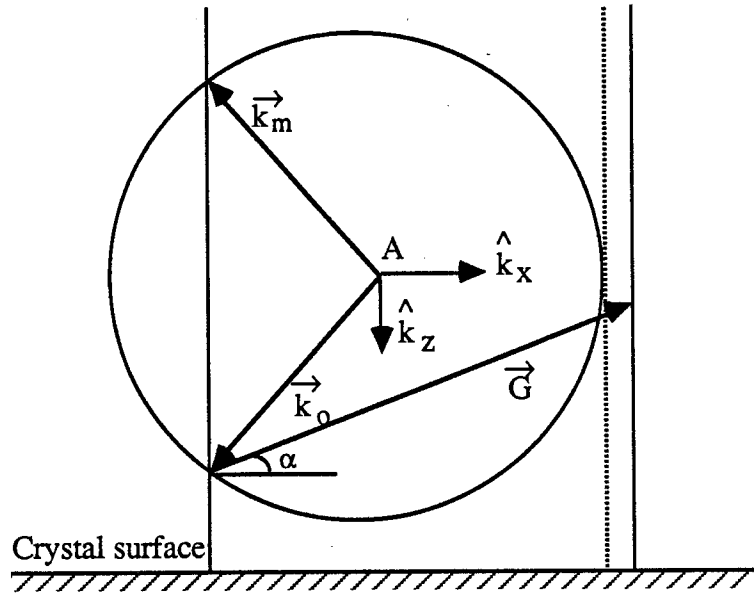
Figure 1.3:- Situation explaining the formation of evanescent surface diffracted
waves

wave vectors. The possible internal wave vectors are determined by solving Schrödinger's equation for the neutron, which contains the periodic neutron-nuclear interaction potential inside the crystal. This determines the relations between the components of the internal wave vectors and the other known quantities such as magnitude of the incident wave vector and the fourier components of the periodic interaction potential. These are called the dispersion relations. A given k_{ox} of the incoming wave will select four internal waves $\vec{K}_O^A$, $\vec{K}_O^B$, $\vec{K}_O^C$ and $\vec{K}_O^D$ all with $K_{ox}^{A,B,C,D} = k_{ox}$ and four coherently generated Bragg diffracted waves $\vec{K}_G^A$, $\vec{K}_G^B$, $\vec{K}_G^C$ and $\vec{K}_G^D$ all with $K_{Gx}^{A,B,C,D} = k_{ox} + G_x$. As $\vec{K}_G = \vec{K}_O + \vec{G}$, the dispersion relations determine the four values of K_{oz} that go with both K_{ox} and K_{Gx}. We now justify these remarks in more detail.

The time independent Schrödinger equation for a neutron inside a crystal is

$$-\frac{\hbar^2}{2m} \nabla^2 \Psi(\vec{r}) + V(\vec{r})\Psi(\vec{r}) = E_O \Psi(\vec{r}), \qquad (1.10)$$

where $V(\vec{r})$ is the interaction potential of the neutron inside the crystal, and E_O is the incident neutron kinetic energy,

$$E_O = \frac{\hbar^2}{2m} k_O^2 . \qquad (1.11)$$

The total energy of the neutron inside the crystal is E_O. For the perfect crystal $V(\vec{r})$ is periodic. If we define a reduced potential with the dimensions of k_O^2,

$$v(\vec{r}) = \frac{2m}{\hbar^2} V(\vec{r}), \qquad (1.12)$$

we can write eq. (1.10) as

$$\nabla^2 \Psi - v(\vec{r})\Psi + k_0^2\, \Psi = 0 \,. \tag{1.13}$$

The reduced periodic neutron-nuclear interaction potential for a rigid array of nuclei can be written as

$$v\,(\vec{r}) = 4\,\pi \sum_l b_l\, \delta(r - R_l),$$

where the position vector of the lth nucleus is denoted by R_l and b_l is the scattering length of that nucleus, or can be expanded in a Fourier series

$$v\,(\vec{r}) = \sum_{\vec{G}} v_{\vec{G}}\, e^{i\,\vec{G}\cdot\vec{r}}.$$

By Fourier analyzing the above expression we will get

$$v_{\vec{G}} = \frac{1}{V_{\text{cell}}}\int v\,(\vec{r})\, e^{-i\vec{G}\cdot\vec{r}}\, dr \;= \frac{4\pi}{V_{\text{cell}}}\int \sum_l b_l\, \delta(r - R_l)\, e^{-i\vec{G}\cdot\vec{r}}\, dr$$

$$= \frac{4\pi}{V_{\text{cell}}} \sum_l b_l\, e^{-i\,\vec{G}\cdot\vec{R}_l} \;= \frac{4\pi}{V_{\text{cell}}} F_{\vec{G}}\,, \tag{1.14}$$

where $F_{\vec{G}} = \sum_l b_l\, e^{-i\,\vec{G}\cdot\vec{R}_l}$ is the unit cell structure factor and V_{cell} is the volume of a unit cell.

Using the assumption that the incident wave vector $\vec{k_0}$ is oriented very close to the exact Bragg condition for the particular reciprocal lattice vector $\vec{G}$, only the Fourier components of the potential associated with $\vec{G}$, normal to the reflecting planes, become important. Thus, we write

$$v(\vec{r}) = v_0 + v_{\vec{G}}\, e^{i\vec{G}\cdot\vec{r}} + v_{-\vec{G}}\, e^{-i\vec{G}\cdot\vec{r}}\,, \tag{1.15}$$

where v_0 is the average potential inside the crystal with respect to the potential outside the crystal which is zero, i.e. the potential which corresponds to zero reciprocal lattice vector. Note that for the silicon crystals $|v(220)| = \sqrt{2} |v(111)| = v_0 e^{-W}$, where w is the Debye-Waller temperature factor. Furthermore, for a non absorbing, centrosymmetric crystal $v_{\vec{G}} = v_{-\vec{G}}$. The typical values of v_0 and $v_{\vec{G}}$ for silicon crystals are given in appendix 1. As the periodic potential couples the incident wave with the diffracted wave, the neutron wave function can be expanded in Bloch functions

$$\Psi(\vec{r}) = \sum_{\vec{G}} \Psi_{\vec{G}} \, e^{i(\vec{K}_0 + \vec{G}) \cdot \vec{r}}$$

Under the same assumption as above, only two amplitudes Ψ_0 and Ψ_G, will be large. Thus we anticipate the solutions of eq. (1.13) to be of the form

$$\Psi(\vec{r}) = \Psi_0 \, e^{i\vec{K}_0 \cdot \vec{r}} + \Psi_G \, e^{i\vec{K}_G \cdot \vec{r}} , \qquad (1.16)$$

where

$$\vec{K}_G = \vec{K}_0 + \vec{G} \qquad (1.17)$$

By substituting this wave function into the Schrödinger equation (1.13) together with (1.15) and comparing the coefficients of the fourier components on both sides, we get a pair of linear algebraic equations:

$$(k_0^2 - v_0 - K_0^2) \, \Psi_0 - v_{-\vec{G}} \, \Psi_G = 0, \qquad (1.18a)$$

$$-v_{\vec{G}} \, \Psi_0 + (k_0^2 - v_0 - K_G^2) \, \Psi_G = 0. \qquad (1.18b)$$

For a non trivial solution of eqs. (1.18) to exist, the determinant of the coefficients of Ψ_0 and Ψ_G must vanish, i.e.

$$(k_0^2 - v_0 - K_0^2) \, (k_0^2 - v_0 - K_G^2) = v_{\vec{G}} \, v_{-\vec{G}} . \qquad (1.19)$$

This is known as a "dispersion relation". (Note that from here onwards we will drop the vector sign appearing in $v_{\vec{G}}$ and $v_{-\vec{G}}$.)

The neutron wave function must be continuous at the boundary and so the components parallel to the surface of the internal and external wave vectors must match. Therefore we can write the following relations for the parallel sided slab:

$$K_O^2 = k_{OX}^2 + K_{OZ}^2 \qquad (1.20a)$$

and

$$K_G^2 = (k_{OX} + G_X)^2 + (K_{OZ} + G_Z)^2 \qquad (1.20b)$$

We see that the dispersion relation {eq. (1.19)} becomes quartic in K_{OZ} by substituting the eqs. (1.20). One can now see that, a given incident plane wave $\Phi_O \exp(\vec{k}_O \cdot \vec{r})$ generates four internal waves having wave vectors $\vec{K}_O^A$, $\vec{K}_O^B$, $\vec{K}_O^C$ and $\vec{K}_O^D$ with $K_{OX}^{A,B,C,D} = k_{OX}$. These four waves in turn generate, and are coherently coupled to, four Bragg diffracted internal waves having wave vectors $\vec{K}_G^A$, $\vec{K}_G^B$, $\vec{K}_G^C$ and $\vec{K}_G^D$ with $K_{GX}^{A,B,C,D} = k_{OX} + G_X$. Consequently the total wave inside the crystal consists of coherent superposition of eight plane waves, i.e.

$$
\begin{aligned}
\Psi(\vec{r}) = {} & \Psi_O^A \exp(\vec{K}_O^A \cdot \vec{r}) \; + \; \Psi_O^B \exp(\vec{K}_O^B \cdot \vec{r}) \\
& + \Psi_O^C \exp(\vec{K}_O^C \cdot \vec{r}) + \Psi_O^D \exp(\vec{K}_O^D \cdot \vec{r}) + \\
& \Psi_G^A \exp(\vec{K}_G^A \cdot \vec{r}) \; + \; \Psi_G^B \exp(\vec{K}_G^B \cdot \vec{r}) \\
& + \Psi_G^C \exp(\vec{K}_G^C \cdot \vec{r}) + \Psi_G^D \exp(\vec{K}_G^D \cdot \vec{r}). \qquad (1.21)
\end{aligned}
$$

To the extent that $v_G v_{-G} \ll K_O^2$ and $v_G v_{-G} \ll K_G^2$ (i.e. $v_G v_{-G} \approx 0$), the quartic relation describes two intersecting spheres, one centered at the origin O and the other at G, both of radius $\sqrt{k_O^2 - v_O}$. These spheres are the asymptotic forms of the dispersion surface. We treat the case where the incident wave vector, the reciprocal lattice vector and

the surface normal all lie in the same plane which cuts the spheres into two circles. The equation of the asymptotic circles is given by

$$(k_O^2 - v_O - K_O^2)\,(k_O^2 - v_O - K_G^2) = 0$$

The solutions selected by the boundary conditions are found by intersecting the dispersion surface with a line which is normal to the crystal surface at the value of k_{OX}. This line intersects the asymptotic circles at four points with coordinates

$$K_{OZ}^{*A} = \sqrt{k_{OZ}^2 - v_O}\,, \tag{1.22a}$$

$$K_{OZ}^{*B} = -\sqrt{k_{OZ}^2 - v_O}\,, \tag{1.22b}$$

$$K_{OZ}^{*C} = -G_Z + \sqrt{k_{OZ}^2 - v_O - \Delta} \tag{1.22c}$$

and

$$K_{OZ}^{*D} = -G_Z - \sqrt{k_{OZ}^2 - v_O - \Delta}\,\,; \tag{1.22d}$$

where $\Delta = G_X^2 + 2\,k_{OX}\,G_X$, $k_{OZ} = k_O \cos(\theta - \alpha)$, $k_{OX} = -k_O \sin(\theta - \alpha)$, $G_Z = -G \sin\alpha$, and $G_X = G \cos\alpha$. The first two roots are for the circle of $(k_O^2 - v_O - K_O^2) = 0$ and the last two roots are for the circle of $(k_O^2 - v_O - K_G^2) = 0$. By knowing these roots, we can rewrite the dispersion relation in the form

$$(K_{OZ} - K_{OZ}^{*A})\,(K_{OZ} - K_{OZ}^{*B})\,(K_{OZ} - K_{OZ}^{*C})\,(K_{OZ} - K_{OZ}^{*D}) = v_G v_{-G} \tag{1.23}$$

with $K_{OX}^{A,B,C,D} = k_{OX}$. The solutions of the above eq. (1.23) give the exact values of K_{OZ}. The term $v_G v_{-G}$ leads to a splitting of the two circles into an outside curve (α - branch) and an inside curve (β - branch) as shown in Fig. 1.4.

Crystal surface

Load line

$\vec{k}_0$

ψ

k_0

$(k_0^2 - v_0)^{1/2}$

$(k_0^2 - v_0)^{1/2}$

$(k_0^2 - v_0)^{1/2}$

α

O

G

C

P

A

D

B
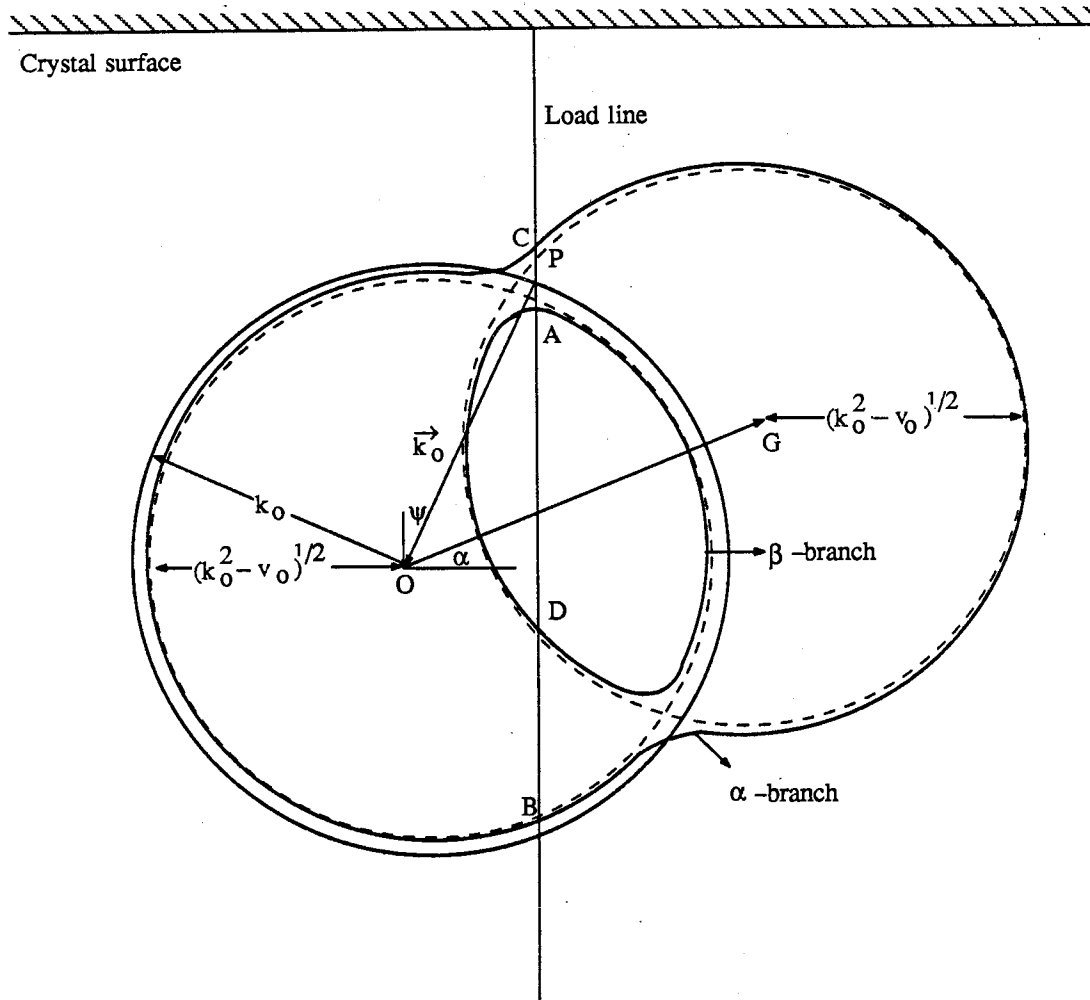
β –branch

α –branch

Figure 1.4:- This diagram shows the splitting of α and β branches from the two asymptotic circles (broken line). The load line is determined by the value of k_{ox}. The tie points A and B are associated with the asymptotic circle at center O. The other two tie points C and D are associated with the asymptotic circle at center G. The radius of both circles is equal to $\sqrt{k_0^2 - v_0}$.

The boundary conditions for the parallel-sided slab then lead to the values for the corresponding eight internal wave amplitudes and four unknown external wave amplitudes in terms of the known incident wave amplitude Φ_0. The boundary conditions at the crystal surfaces are

    – the continuity of the waves,

    – the continuity of the gradients of the waves normal to the surface.

If quartic equations were sufficiently transparent, one would just write down the expressions for the eight waves and let it go at that. These things are handled readily by computers using complex arithmetic. To obtain useful analytic expressions some approximations are called for. These approximations, corresponding to different situations, are explained later in this chapter. This approach of solving the parallel-sided slab problem is known as the "eikonal approach".

There is an alternative mathematical approach to solve the parallel-sided slab problem. In this approach, we again solve the Schrödinger's equation (1.13), but now the amplitudes $\Psi_0(\vec{r})$ and $\Psi_G(\vec{r})$ of the waves inside the crystal are allowed to depend upon position. Under the assumption that the incident wave vector $\vec{k_0}$ is oriented very close to the exact Bragg condition for a particular reciprocal lattice vector, we again anticipate the solution inside the crystal of the form

$$\Psi(\vec{r}) = = \Psi_0(\vec{r})\, e^{i\vec{K_0}\cdot\vec{r}} + \Psi_G(\vec{r})\, e^{i\vec{K_G}\cdot\vec{r}} , \qquad (1.24)$$

where again $\vec{K_G} = \vec{K_0} + \vec{G}$.

In particular, we will choose the internal wave vector $\vec{K_0}$ to satisfy the exact Bragg condition for one particular scattering wave vector $\vec{G}$ and to have magnitude

$$|\vec{K_0}| = K = \sqrt{k_0^2 - v_0}$$ (1.25)

Note that the external Bragg angle θ_B is given by

$$\sin\theta_B = \frac{G}{2k_0}$$ (1.26a)

whereas the internal Bragg angle θ_B^* is given by

$$\sin\theta_B^* = \frac{G}{2K}$$ (1.26b)

We set up an oblique coordinate system choosing unit vectors $\hat{S}_0$ along $\vec{K}_0$ and $\hat{S}_G$ along $\vec{K}_G$ as shown in Fig. 1.5. The relations between the oblique coordinate system (S_0, S_G) and the rectangular axes chosen to be parallel (x) and perpendicular (z) to the surface of the slab (see Fig.1.5) are:

$$s_0 = \frac{1}{\sin 2\theta_B^*} \left\{ z \sin (\theta_B^* + \alpha) - x \cos (\theta_B^* + \alpha) \right\}$$ (1.27a)

and

$$s_G = \frac{1}{\sin 2\theta_B^*} \left\{ z \sin (\theta_B^* - \alpha) + x \cos (\theta_B^* - \alpha) \right\}.$$ (1.27b)

By substituting eq. (1.24) into eq. (1.13), Schrödinger's equation becomes

$$\left(\nabla^2 + k_0^2\right)\left(\Psi_0 e^{iK\hat{S}_0 \cdot \vec{r}} + \Psi_G e^{iK\hat{S}_G \cdot \vec{r}} \right) - \Psi_0 v_G e^{iK\hat{S}_G \cdot \vec{r}} - \Psi_G v_0 e^{iK\hat{S}_G \cdot \vec{r}}$$
$$- \Psi_0 v_0 e^{iK\hat{S}_0 \cdot \vec{r}} - \Psi_G v_{-G} e^{iK\hat{S}_0 \cdot \vec{r}} = 0$$ (1.28)

We know that

$$\nabla^2 \Psi_o e^{iK\hat{S}_o \cdot \vec{r}} = e^{iK\hat{S}_o \cdot \vec{r}} \left\{ \nabla^2 \Psi_o + 2i\vec{\nabla} \Psi_o \cdot K\hat{S}_o - K^2 \Psi_o \right\} \qquad (1.29a)$$

and

$$\nabla^2 \Psi_G e^{iK\hat{S}_G \cdot \vec{r}} = e^{iK\hat{S}_G \cdot \vec{r}} \left\{ \nabla^2 \Psi_G + 2i\vec{\nabla} \Psi_G \cdot K\hat{S}_G - K^2 \Psi_G \right\} \ . \quad (1.29b)$$

Requiring that the coefficients of each wave vanish separately in eq. (1.28) together with (1.29), yields a pair of coupled differential equations:

$$\nabla^2 \Psi_o + 2iK\vec{\nabla} \Psi_o \cdot \hat{S}_o - (K^2 - k_o^2 + v_o) \Psi_o - v_{-G} \Psi_G = 0 \qquad (1.30a)$$

$$\nabla^2 \Psi_G + 2iK\vec{\nabla} \Psi_G \cdot \hat{S}_G - (K^2 - k_o^2 + v_o) \Psi_G - v_G \Psi_o = 0, \qquad (1.30b)$$

Where $\nabla^2 = \dfrac{1}{\sin^2 2\theta_B^*} \left\{ \dfrac{\partial^2}{\partial s_o^2} + \dfrac{\partial^2}{\partial s_G^2} - 2 \cos 2\theta_B^* \dfrac{\partial^2}{\partial s_G \partial s_o} \right\}$ (1.31a);

$$\vec{\nabla} \cdot \hat{S}_o = \frac{\partial}{\partial s_o} \qquad (1.31b)$$

and

$$\vec{\nabla} \cdot \hat{S}_G = \frac{\partial}{\partial s_G} \ . \qquad (1.31c)$$

The magnitude of the internal wave vector has been chosen so that the third terms vanish in eqs. (1.30). Finding a general solution of eqs. (1.30) is very difficult. One could solve the above coupled differential equations together with boundary conditions (see page 15) by computer with great difficulty. But we know from the eikonal method that the internal wave function can be written as a superposition of plane waves for the parallel-sided slab problem. With this in mind we can try a plane wave type solutions for internal wave amplitudes in the incident and the diffracted directions, i.e.

$$\Psi_0(\vec{r}) = C_0 \, e^{i(a\,\hat{a} + b\,\hat{b})\cdot(s_0\,\hat{S}_0 + s_G\,\hat{S}_G)}$$

where $(a\,\hat{a} + b\,\hat{b})$ represents a vector in k-space and $(s_0\,\hat{S}_0 + s_G\,\hat{S}_G)$ is the position vector $\vec{r}$. We choose the unit vectors $\hat{a}$ and $\hat{b}$ are perpendicular to $\hat{S}_G$ and $\hat{S}_0$. Therefore, the (a,b) space represents the reciprocal space to the (s_0,s_G) real space. Note that, since (s_0,s_G) is an oblique coordinate system in real space, the (a,b) is an oblique coordinate system as well in the reciprocal space. Furthermore we know that $\hat{a}\cdot\hat{S}_0 = \hat{b}\cdot\hat{S}_G = \sin 2\theta_B^*$. The above expression for the $\Psi_0(\vec{r})$ can be rewritten as

$$\Psi_0(\vec{r}) = C_0 \, e^{i \sin 2\theta_B^* (as_0 + bs_G)} . \tag{1.32a}$$

From eqs. (1.30a), (1.31a) and (1.31b), the amplitude of the internal wave function in the diffracted direction can be written in the form:

$$\Psi_G(\vec{r}) = C_G \, e^{i \sin 2\theta_B^* (as_0 + bs_G)} . \tag{1.32b}$$

Here C_0 and C_G are constants and are related to each other. The relation between C_0 and C_G can be found by using either eq. (1.30a) or eq. (1.30b). By substituting eqs. (1.32) into eqs. (1.30) combining with eqs. (1.31), we will get

$$\left\{ (a^2 + b^2 - 2\cos 2\theta_B^* ab) + 2Ka \sin 2\theta_B^* \right\} \Psi_0 + v_{-G} \Psi_G = 0 \tag{1.33a}$$

$$\left\{ (a^2 + b^2 - 2\cos 2\theta_B^* ab) + 2Kb \sin 2\theta_B^* \right\} \Psi_G + v_G \Psi_0 = 0 \tag{1.33b}$$

Again, for a non trivial solution of eqs. (1.33) to exist, the determinant of the coefficients of Ψ_0 and Ψ_G must vanish, i.e.

$$\left\{ (a^2 + b^2 - 2 \cos 2\theta_B^* \, ab) + 2Ka \sin 2\theta_B^* \right\}$$

$$\left\{ (a^2 + b^2 - 2 \cos 2\theta_B^* \, ab) + 2Kb \sin 2\theta_B^* \right\} = v_G v_{-G} \qquad (1.34)$$

Eq. (1.34) is somewhat similar to the dispersion relation (1.19). To the extent that $v_G v_{-G} \approx 0$ the above eq. (1.34) reduces to

$$\left\{ (a^2 + b^2 - 2 \cos 2\theta_B^* \, ab) + 2Ka \sin 2\theta_B^* \right\}$$

$$\left\{ (a^2 + b^2 - 2 \cos 2\theta_B^* \, ab) + 2Kb \sin 2\theta_B^* \right\} = 0 \qquad (1.35)$$

which describes the asymptotic form. This asymptotic form describes the two intersecting circles (both passing through the origin) in (a,b) space as shown in Fig. (1.6). The load line, which describes the relation between a and b, can be obtained by matching the exponential component of the wave function (internal and external) parallel to the crystal surface, i.e.

$$- K \sin (\theta_B^* - \alpha) + \sin 2\theta_B^* \, [a \, s_O + b \, s_G]_X = - k_O \sin (\theta - \alpha), \qquad (1.36)$$

where $\sin 2\theta_B^* \, [a \, s_O + b \, s_G]_X = - a \, \cos (\theta_B^* + \alpha) + b \, \cos (\theta_B^* - \alpha).$ $\qquad (1.37)$

We see that by substituting the linear relation between a and b (eq. 1.36) into eq. (1.34), the latter becomes quartic either in a or in b. The constants C_O and C_G, corresponding to four sets of a's and b's, can be calculated using both boundary conditions (see page 15). Now we have four internal plane waves in the incident direction and four internal plane waves in the diffracted direction corresponding to the four sets of a and b. With the following transformations,
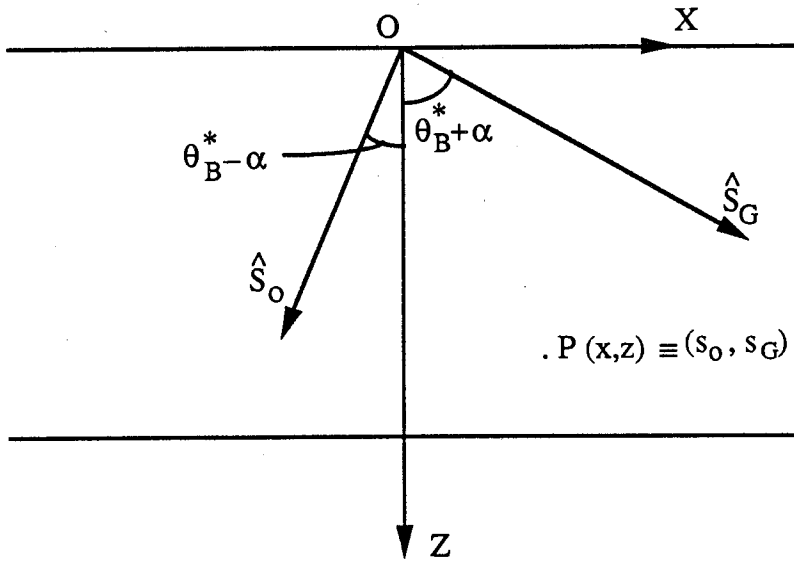
Figure 1.5:- Relation between the oblique coordinate system and rectangular coordinate system
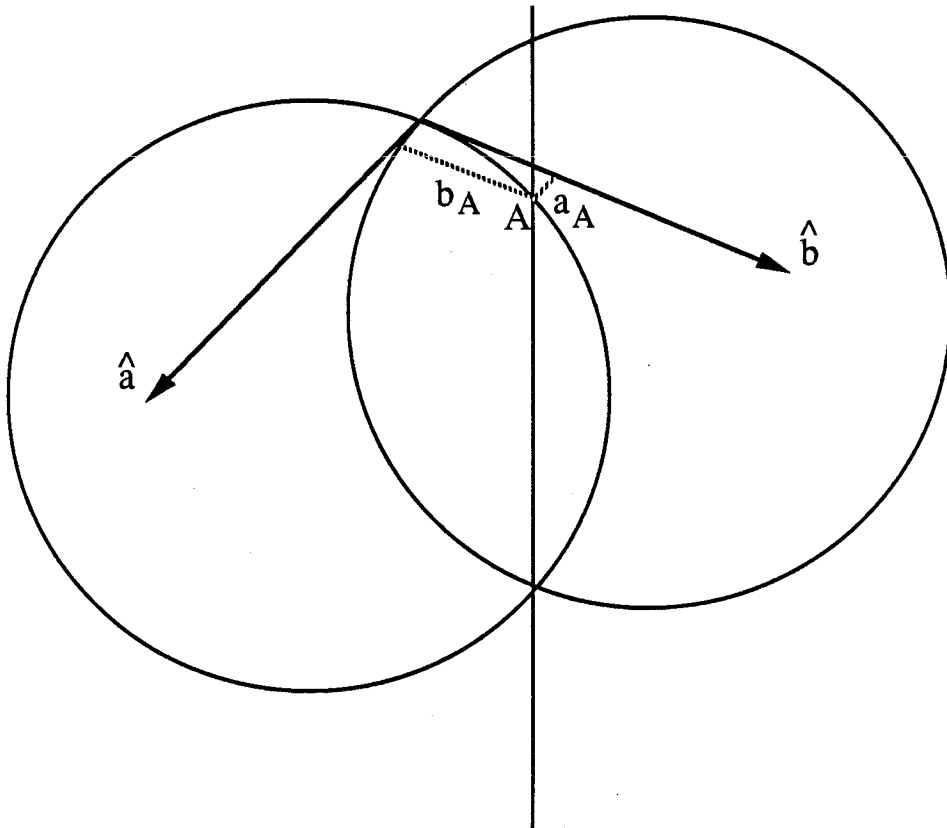
Figure 1.6:- The circles decribing the asymptotic form (eq. 1.35) in (a,b) space

$$K_X = -K \sin(\theta_B^* - \alpha) - a \cos(\theta_B^* + \alpha) + b \cos(\theta_B^* - \alpha) \qquad (1.38a)$$

$$K_Z = K \cos(\theta_B^* - \alpha) + a \sin(\theta_B^* + \alpha) + b \sin(\theta_B^* - \alpha) \qquad (1.38b)$$

$\{(K_X, K_Z)$ are components of the internal wave vector in the eikonal approach.$\}$, we could recover all the eight internal waves which we got in the eikonal approach. Thus we would get nothing new. However, the advantage of this method in certain geometries and also in treating the strain problem (under some assumptions suitable for these situations) are briefly discussed later in this chapter. I will call this second approach the "spatially dependent amplitude method" in rest of my thesis.

1.3   The scope of this thesis

When treating the strain gradient problem we will look for approximate solutions of Schrödinger's equation. The approximations in the eikonal method and in the spatially dependent amplitude method are conceptually different. We will show for the unstrained crystal slab that they lead to almost the same results in most cases. In order to understand some of the differences, we will study some extreme cases in which either the incoming or outgoing beam is very close to paralleling the surface. When we treat the elastic strain gradient problem we will do it using the spatially dependent amplitude method. But we will already have some understanding of the effects that cannot be obtained from this method in the unstrained crystal. The approximate treatment using the spatially dependent amplitude method is commonly referred to as the T-T method in the literature in recognition of the contributions of Takagi and Taupin.

To discuss what comes into the T-T method applied to crystals with strain gradients it is first necessary to discuss the T-T method applied to the unstrained crystal. After this we will return to outline what is involved in the study of diffraction from crystals with strain

gradients and also to discuss the strain itself and how it is determined using elasticity theories for single crystals in the form of thin plates.

1.3.1 Approximations in the eikonal approach

In the eikonal approach, only four internal waves out of eight internal waves become important in most cases except extreme asymmetric cases. In other words the amplitudes of the other four internal waves are negligible. In the literature, researchers in this field use different approximations in order to reduce the eight wave problem into a four wave problem. Sometimes these approximations confuse the reader. Therefore we will state the approximations very clearly.

For example we will consider the non extreme asymmetric Laue geometry and will state all the approximations. The dispersion surfaces, which determine the internal wave vectors, for this particular case are shown in Fig. 1.4 (page 14). The tie points A and C are closer to one end (P) of the incident wave vector. The four internal waves with wave vectors $\vec{K}_O^A$, $\vec{K}_G^A$, $\vec{K}_O^C$ and $\vec{K}_G^C$, corresponding to these two tie points (A and C) are important here. Note that the two z components K_{OZ}^A and K_{OZ}^C are close to each other and to the value of k_{OZ} (z component of the incident wave vector). Therefore these two z components have to be calculated more accurately using the dispersion relation (1.23). We can rewrite the dispersion relation (1.23) in the form

$$(K_{OZ} - K_{OZ}^{*A})(K_{OZ} - K_{OZ}^{*C}) = \frac{v_G v_{-G}}{(K_{OZ} - K_{OZ}^{*B})(K_{OZ} - K_{OZ}^{*D})}. \qquad (1.39)$$

We can approximate the above equation (1.39) to

$$(K_{OZ} - K_{OZ}^{*A})(K_{OZ} - K_{OZ}^{*C}) \approx \frac{v_G v_{-G}}{(K_{OZ}^{*A} - K_{OZ}^{*B})(K_{OZ}^{*C} - K_{OZ}^{*D})} \equiv \varepsilon \qquad (1.40)$$

in this particular case. This has been done by replacing K_{OZ} by K_{OZ}^{*A} and K_{OZ}^{*C} in the right

hand side of the equation (1.39) which is small. Note that the asymptotic roots K_{OZ}^{*A} and

K_{OZ}^{*B} correspond to the asymptotic circle with center at O while the other two roots K_{OZ}^{*C}

and K_{OZ}^{*D} correspond to the asymptotic circle which center is at G. Thus, the right hand

side of the eq. (1.40) will take the simplest form. The quantity ε is an energy in reduced

units of (inverse length)^2. It sets the length scale for pendellösung effects in dynamical

theory, as will be seen in chapter 2. By solving the above quadratic equation (1.40), we

can calculate accurate values for K_{OZ}^{A} and K_{OZ}^{C}. Since the tie points B and D are far away

from point P, we can use the asymptotic values K_{OZ}^{*B} and K_{OZ}^{*D} for K_{OZ}^{B} and K_{OZ}^{D}.

By using the two boundary conditions mentioned earlier, one could calculate all eight

internal wave amplitudes and four unknown external wave amplitudes. This can be done

numerically very easily, but we see that the amplitudes of the four internal waves

corresponding to the tie points B and D are negligible. We take them to be zero.

Furthermore, the amplitudes of two external waves (mirror reflection of the incoming wave

and of Bragg diffracted wave) are negligible in this case. For simplicity we take them to be

zero as well. Now we have only four internal waves and three external waves including

the incoming wave. By using the boundary condition, continuity of internal and external

waves at the crystal surfaces, we can find analytical expressions for the amplitudes of the

four internal waves and of the two unknown external waves in terms of the known

incoming wave amplitude Φ_O. Since we have omitted four internal waves and two external

waves, it is unnecessary to invoke the second boundary condition, continuity of the

gradients of the waves normal to surface. Similar approximations are applicable to the non

extreme asymmetric Bragg geometry. Calculations in these cases are made and analytical

expressions are given in chapter 2.

1.3.2 The T-T method

In these non extreme cases, we can reduce the spatially dependent amplitude method to the T-T method. Here, we take advantage of the fact that the amplitudes of the wave function (eq. 1.24) inside the crystal are slowly varying (much slower than that of the carrier wave), so that terms involving $\nabla^2 \Psi_o$ which are numerically small compared to $K \hat{S}_o \cdot \vec{\nabla} \Psi_o$, are neglected. This assumption has an effect similar to the omission of four internal waves in the eikonal approach. Now using the oblique coordinates, one obtains a simple form to the coupled differential equations (1.30a & b):

$$2iK \frac{\partial \Psi_o}{\partial s_o} = v_{-G} \Psi_G \tag{1.41a}$$

and

$$2iK \frac{\partial \Psi_G}{\partial s_G} = v_G \Psi_o \tag{1.41b}$$

which combine to give a second order partial differential equation for Ψ_G:

$$4K^2 \frac{\partial^2 \Psi_G}{\partial s_G \partial s_o} + v_G v_{-G} \Psi_G = 0 . \tag{1.41c}$$

We can solve the equations (1.41) together with the boundary condition, continuity of waves at the crystal surfaces, and determine the amplitudes of the internal and external waves. By rearranging the complete internal wave function, we will get four plane waves which seem similar to those obtained in the eikonal approach. But the results obtained by these two methods are not quite same because the approximations are different. These remarks are justified in more detail in chapter 2.

The T-T method has a unique advantage. For certain geometries, the solutions of the equations (1.41) are straight forward. For a "δ - function" incident beam (narrow slit

geometry), the solutions are in the form of Bessel functions [7]. This spatially dependent amplitude method with the above mentioned assumption was first developed by Takagi [8] and Taupin [9] to study the effects of strain in the dynamical diffraction of x-rays and more recently utilized by Werner [10] to calculate the effects of gravitational and magnetic fields on the diffraction of neutrons.

We have calculated the integrated diffracted beam intensity (at the exit surface) as a function of crystal thickness for non extreme asymmetric Laue cases. In order to verify these results, experiments were performed in the symmetric and non extreme asymmetric Laue geometry. In these experiments, we have measured the dependence of the diffracted beam intensity as a function of thickness of Si wafers successively etched to thinner and thinner dimensions. The comparison of theory and experiments are given in chapter 2.

1.3.3 The extreme cases

The above described four wave theory (conventional theory) starts to fail in extreme asymmetric cases. These extreme cases can be divided into four categories. They are

1. incident beam almost parallel to the crystal surface (Laue geometry)

2. Bragg diffracted beam almost parallel to the crystal surface (Laue geometry)

3. Bragg diffracted beam almost parallel to the crystal surface (Bragg geometry)

4. incident beam almost parallel to the crystal surface (Bragg geometry).

Theoretically, these cases are obtained by rotating the incident beam and the reciprocal lattice vector with respect to the crystal surface. In experiments, one can obtain these cases by cutting the crystal surface at different angles with respect to the reciprocal lattice vector and by choosing the proper incident beam where the incident beam is oriented very close to satisfying the exact Bragg condition for that particular reciprocal lattice vector.

In the extreme asymmetric cases, more than four waves become important. We consider the case where the incident beam is almost parallel to the crystal surface as an example. The dispersion surface which gives the internal wave vectors are shown in Fig. 1.7 for this particular case. As we see from the Fig. 1.7, the tie points A, B and C are close to each other and to point P. Therefore, six waves corresponding to these tie points A, B and C are important in this case. The three z components (K_{oz}^{A}, K_{oz}^{B} and K_{oz}^{C}) can be determined accurately using the dispersion relation in the form

$$(K_{oz} - K_{oz}^{*A})(K_{oz} - K_{oz}^{*B})(K_{oz} - K_{oz}^{*C}) = \frac{v_G v_{-G}}{(K_{oz} - K_{oz}^{*D})} \, .$$

We can approximate the above equation to

$$(K_{oz} - K_{oz}^{*A})(K_{oz} - K_{oz}^{*B})(K_{oz} - K_{oz}^{*C}) \approx \frac{v_G v_{-G}}{(K_{oz}^{*C} - K_{oz}^{*D})} \, ,$$

which is a cubic equation with coefficients as shown:

$$K_{oz}^{3} - K_{oz}^{2}(K_{oz}^{*A} + K_{oz}^{*B} + K_{oz}^{*C}) + K_{oz}(K_{oz}^{*A}.K_{oz}^{*B} + K_{oz}^{*B}.K_{oz}^{*C} + K_{oz}^{*C}.K_{oz}^{*A})$$

$$- K_{oz}^{*A}.K_{oz}^{*B}.K_{oz}^{*C} - \frac{v_G v_{-G}}{(K_{oz}^{*C} - K_{oz}^{*D})} \approx 0. \qquad (1.42)$$

Since the tie point D is far away from point P (see Fig. 1.7), we have used the asymptotic value K_{oz}^{*D} for K_{oz}^{D}.

Furthermore the amplitude of the mirror reflection of the incident wave becomes significant. In this case we see that at least six internal waves and four external waves, including the incident wave, are important (i.e. the amplitudes of these waves have significant values.). The amplitudes of the internal wave associated with the tie point D and
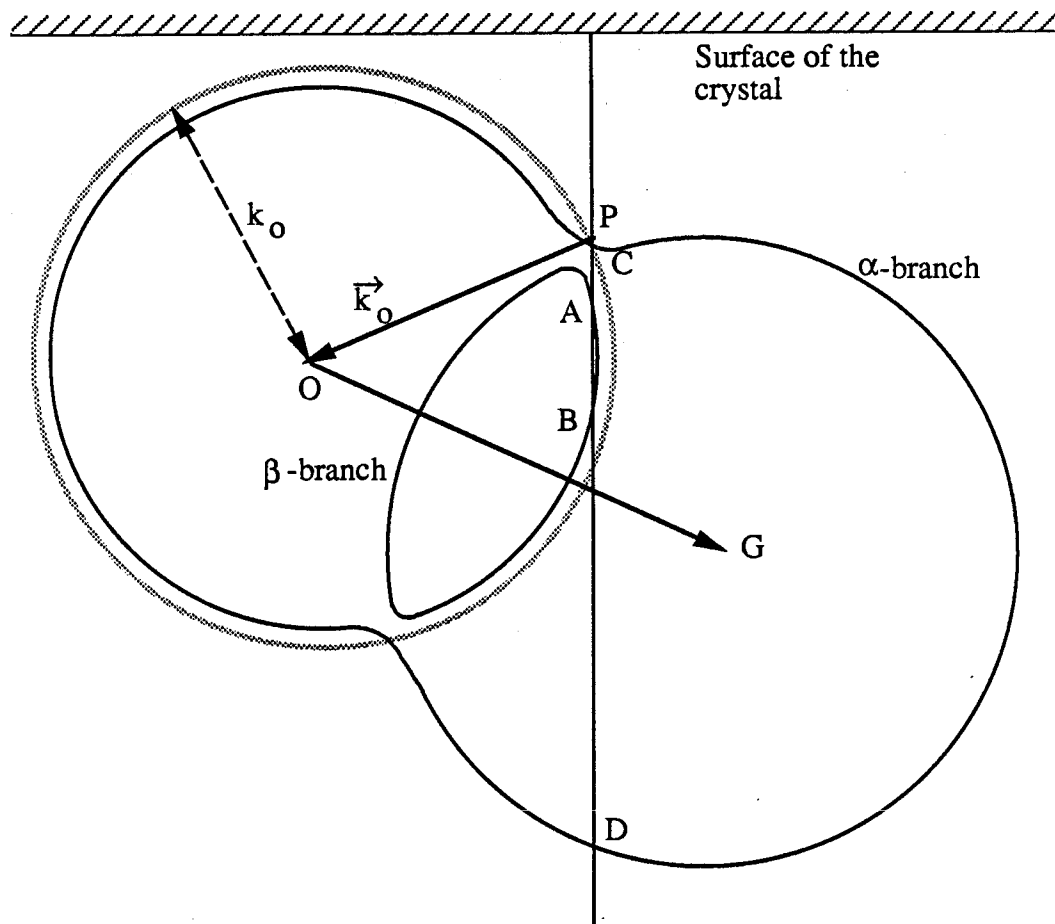
Figure 1.7:- This diagram shows the dispersion surfaces in the extreme asymmetric case where the incident beam is almost parallel to the crystal surface (Laue geometry). The tie points A, B and C are closer to point P and the tie point D is far away from point P.

of the mirror reflection of the Bragg diffracted wave are negligible in this case. For simplicity we assume them to be zero. To calculate the amplitudes of the important internal and external waves, we have to use both boundary conditions mentioned earlier. Using these boundary conditions and ratio of amplitudes (from eqs. (1.18)), we will get a number of equations which is more than the number of unknowns. One will find easily that two of these equations become approximately equivalent to two other equations. Therefore, among the equivalent equations, one of each pair can be omitted in calculating the unknown internal and external wave amplitudes. Now, we have a number of equations which is equal to the number of unknowns. The detailed calculations are shown in chapter 3. The discrepancies among the results obtained using the four wave conventional theory and the above described modified theory in extreme cases, are discussed in the same chapter. In addition, the other three extreme cases with detailed calculations are also described. Note that in all of these four extreme cases, only three tie points are close to the point P. So we have to calculate at most three values z components of the internal wave vectors more accurately. Therefore we need not solve the quartic equation except in the extreme extreme case of both incoming and out going wave vectors being close to parallel to the surface.

In the spatially dependent amplitude method, terms like $\nabla^2 \Psi_O$ and $\nabla^2 \Psi_G$ cannot be neglected in these extreme cases. So we have to solve the coupled differential equations (1.30) together with boundary conditions. First we have to calculate four sets of values for a and b from the eqs. (1.34), (1.36) and (1.37). Only three sets of a and b which are close to zero, are important in the extreme cases. One could proceed and solve the problem in the same way as we did in the eikonal approach. However, here we have two variables a and b instead of the one variable K_{oz} in the eikonal approach. Furthermore, the asymptotic values of a and b are not trivial. But, the asymptotic value of K_{oz} (K_{oz}^*) is known. Therefore the eikonal approach becomes easier than the spatially dependent amplitude method in solving the extreme cases of parallel-sided slab geometries.

1.3.4 Elastically deformed crystals

We have treated the elastically deformed crystal problem in the case of a uniform strain gradient in the plane of diffraction using the T-T method. The effects of the elastic strain gradient is to modify the coupled differential equations for the amplitudes of the waves along the incident and diffracted directions by including a phase factor that depends upon the component of the displacements along the scattering vector. That is eqs. (1.41) become

$$2iK\frac{\partial \Psi_0}{\partial s_0} = v_{-G} e^{i\vec{G}\cdot\vec{u}} \Psi_G \qquad (1.43a)$$

and

$$2iK\frac{\partial \Psi_G}{\partial s_G} = v_G e^{-i\vec{G}\cdot\vec{u}} \Psi_0, \qquad (1.43b)$$

where $\vec{u}(\vec{r})$ is the displacement of a given lattice site from its unstrained position. The solutions of the above coupled differential equations have been expressed in terms of confluent hypergeometric functions by Chukhovskii and Petrashen [11] in the case of uniform strain gradient. The complications of this treatment have been such that little use has been made of their approach by workers in this field. We have eliminated the mathematical obscurity by expressing the confluent hypergeometric function in terms of Chebyshev polynomials. The results are in a form suitable for numerical computation of the variation of intensity of neutron scattering with crystal thickness and amplitude of the strain gradient.

The theory is worked out for uniform strain gradients, that is for displacements $\vec{u}(\vec{r})$ containing terms up to the second order in the distance from the origin taken from the middle of the Borrmann triangle. The Borrmann triangle is formed by an incoming wave, a diffracted wave and the crystal surface. As long as the strain gradient is constant over the

Borrmann triangle standard treatment using the T-T method is applicable. The solutions for uniform strain gradients will apply point by point along the crystal as long as the strain gradients vary very slowly on the scale of the Borrmann triangle. For example the theory would apply in the far field of a single dislocation even though it would be quite suspect if the dislocation was in the middle of the Borrmann triangle.

1.3.5 Elastic strain gradients

The bending of a thin crystal is described in terms of the displacements of its mid-surface from its equilibrium position. In our model the crystal is cubic and the coordinate axes, which are parallel to the edges of the crystal, are parallel to the cubic edges. For a crystal lying in the xy plane and bent cylindrically about x- axis by some externally applied forces, the displacement in the z direction of the mid-surface would be

$$w(x,y,0) = \frac{y^2}{2R} .$$

Away from the mid-surface the displacement in the z direction is given by

$$w(x,y,z) = \frac{y^2}{2R} + \frac{C_{12}}{C_{11}} \frac{z^2}{2R} ,$$

where C_{12} and C_{11} are the elastic constants in an appropriate coordinate system, to be explained later. The displacement in the y direction is given by

$$v(x,y,z) = -\frac{yz}{R} .$$

If the scattering vector is in the xz plane, then only the strain in the z direction will influence the neutron diffraction through the term $\vec{G} . \vec{u}$. Thus there would be no effect on the diffracted intensity of a crystal bent cylindrically about the x-axis if the scattering vector $\vec{G}$ was exactly along the x-axis. For a scattering vector in the xz plane the factor,

$$\exp(-i \vec{G} . \vec{u}) = \exp\left\{ -i \frac{C_{12}}{C_{11}} \frac{G_z z^2}{2R} \right\} ,$$

enters the T-T equation and determines the deviation from the behaviour of the unstrained

crystal.

The actual shapes of the bent crystals are not this simple. The crystal wafer does not bend to form a perfect cylindrical shape. There is curvature along the x-axis that comes about because of the finite length in the x direction. The deviations are noticeable optically near the free edges ($x = \pm a$) of a crystal that is bent by applying boundary conditions at $y = \pm b$ to a crystal plate of length 2a and width 2b. The free edges at $x = \pm a$ do not follow a cylindrical bend. (Even if one were to use cylindrical mold to force the cylindrical bend, there would still be some deviations because of the elastic stress resisting the mold, but the effects would be reduced.) Because of these effects one will see a change in the diffracted intensity even when the scattering vector lies in the x direction, not because there is any thing wrong with the T-T method, but because there will be a real strain gradient component along the x-axis, particularly if the crystal is bent as described above using the edge couples. Thus the strains will be determined by the displacement of the mid-surface in the form

$$w(x,y,0) = \frac{x^2}{2R_x} + \frac{y^2}{2R_y} + \frac{xy}{R_{xy}},$$

where R_x, R_y and R_{xy} are the radii of curvature of the mid-surface in planes parallel to the xz, yz and xy planes respectively. These radii of curvature can be found either from the elasticity theory with boundary conditions or from experiment by measuring $w(x,y,\frac{t}{2})$, where t is the thickness of the crystal. In the above expression for the displacement of the mid-surface there would be some constant and linear terms which won't really matter in calculating the intensity of the diffracted beam. The displacements associated with a given $w(x,y,0)$ are

$$u = -\frac{xz}{R_x} - \frac{yz}{R_{xy}}, \qquad v = -\frac{yz}{R_y} - \frac{xz}{R_{xy}}$$

and

$$w(x,y,z) = \frac{x^2}{2R_x} + \frac{y^2}{2R_y} + \frac{xy}{R_{xy}} + \frac{C_{12}}{2C_{11}} \left\{ \frac{1}{R_x} + \frac{1}{R_y} \right\} z^2 .$$

The displacement that will effect the diffracted intensity when the scattering vector lies along the x direction is $u = -\frac{xz}{R_x} - \frac{yz}{R_{xy}}$.

The calculation of the strain gradients in elastically deformed crystals is treated in the first approximation by the conventional elasticity theory of thin crystal plates in which the basic differential equation is in the form:

$$\frac{\partial^4 w}{\partial x^4} + \frac{2(C_{12} + 2\,C_{44})}{C_{11}} \frac{\partial^4 w}{\partial x^2 \partial y^2} + \frac{\partial^4 w}{\partial y^4} = 0,$$

where the xyz coordinate system of the bending is parallel to the cubic axes of the crystal. If the coordinate system is not parallel to the cubic axes one must carry out some matrix transformations of the tensor quantities. In deriving the above differential equation the influence of strain in the z direction has been neglected because it has only little consequence in the elasticity theory. The strain gradients in the z direction are the main effect in diffraction. The boundary conditions of the free edges give rise to two differential equations:

$$\frac{\partial^2 w}{\partial x^2} + \frac{C_{12}}{C_{11}} \frac{\partial^2 w}{\partial y^2} = 0$$

$$\frac{\partial^3 w}{\partial x^3} + \frac{(C_{12} + 4\,C_{44})}{C_{11}} \frac{\partial^3 w}{\partial x \partial y^2} = 0$$

Solutions are attempted by Ritz methods with polynomial expansion. The results are given in chapter 4.

Conventional elasticity theory becomes suspect when the displacements move the mid-surface of the plate outside the boundaries of the undistorted plate. For bending this corresponds to a radius of curvature

$$R = \frac{b^2}{t}$$

where 2b is the width and t is the thickness of the plate. For our cut silicon wafers 2b = 0.06 m and t = 0.3 to 0.5 mm. These give radii of curvature of 1.8 to 3 meters. This is in the middle of the range of our experiments, which go down to curvatures as sharp as 0.5 meters, which generally breaks the crystal, and are usually as sharp as 1 meter.

The question of what replaces the conventional elasticity theory when the displacements become too large is ignored in most texts. What is happening on large bends is that the material develops what can be called hoop stress because of the curvature. This is missing from the simple differential equation. What is needed is to take into account the stress fields as well as the strains. This yields two coupled differential equations as shown by Rostovtsev in 1940 (see the book by Lekhnitskii [12]):

$$a_{11}\frac{\partial^4 F}{\partial x^4} + (2a_{12} + a_{44}) \frac{\partial^4 F}{\partial x^2 \partial y^2} + a_{11}\frac{\partial^4 F}{\partial y^4} = \left(\frac{\partial^2 w}{\partial x \partial y}\right)^2 - \frac{\partial^2 w}{\partial x^2} \cdot \frac{\partial^2 w}{\partial y^2}$$

$$D_{11} \frac{\partial^4 w}{\partial x^4} + 2 (D_{12} + 2D_{44}) \frac{\partial^4 w}{\partial x^2 \partial y^2} + D_{11} \frac{\partial^4 w}{\partial y^4} =$$

$$t\left(\frac{\partial^2 F}{\partial y^2} \cdot \frac{\partial^2 w}{\partial x^2} - 2 \frac{\partial^2 F}{\partial x \partial y} \cdot \frac{\partial^2 w}{\partial x \partial y} + \frac{\partial^2 F}{\partial x^2} \cdot \frac{\partial^2 w}{\partial y^2}\right)$$

(see appendix 9 for more details including nomenclature.) There are no known non trivial solutions to these equations. They can be treated by Ritz methods or by relaxation methods without unduly complicating the computations. These applications of elasticity theory lie just outside the scope of this thesis. The next stage in our work would encompass this.

The scope of the thesis is to show how to apply the T-T equations to a bent crystal when the local curvatures, R_x, R_y and R_{xy}, are known theoretically or experimentally. We will show how to do this in Chapter 4.

CHAPTER 2

CONVENTIONAL DYNAMICAL THEORY OF DIFFRACTION

2.1 The eikonal approach

Here we give detailed calculations of internal wave vectors (important ones only) and of corresponding internal wave amplitudes in the case of symmetric and non extreme asymmetric Laue and Bragg geometries. We distinguish now between the Laue case (Fig. 2.1a) and the Bragg case (Fig. 2.1b). There are some differences in solving the parallel-sided slab problem between Laue and Bragg cases. We will state the differences wherever they occur.

As mentioned in the previous chapter, we rewrite the approximate form of the dispersion relation (eq. 1.40) for the non extreme asymmetric Laue geometry as:

$$K_{oz}^2 - (K_{oz}^{*A} + K_{oz}^{*C}) K_{oz} + K_{oz}^{*A} K_{oz}^{*C} - \varepsilon \approx 0 , \qquad (2.1)$$

where $$\varepsilon = \frac{v_G \, v_{-G}}{(K_{oz}^{*A} - K_{oz}^{*B}) (K_{oz}^{*C} - K_{oz}^{*D})} \qquad (2.2)$$

As mentioned before, ε is an energy in reduced units that sets the length scale for diffraction phenomena. In usual diffraction experiments, ε is essentially a constant for a given reflection (see appendix 1 for typical values). From eqs. 1.22

$$(K_{oz}^{*A} - K_{oz}^{*B}) = 2 \sqrt{k_{oz}^2 - v_o} = 2 \sqrt{k_o^2 \cos^2(\theta - \alpha) - v_o}$$

$$\approx 2 \sqrt{k_o^2 \cos^2(\theta_B - \alpha) - v_o}$$

and

$$(K_{oz}^{*C} - K_{oz}^{*D}) = 2 \sqrt{k_{oz}^2 - v_o - \Delta}$$

incident beam

$\vec{k}_O$

$\theta - \alpha$

O

X

Bragg
planes

$\vec{K}_O$

$\vec{K}_G$

$\vec{G}$

α

t

Bragg diffracted
beam

Z

$\vec{k}_G$

transmitted
beam

$\vec{k}_O$

(a)

incident beam

Bragg diffracted
beam

$\vec{k}_O$

$\vec{k}_G$

$\theta - \alpha$

X

O

Bragg
planes

$\vec{K}_G$

$\vec{G}$

$\vec{K}_O$

α

t

Z

$\vec{k}_O$

transmitted
beam

(b)
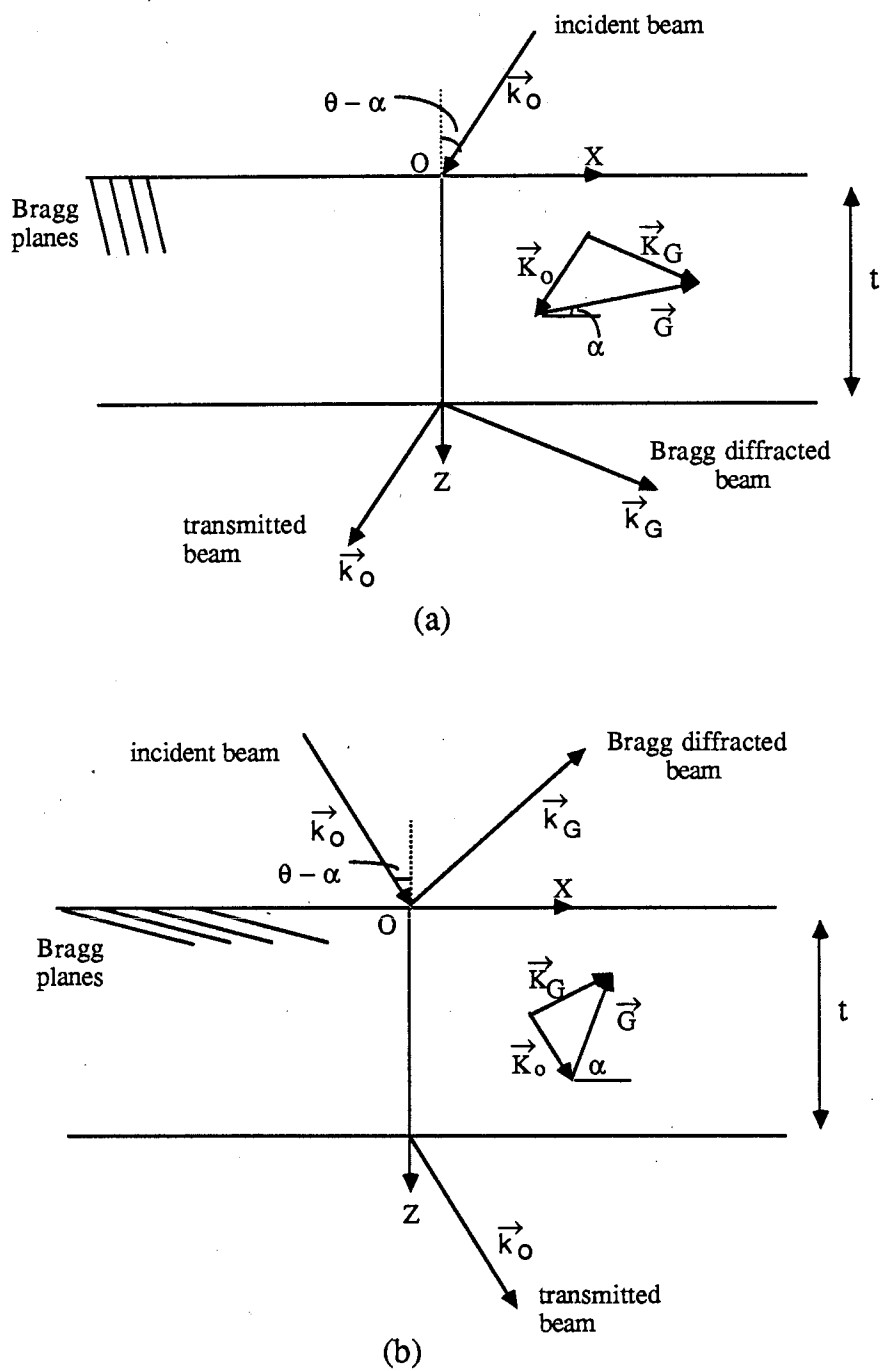
Figure 2.1:- Sketch of (a) the Laue case (b) the Bragg case.

$$= 2 \sqrt{k_0^2\cos^2(\theta-\alpha) - v_0 - G^2\cos^2\alpha + 2k_0 G\sin(\theta-\alpha)\cos\alpha}$$

$$\approx 2 \sqrt{k_0^2\cos^2(\theta_B-\alpha) - v_0 - G^2\cos^2\alpha + 2k_0 G\sin(\theta_B-\alpha)\cos\alpha} \ .$$

Similarly, for the non extreme asymmetric Bragg geometry, the approximate dispersion relation will be in the following form,

$$K_{oz}^2 - (K_{oz}^{*A} + K_{oz}^{*D}) K_{oz} + K_{oz}^{*A} K_{oz}^{*D} + \epsilon \approx 0 \ . \qquad (2.3)$$

In these Bragg cases, all the approximations that we have stated for the non extreme asymmetric Laue geometry (pages 22 & 23) are valid. The only difference is that the tie points A and D (closer to the point P) become important in the Bragg cases compared to the tie points A and C which are important in the non extreme asymmetric Laue geometry. Note that in all cases $K_{ox}^{A,B,C,D} = k_{ox}$. The solutions for K_{oz} of eqs. (2.1) and (2.3) combined with the boundary condition $K_{ox} = k_{ox}$ {(K_{ox}, K_{oz}) determine the internal wave vector}, are described by two hyperbolae as shown as in Fig. 2.2a (Laue case) and 2.2b (Bragg case). The allowed values of K_{oz} (solutions of eq. 2.1) in the case of the non extreme asymmetric Laue geometry are given by

$$K_{oz}^A = \frac{(K_{oz}^{*A} + K_{oz}^{*C})}{2} + \frac{\sqrt{(K_{oz}^{*A} - K_{oz}^{*C})^2 + 4\epsilon}}{2} \qquad (2.4a)$$

and

$$K_{oz}^C = \frac{(K_{oz}^{*A} + K_{oz}^{*C})}{2} - \frac{\sqrt{(K_{oz}^{*A} - K_{oz}^{*C})^2 + 4\epsilon}}{2} \ . \qquad (2.4b)$$

Similarly, the solutions of eq. (2.3) give the z component of the internal wave vectors in the case of Bragg geometry. The solutions are

$$K_{OZ}^A = \frac{(K_{OZ}^{*A} + K_{OZ}^{*D})}{2} + \frac{\sqrt{(K_{OZ}^{*A} - K_{OZ}^{*D})^2 - 4\varepsilon}}{2} \qquad (2.5a)$$

and

$$K_{OZ}^D = \frac{(K_{OZ}^{*A} + K_{OZ}^{*D})}{2} - \frac{\sqrt{(K_{OZ}^{*A} - K_{OZ}^{*D})^2 - 4\varepsilon}}{2} . \qquad (2.5b)$$

Note that K_{OZ}^A and K_{OZ}^C are always real for the values of (k_{OX}, k_{OZ}) (where $\vec{k_O}$ is very close to satisfying the exact Bragg condition) in the Laue geometry (see Fig. 2.2a). In the case of Bragg reflection, K_{OZ}^A and K_{OZ}^D are complex in a certain range of values of (k_{OX}, k_{OZ}) (see Fig. 2.2b), i.e. the surface normal does not intersect either of the two dispersion surfaces. This region is known as the total-reflection region. We know that, for an incident plane wave, two waves in the incident direction and the other two waves in the diffracted direction have considerable amplitudes. Note that, Ψ_O^A, Ψ_O^C, Ψ_G^A and Ψ_G^C have considerable value in the case of Laue geometry while Ψ_O^A, Ψ_O^D, Ψ_G^A and Ψ_G^D are important in the Bragg cases. By knowing these wave amplitudes, we can calculate the amplitudes of the transmitted and Bragg diffracted waves outside the crystal. Note that the amplitudes of mirror reflections of the incoming wave and of Bragg diffracted wave are negligible in these non extreme asymmetric Laue and Bragg cases.

In the Laue geometry, we will get the following relations between the external incident wave amplitude Φ_O and the internal wave amplitudes (Ψ_O^A, Ψ_O^C, Ψ_G^A and Ψ_G^C) by applying the boundary condition, continuity of waves across the entrance surface of the crystal

$$\Psi_O^A + \Psi_O^C = \Phi_O \qquad (2.6a)$$

and

$$\Psi_G^A + \Psi_G^C = 0 . \qquad (2.6b)$$
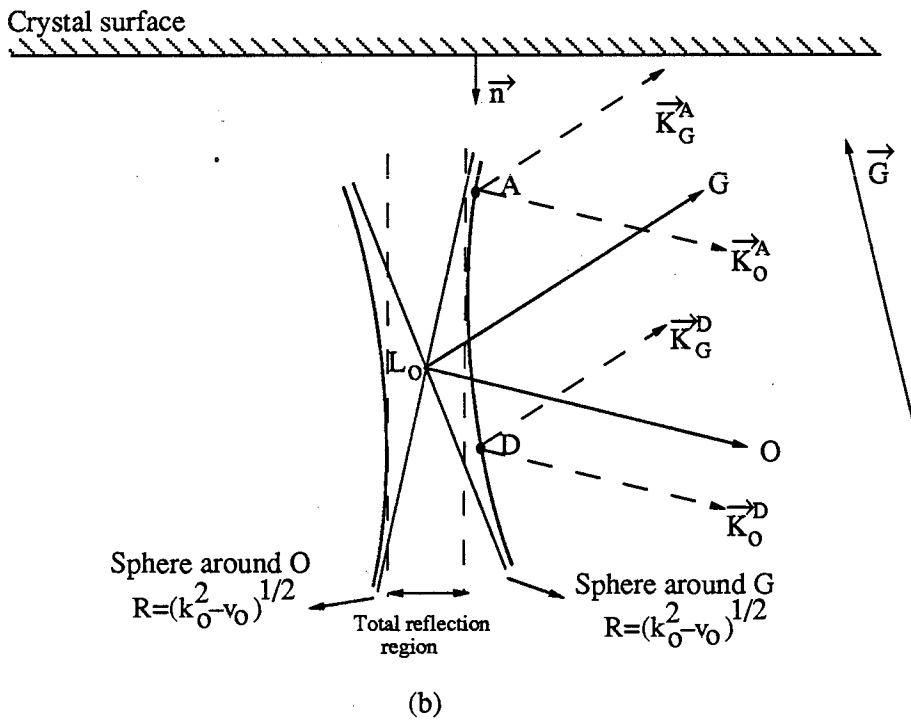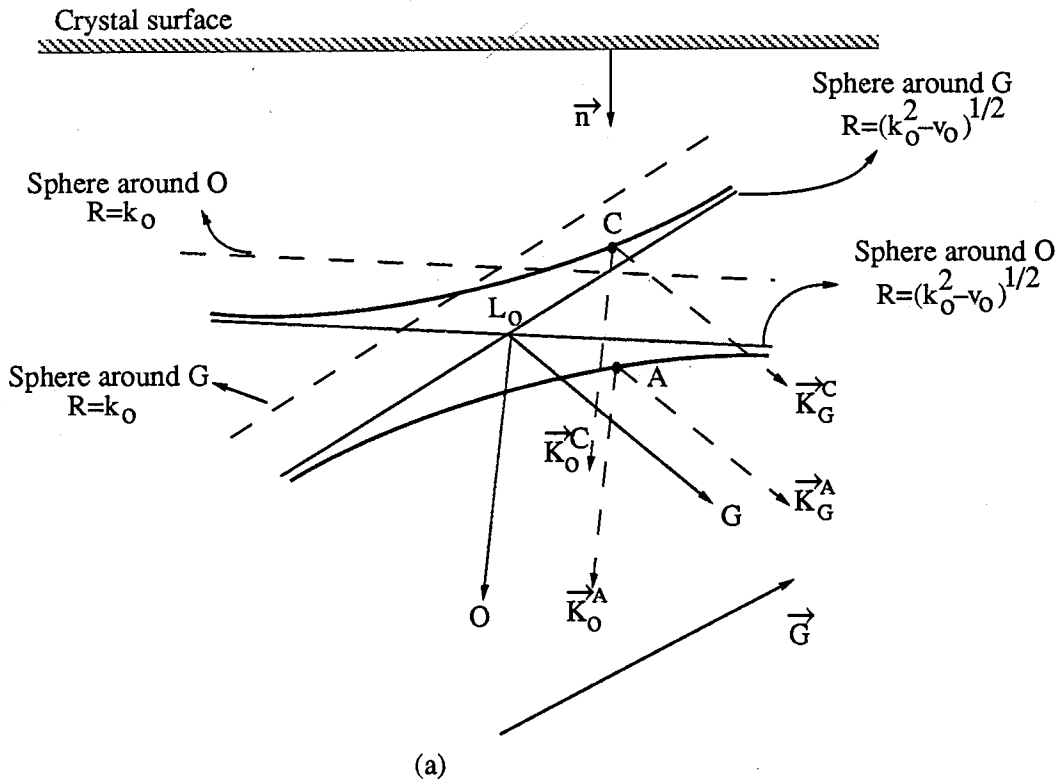
Figure 2.2:- Dispersion surfaces in the reciprocal space for (a) Laue case (b) Bragg reflection.

The first relation (2.6a) makes the total internal incident wave match the external incident plane wave while the second relation makes the total diffracted wave vanish at the entrance surface of the crystal.

By applying the same boundary condition at the exit surface (lower surface of the crystal in the case of Laue geometry), we will get the relations for the amplitudes of transmitted and Bragg diffracted waves in terms of internal wave amplitudes. They are

$$\Phi_t \, e^{ik_{oz}t} = \Psi_o^A \, e^{iK_{oz}^A t} + \Psi_o^C \, e^{iK_{oz}^C t} \tag{2.7a}$$

and

$$\Phi_d \, e^{ik_{Gz}t} = \Psi_G^A \, e^{iK_{Gz}^A t} + \Psi_G^C \, e^{iK_{Gz}^C t} \,, \tag{2.7b}$$

where Φ_t and Φ_d are the amplitudes of transmitted and diffracted waves respectively; $K_{Gz}^{A,C} = K_{oz}^{A,C} + G_z$.

In the Bragg geometry, the diffracted beam emerges from the crystal at the upper surface (see Fig. 2.1b). Therefore the total internal wave in the diffracted direction must vanish at the lower surface of the crystal. By applying the boundary condition, continuity of waves across the crystal surfaces, we will get the following relations:

$$\Psi_o^A + \Psi_o^D = \Phi_o \tag{2.8a}$$

$$\Psi_G^A + \Psi_G^D = \Phi_d \tag{2.8b}$$

$$\Psi_o^A \, e^{iK_{oz}^A t} + \Psi_o^D \, e^{iK_{oz}^D t} = \Phi_t \, e^{ik_{oz}t} \tag{2.8c}$$

$$\Psi_G^A \, e^{iK_{Gz}^A t} + \Psi_G^D \, e^{iK_{Gz}^D t} = 0 \,. \tag{2.8d}$$

Note that the first two relations (2.8a & b) correspond to the upper surface while the last two relations (2.8c & d) correspond to the lower surface of the crystal. In order to calculate the internal wave amplitudes, we need only eqs. (2.6a & b) in the case of Laue geometry and eqs. (2.8a & d) in the Bragg case. We also need the ratio of the internal amplitudes which can be found from eq. (1.18a), i.e.

$$\frac{\Psi_0^A}{\Psi_G^A} = \frac{v_{-G}}{\{k_0^2 - v_0 - K_0^{A2}\}} = \frac{v_{-G}}{\{k_{0z}^2 - v_0 - K_{0z}^{A2}\}} \tag{2.9a}$$

and

$$\frac{\Psi_0^C}{\Psi_G^C} = \frac{v_{-G}}{\{k_{0z}^2 - v_0 - K_{0z}^{C2}\}} ; \tag{2.9b}$$

or

$$\frac{\Psi_0^D}{\Psi_G^D} = \frac{v_{-G}}{\{k_{0z}^2 - v_0 - K_{0z}^{D2}\}} . \tag{2.9c}$$

By solving the eqs. (2.6a), (2.6b), (2.9a) and (2.9b), we will get all the internal wave amplitudes in the case of Laue geometry. They are

$$\Psi_G^A = \frac{\{k_{0z}^2 - v_0 - K_{0z}^{A2}\} \{k_{0z}^2 - v_0 - K_{0z}^{C2}\}}{v_{-G}\{K_{0z}^{A2} - K_{0z}^{C2}\}} \Phi_0 , \tag{2.10a}$$

$$\Psi_G^C = - \frac{\{k_{0z}^2 - v_0 - K_{0z}^{A2}\} \{k_{0z}^2 - v_0 - K_{0z}^{C2}\}}{v_{-G}\{K_{0z}^{A2} - K_{0z}^{C2}\}} \Phi_0 , \tag{2.10b}$$

$$\Psi_0^A = \frac{\{k_{0z}^2 - v_0 - K_{0z}^{C2}\}}{\{K_{0z}^{A2} - K_{0z}^{C2}\}} \Phi_0 \tag{2.10c}$$

and

$$\Psi_0^C = - \frac{\{k_{0z}^2 - v_0 - K_{0z}^{A2}\}}{\{K_{0z}^{A2} - K_{0z}^{C2}\}} \Phi_0 \tag{2.10d}$$

Similarly, we will get the following expressions for the internal wave amplitudes by solving the eqs. (2.8a), (2.8d), (2.9a) and (2.9c) in the case of Bragg geometry:

$$\Psi_G^A = \frac{\{k_{0z}^2 - v_0 - K_{0z}^{A\,2}\}\{k_{0z}^2 - v_0 - K_{0z}^{D\,2}\}}{v_{-G}\left(\{k_{0z}^2 - v_0 - K_{0z}^{D\,2}\}e^{iK_{Gz}^D t} - \{k_{0z}^2 - v_0 - K_{0z}^{A\,2}\}e^{iK_{Gz}^A t}\right)}\Phi_0\, e^{iK_{Gz}^D t}$$

(2.11a)

$$\Psi_G^D = -\frac{\{k_{0z}^2 - v_0 - K_{0z}^{A\,2}\}\{k_{0z}^2 - v_0 - K_{0z}^{D\,2}\}}{v_{-G}\left(\{k_{0z}^2 - v_0 - K_{0z}^{D\,2}\}e^{iK_{Gz}^D t} - \{k_{0z}^2 - v_0 - K_{0z}^{A\,2}\}e^{iK_{Gz}^A t}\right)}\Phi_0\, e^{iK_{Gz}^A t}$$

(2.11b)

$$\Psi_0^A = \frac{\{k_{0z}^2 - v_0 - K_{0z}^{D\,2}\}}{\left(\{k_{0z}^2 - v_0 - K_{0z}^{D\,2}\}e^{iK_{Gz}^D t} - \{k_{0z}^2 - v_0 - K_{0z}^{A\,2}\}e^{iK_{Gz}^A t}\right)}\Phi_0\, e^{iK_{Gz}^D t}$$

(2.11c)

$$\Psi_0^D = -\frac{\{k_{0z}^2 - v_0 - K_{0z}^{A\,2}\}}{\left(\{k_{0z}^2 - v_0 - K_{0z}^{D\,2}\}e^{iK_{Gz}^D t} - \{k_{0z}^2 - v_0 - K_{0z}^{A\,2}\}e^{iK_{Gz}^A t}\right)}\Phi_0\, e^{iK_{Gz}^A t}.$$

(2.11)

Now we know all the internal wave vectors and corresponding internal wave amplitudes. By knowing these, one could calculate the diffracted wave amplitude (Φ_d) from eq. (2.7b) in the Laue case (at the lower surface of the crystal) and from eq. (2.8b) in the Bragg case (at the upper surface of the crystal) in order to verify the theory experimentally. Details are given later in this chapter. Before calculating the external unknown wave amplitudes (transmitted and Bragg diffracted), we will see the detailed calculations of solutions to the parallel-sided slab problem in the non extreme asymmetric cases using the Takagi-Taupin approach.

2.2 The T-T approach

As we mentioned in chapter 1, we have to solve eqs. (1.41) together with the boundary conditions, in order to calculate the internal wave function in the non extreme asymmetric Laue and Bragg geometries.

Solutions of eq. (1.41c) are of the form

$$\Psi_G = C_G \, e^{\, i \left(\frac{qv_{-G}}{2K} s_0 + \frac{v_G}{2Kq} s_G \right)}. \tag{2.12}$$

From eq. (1.41b), we get

$$\Psi_0 = -\frac{C_G}{q} \, e^{\, i \left(\frac{qv_{-G}}{2K} s_0 + \frac{v_G}{2Kq} s_G \right)}. \tag{2.13}$$

There should be two solutions for q in the case of a parallel-sided slab problem. This becomes evident in the process of matching the boundary conditions which also determine the coefficient C_G. (For a general boundary there can be an infinite number of solutions for q). For incoming wave vector $\vec{k_0}$ which makes an angle $(\theta - \alpha)$ with respect to the surface normal, the continuity of the internal and the external wave functions at the entrance surface requires

$$\Psi_0 \, (x, z=0) \, e^{\, iKx \, \hat{S}_0 \cdot \hat{x}} = \Phi_0 \, e^{\, ik_{0x}x} \tag{2.14a}$$

and

$$\Psi_G \, (x, z=0) \, e^{\, iKx \, \hat{S}_G \cdot \hat{x}} = 0 \tag{2.14b}$$

in the case of non extreme asymmetric Laue geometry. By matching the x component of the phase factor in eq. (2.14a) together with eqs. (1.27), we get

$$\frac{qv_{-G}}{2K} \cdot \frac{-\cos(\theta_B^* + \alpha)}{\sin 2\theta_B^*} + \frac{v_G}{2Kq} \cdot \frac{\cos(\theta_B^* - \alpha)}{\sin 2\theta_B^*} - K\sin(\theta_B^* - \alpha) = k_O \sin(\theta - \alpha),$$

i.e. $\{q \cos(\theta_B^* + \alpha) - \frac{1}{q}\cos(\theta_B^* - \alpha)\}$

$$= \frac{2K\sin 2\theta_B^*}{v_G}\{k_O \sin(\theta - \alpha) - K\sin(\theta_B^* - \alpha)\} \qquad (2.15a)$$

(Note that here we assume $v_G = v_{-G}$.) Eq. (2.15a) is quadratic in q and gives the two solutions of q (say q_1 and q_2) in the case of a parallel-sided slab problem. They are:

$$q_1 = p + \sqrt{p^2 + \frac{\cos(\theta_B^* - \alpha)}{\cos(\theta_B^* + \alpha)}} \qquad (2.15b)$$

and

$$q_2 = p - \sqrt{p^2 + \frac{\cos(\theta_B^* - \alpha)}{\cos(\theta_B^* + \alpha)}}, \qquad (2.15c)$$

where $p = \frac{K^2 \sin 2\theta_B^*}{v_G \cos(\theta_B^* + \alpha)}\left\{\frac{k_O \sin(\theta - \alpha)}{K} - \sin(\theta_B^* - \alpha)\right\}.$ $\qquad (2.15d)$

We also get the following relations by matching the coefficients of exponential components on both sides of eqs. (2.14):

$$(C_G)_{q_1} + (C_G)_{q_2} = 0 \qquad (2.16a)$$

$$-\frac{(C_G)_{q_1}}{q_1} - \frac{(C_G)_{q_2}}{q_2} = \Phi_O. \qquad (2.16b)$$

From these two relations {eqs. (2.16a) & (b)}, we obtain $(C_G)_{q_1}$ and $(C_G)_{q_2}$ in terms of q_1, q_2 and Φ_O, i.e.

$$(C_G)_{q_1} = -(C_G)_{q_2} = \frac{q_1\, q_2}{(q_1 - q_2)}\Phi_0 \qquad (2.17)$$

We see that the spectrum of separation constants q is discrete, (q_1, q_2) in this case, involving only two amplitudes $(C_G)_{q_1}$ and $(C_G)_{q_2}$. Thus, we can write the internal wave functions in the incident and the diffracted directions as,

$$\Psi_0(r)\, e^{iK\hat{S}_0 \cdot \vec{r}} = \left\{ -\frac{(C_G)_{q_1}}{q_1}\, e^{i\left(\frac{q_1 v_{-G}}{2K} s_0 + \frac{v_G}{2Kq_1} s_G \right)} \right.$$

$$\left. - \frac{(C_G)_{q_2}}{q_2}\, e^{i\left(\frac{q_2 v_{-G}}{2K} s_0 + \frac{v_G}{2Kq_2} s_G \right)} \right\} e^{iK\hat{S}_0 \cdot \vec{r}} \qquad (2.18a)$$

and

$$\Psi_G(r)\, e^{iK\hat{S}_G \cdot \vec{r}} = \left\{ (C_G)_{q_1}\, e^{i\left(\frac{q_1 v_{-G}}{2K} s_0 + \frac{v_G}{2Kq_1} s_G \right)} \right.$$

$$\left. + (C_G)_{q_2}\, e^{i\left(\frac{q_2 v_{-G}}{2K} s_0 + \frac{v_G}{2Kq_2} s_G \right)} \right\} e^{iK\hat{S}_G \cdot \vec{r}}. \qquad (2.18b)$$

The total internal wave function $\Psi(r)$ ($= \Psi_0(r)\, e^{iK\hat{S}_0 \cdot \vec{r}} + \Psi_G(r)\, e^{iK\hat{S}_G \cdot \vec{r}}$) consists of the superposition of four plane waves which can be obtained by combining the amplitude modulations with the carrier wave vector. The z component of the wave vector can be written as

$$K_z = K\cos(\theta_B^* - \alpha) + \frac{q v_{-G}}{2K} \cdot \frac{\sin(\theta_B^* + \alpha)}{\sin 2\theta_B^*} + \frac{v_G}{2Kq} \cdot \frac{\sin(\theta_B^* - \alpha)}{\sin 2\theta_B^*}. \qquad (2.19)$$

If one compares eq. (2.19) with q_1 and q_2 with eqs. (2.4a & b) there appears to be little in common. But numerically they are very close. To show this analytically involves considerable expansion of square roots and lots of algebra, after which the differences appear in the higher order terms which are many orders of magnitude smaller. Thus numerically one can show that the z component of the internal wave vectors and

corresponding wave amplitudes, which are calculated using both eikonal and T-T approach, are very nearly equal in the non extreme asymmetric Laue cases. The x component of the internal wave vectors in both approaches are equal to k_{OX}, of course. The different approximations in both methods create the very small differences in the z component of the internal wave vectors and in the corresponding wave amplitudes.

Similarly, one could calculate the total internal wave function in the case of Bragg geometry.

2.3 Calculation of diffracted beam intensity

We have measured the diffracted beam intensity experimentally as a function of thickness of the crystal. Details are given later in this chapter. Since we have performed the experiments in the Laue geometry mostly, we will calculate the diffracted beam intensity at the lower surface of the crystal in that geometry. We know that the diffracted wave amplitude is given by eq. (2.7b), i.e.

$$\Phi_d = e^{-ik_{Gz}t} \{ \Psi_G^A e^{iK_{Gz}^A t} + \Psi_G^C e^{iK_{Gz}^C t} \}. \qquad (2.20)$$

Inserting the wave function of the diffracted wave into the quantum mechanical prescription for calculating the intensity,

$$I_d = \Psi(r) \cdot \Psi(r)^*$$

one finds

$$I_d = \Phi_d \Phi_d^*$$

$$= \{ \Psi_G^A e^{iK_{Gz}^A t} + \Psi_G^C e^{iK_{Gz}^C t} \} \{ \Psi_G^{A*} e^{-iK_{Gz}^A t} + \Psi_G^{C*} e^{-iK_{Gz}^C t} \} \qquad (2.21)$$

Since Ψ_G^A and Ψ_G^C are real and $\Psi_G^A = -\Psi_G^C$, eq. (2.21) reduces to

$$I_d = \Psi_G^{A2} + \Psi_G^{C2} + 2 \Psi_G^A \Psi_G^C \cos (K_{Gz}^A - K_{Gz}^C) t$$

$$= 4 \, \Psi_G^{A2} \sin^2 \frac{(K_{GZ}^A - K_{GZ}^C) \, t}{2}$$

$$= \frac{16 \, \varepsilon^2 \, K_{oz}^{*A2} \, \Phi_0^2}{v_{-G}^2 \, \{ (K_{oz}^{*A} - K_{oz}^{*C})^2 + 4 \, \varepsilon \}} \sin^2 \{ \frac{\sqrt{(K_{oz}^{*A} - K_{oz}^{*C})^2 + 4 \, \varepsilon}}{2} \, t \}$$

(2.22)

This expression is derived in appendix 2. It gives the intensity in terms of the intersections $K_{oz}^{*A,B,C,D}$ of the unperturbed spheres, the magnitude of the perturbations v_G^2, and ε which depends upon these variables through eq. (2.2). In an experiment there will be a range of incoming neutron wave vectors. The quantity $(K_{oz}^{*A} - K_{oz}^{*C})$ will vary rapidly over that range, but the quantities K_{oz}^{*A}, ε and v_G will be constant or sufficiently constant to be treated as such. The dependence of the incoming flux Φ_0^2 (determined by the experimental arrangement) upon the incoming wave vectors will set the limits of integration in calculating the integrated intensity.

Turning to experimental verification of dynamical theory, we consider the effects of wavelength spread of the incoming neutrons and its angular spread. Generally researchers in this field calculate the effects on diffracted beam intensity profiles due to the angular spread only, assuming that the incident beam has constant energy. The intensity profiles of the diffracted beams are broadened by a convolution of $\Delta\theta$ (angular spread) and ΔK (magnitude of wave vector spread) whose effects are convoluted. The single variable $(K_{oz}^{*A} - K_{oz}^{*C})$ which is a function of $\Delta\theta$ and ΔK (see appendix 3) better describes the diffraction profiles. In the limits of $\Delta\theta \to 0$ (or $\Delta K \to 0$), the variable is linear in ΔK (or $\Delta\theta$). Let us examine eq. (2.22) further.

From eq. (2.22), we see that the intensity of the diffracted beam is a function of $(K_{oz}^{*A} - K_{oz}^{*C})$, K_{oz}^{*A} and ε for a particular thickness of the crystal. We know that K_{oz}^{*A} and ε are slowly varying variables of wavelength spread and angular spread of neutron

source while ($K_{OZ}^{*A} - K_{OZ}^{*C}$) is a rapidly varying variable. The diffracted beam intensity profile is shown in Fig. 2.3 as a function of K_{OZ}^{*A} and ($K_{OZ}^{*A} - K_{OZ}^{*C}$). Note that, here we assume ε as a constant. From Fig. 2.3, we see that the diffracted beam intensity is a rapidly varying function of ($K_{OZ}^{*A} - K_{OZ}^{*C}$) and a slowly varying function of K_{OZ}^{*A}. The intensity profile of the diffracted beam is mainly determined by a single variable ($K_{OZ}^{*A} -$ K_{OZ}^{*C}). If we neglect the variation in K_{OZ}^{*A} and in ε due to the neutron source wavelength spread and its angular spread, eq. (2.22) will represent a curve which is a rapidly oscillating function of variable ($K_{OZ}^{*A} - K_{OZ}^{*C}$), having a Lorentzian envelope given by

$$\frac{16 \, \varepsilon^2 \, K_{OZ}^{*A^2} \, \Phi_0^2}{v_{-G}^2 \, \{ (K_{OZ}^{*A} - K_{OZ}^{*C})^2 + 4 \, \varepsilon \}}$$. These results are illustrated in Fig. 2.4. The peak

of the above Lorentzian envelope occurs when $K_{OZ}^{*A} = K_{OZ}^{*C}$. This can be represented by a set of lines ($K_{OZ}^{*A} - K_{OZ}^{*C} = 0$) in ($\Delta\theta$, ΔK) space depending upon the value of α (see Fig. 2.5a). Furthermore, the peak value of the Lorentzian envelope is given by

$$\text{Peak intensity} = \frac{4 \, \varepsilon \, K_{OZ}^{*A^2} \, \Phi_0^2}{v_{-G}^2} \qquad (2.23)$$

The Lorentzian envelope falls to half of its maximum when ($K_{OZ}^{*A} - K_{OZ}^{*C}$)^2 = 4 ε. This corresponds to a full width at half maximum of

$$(K_{OZ}^{*A} - K_{OZ}^{*C})_L - (K_{OZ}^{*A} - K_{OZ}^{*C})_R = 4 \sqrt{\varepsilon} \qquad (2.24)$$

This also can be represented by a set of lines in ($\Delta\theta$, ΔK) space for various values of α (see Fig. 2.5b). These parameters are very useful in designing high reflectivity monochromators.

2.4 Calculation of integrated intensity of the diffracted beam

In general, the incident plane wave has a finite wavelength spread and angular
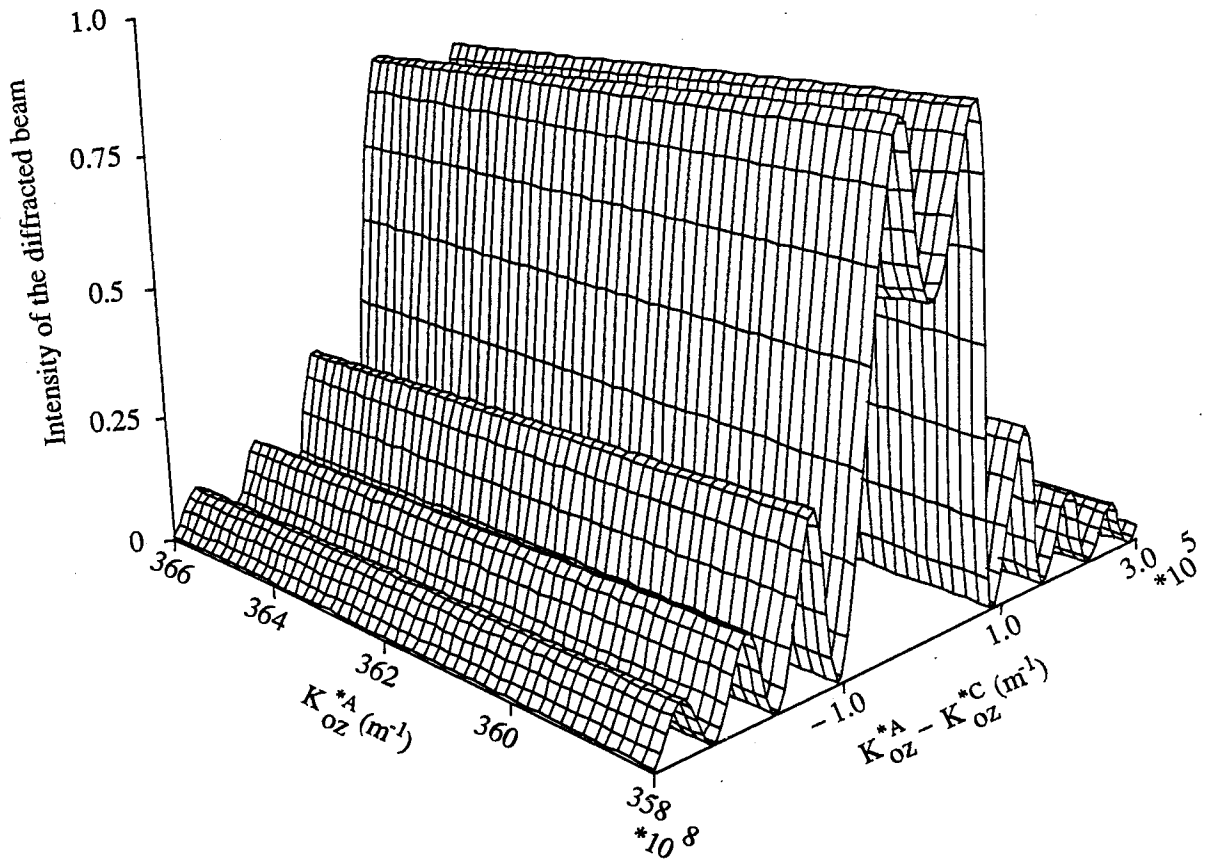
Figure 2.3:- Intensity of the diffracted wave (at the lower surface of the crystal) as a function of K_{oz}^{*A} and ($K_{oz}^{*A} - K_{oz}^{*C}$). Here we assume ε as a constant.
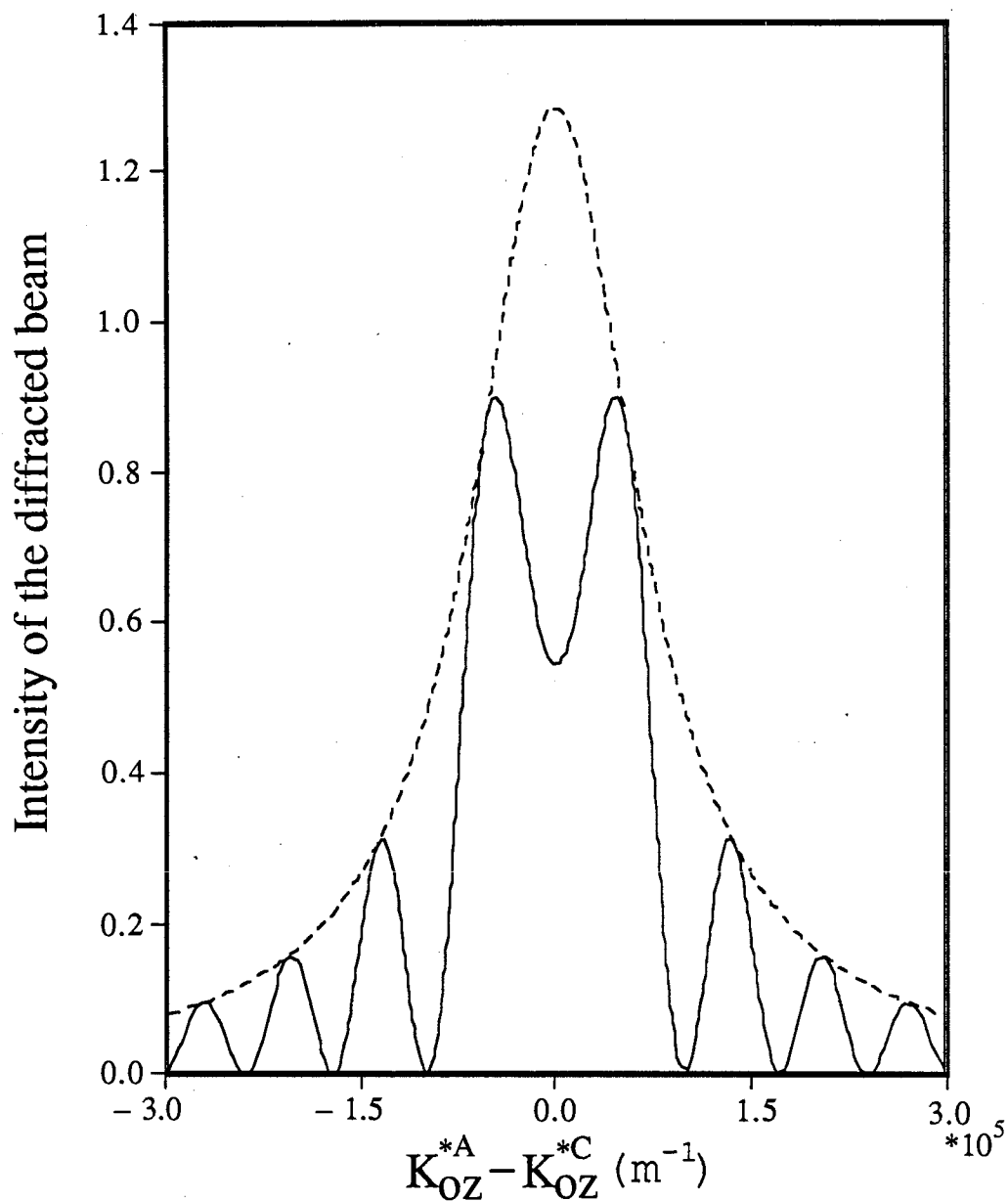
Figure 2.4:- Intensity of the diffracted beam as a function of ($K_{OZ}^{*A} - K_{OZ}^{*C}$). Here we neglect the variation in K_{OZ}^{*A} and in ε due to the wavelength spread and the angular spread of the incoming neutron beam.
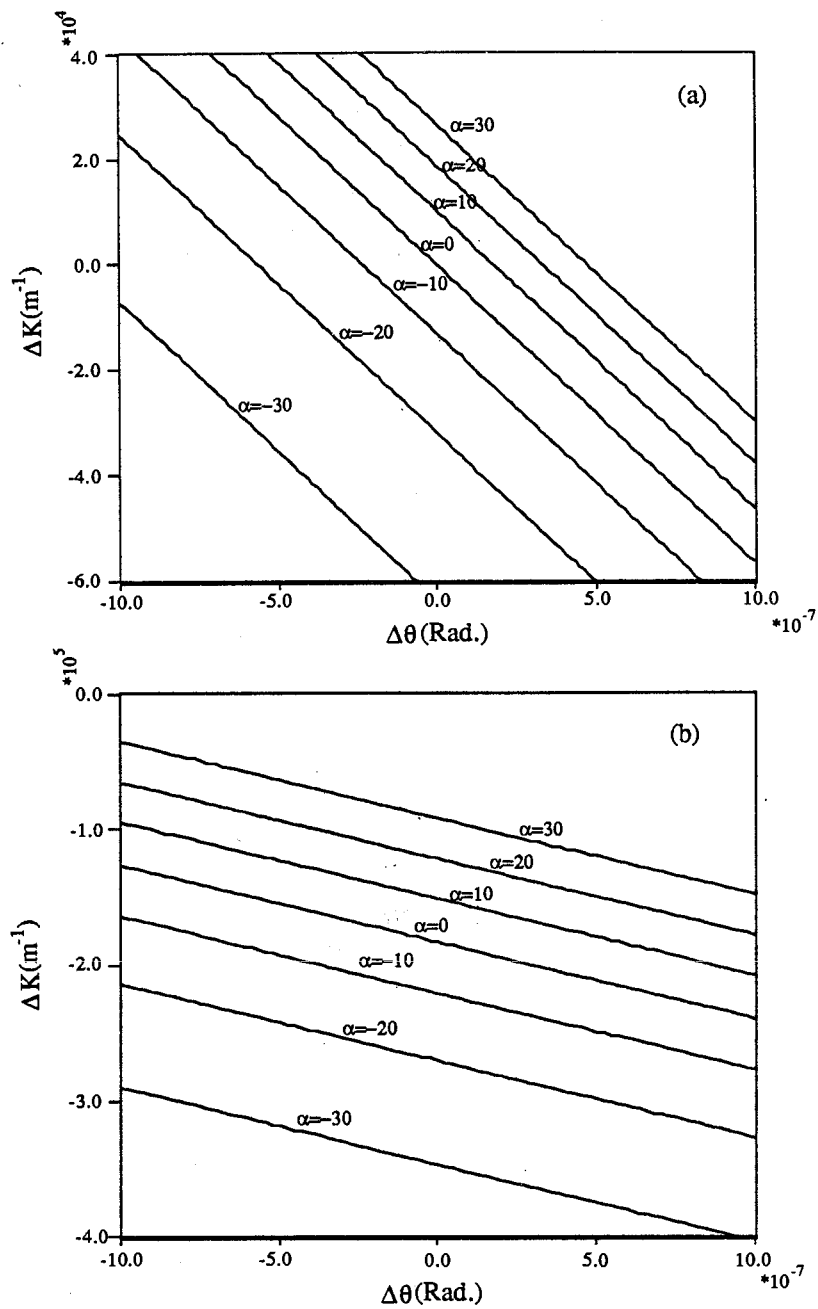
Figure 2.5:- (a) Lines ($K_{OZ}^{*A} - K_{OZ}^{*C} = 0$) representing the positions where the Lorentzian envelope has the peak value in ($\Delta\theta$, ΔK) space.

(b) A set of lines (($K_{OZ}^{*A} - K_{OZ}^{*C}$)$_L$ – ($K_{OZ}^{*A} - K_{OZ}^{*C}$)$_R$ = 4 $\sqrt{\varepsilon}$) corresponds to full width at half maximum of the Lorentzian envelope.

divergence. So one can represent the incident beam profile by a set of contours in k-space ((k_X, k_Z) plane) depending upon the experimental situations. Therefore, one has to take the wavelength spread and the angular spread of the incoming beam into account in calculating the integrated intensity. The integrated intensity of the diffracted beam can be defined as

$$I = \int \int I_d \, dk_{ox} \, dk_{oz} \, . \tag{2.25}$$

As we mentioned earlier, the diffracted beam intensity is a rapidly varying function of ($K_{oz}^{*A} - K_{oz}^{*C}$) and a slowly varying function of K_{oz}^{*A}. One can evaluate the above double integration (eq. 2.25) by the change of variable method, i.e.

$$I = \int \int I_d(\, k_{ox}, k_{oz}) \, dk_{ox} \, dk_{oz}$$

$$= \iint I_d(\, K_{oz}^{*A} - K_{oz}^{*C}, \, K_{oz}^{*A}) \, J(\, K_{oz}^{*A} - K_{oz}^{*C}, \, K_{oz}^{*A}) \, d(\, K_{oz}^{*A} - K_{oz}^{*C}) \, d(\, K_{oz}^{*A}), \tag{2.26a}$$

where the Jacobian $J(\, K_{oz}^{*A} - K_{oz}^{*C}, \, K_{oz}^{*A}) \approx \dfrac{\cos(\theta_B + \alpha)}{2 \sin \theta_B \cos \alpha} \tag{2.26b}$

(for details see appendix 4).

Substituting the diffracted beam intensity I_d {from eq. (2.22)} into eq. (2.26a) we will get,

$$I = \int \int \frac{16 \, \varepsilon^2 \, K_{oz}^{*A2} \, \Phi_o^2}{v_{-G}^2 \, \{(\, K_{oz}^{*A} - K_{oz}^{*C})^2 + 4 \, \varepsilon\}} \, \sin^2 \{\frac{\sqrt{(\, K_{oz}^{*A} - K_{oz}^{*C})^2 + 4 \, \varepsilon}}{2} \, t\}$$

$$\cdot \frac{\cos(\theta_B + \alpha)}{2 \sin \theta_B \cos \alpha} \, d(\, K_{oz}^{*A} - K_{oz}^{*C}) \, d(\, K_{oz}^{*A}) \, . \tag{2.27}$$

We see from Fig. 2.3 that the intensity of the diffracted beam decreases rapidly with increasing or decreasing value of $(K_{oz}^{*A} - K_{oz}^{*C})$ from zero. A small spread in wavelength and in angle of the incoming beam gives a range of values for the variable $(K_{oz}^{*A} - K_{oz}^{*C})$ in

which the intensity of the diffracted beam has a significant value. For simplicity, we assume that the incident beam profile is constant over this region. Furthermore the intensity of the diffracted beam is a slowly varying function of K_{OZ}^{*A} over a wide range (see Fig. 2.3). Therefore one has to take the incident beam profile dependence on K_{OZ}^{*A} into account in the integrated intensity calculation. The variation of the incident beam profile with the variable $(K_{OZ}^{*A} - K_{OZ}^{*C})$ can be neglected within the range in which the intensity of the diffracted beam has a significant value. Furthermore, we have neglected also the variation of ε due to the wavelength spread and the angular spread of the incoming neutrons. With the above assumptions, the double integral {eq. (2.27)} can be split into two single integrals, i.e.

$$I = \frac{16\,\varepsilon^2}{v_{-G}^2} \cdot \frac{\cos(\theta_B + \alpha)}{2\sin\theta_B \cos\alpha} \int K_{OZ}^{*A2}\, \Phi_0^2\,(K_{OZ}^{*A})\, d\,(K_{OZ}^{*A}) \, .$$

$$\int_{-\infty}^{\infty} \frac{\sin^2\left\{ \frac{\sqrt{(K_{OZ}^{*A} - K_{OZ}^{*C})^2 + 4\,\varepsilon}}{2}\, t \right\}}{\left\{ (K_{OZ}^{*A} - K_{OZ}^{*C})^2 + 4\,\varepsilon \right\}}\, d\,(K_{OZ}^{*A} - K_{OZ}^{*C}) \, . \quad (2.28)$$

The second integral is a function of thickness of the crystal (t). The first integral, which is independent of crystal thickness, is determined by the incident beam profile. For a particular experimental set up, one could assume that the value of the first integral is constant (say C). Then we can rewrite eq. (2.28) as

$$I = \frac{16\,\varepsilon^2 C}{v_{-G}^2} \cdot \frac{\cos(\theta_B + \alpha)}{2\sin\theta_B \cos\alpha} \int_{-\infty}^{\infty} \frac{\sin^2\left\{ \frac{\sqrt{(K_{OZ}^{*A} - K_{OZ}^{*C})^2 + 4\,\varepsilon}}{2}\, t \right\}}{\left\{ (K_{OZ}^{*A} - K_{OZ}^{*C})^2 + 4\,\varepsilon \right\}} \cdot$$

$$d\,(K_{OZ}^{*A} - K_{OZ}^{*C}).$$

Our ultimate aim is to calculate the integrated intensity as a function of thickness of the crystal for several scattering vectors making various angles with respect to the surface of

the crystal. By defining new dimensionless variables

$$V = \frac{\sqrt{(K_{OZ}^{*A} - K_{OZ}^{*C})^2 + 4\,\varepsilon}}{2\sqrt{\varepsilon}} \quad \text{and} \quad T = \sqrt{\varepsilon}\,t \text{, the above equation can be further}$$

reduced to

$$I = \frac{16\,\varepsilon^2 C}{v_{-G}^2} \cdot \frac{\cos(\theta_B + \alpha)}{2\sin\theta_B \cos\alpha} \frac{1}{2\sqrt{\varepsilon}}\,2 \int_{1+}^{\infty} \frac{\sin^2(VT)}{V\sqrt{V^2 - 1}}\,dV.$$

One can rearrange this equation in the following form

$$\left\{ \frac{v_{-G}^2 \sin\theta_B \cos\alpha}{4\,\varepsilon^{3/2}\cos(\theta_B + \alpha)\,C} \right\} I = 2 \int_{1+}^{\infty} \frac{\sin^2(VT)}{V\sqrt{V^2 - 1}}\,dV. \qquad (2.29)$$

The right hand side of eq. (2.29) depends only on T $(= \sqrt{\varepsilon}\,t)$, the normalized crystal thickness. Now we define I_0 as the normalized integrated intensity

$$I_0 = \left\{ \frac{v_{-G}^2 \sin\theta_B \cos\alpha}{4\,\varepsilon^{3/2}\cos(\theta_B + \alpha)\,C} \right\} I. \qquad (2.30)$$

The curve of normalized integrated intensity versus normalized thickness is a universal curve as shown as in Fig. 2.6. The period of thickness oscillation is 3.102 in normalized units. From this curve, one can calculate the integrated intensity as a function of thickness of the crystal for all possible cases of Laue-transmission geometries by multiplying with the scaling factors (corresponding to the integrated intensity as well as the thickness of the crystal). The scaling factors differ from case to case. The period of thickness oscillation is $3.102\,\varepsilon^{-1/2}$ $\{\varepsilon^{-1/2}$ is the characteristic length given by eq. (2.2)$\}$. These results are verified experimentally and details are given later in this chapter. One has to notice that we have neglected the variation in ε due to the angular spread and the wavelength spread of the
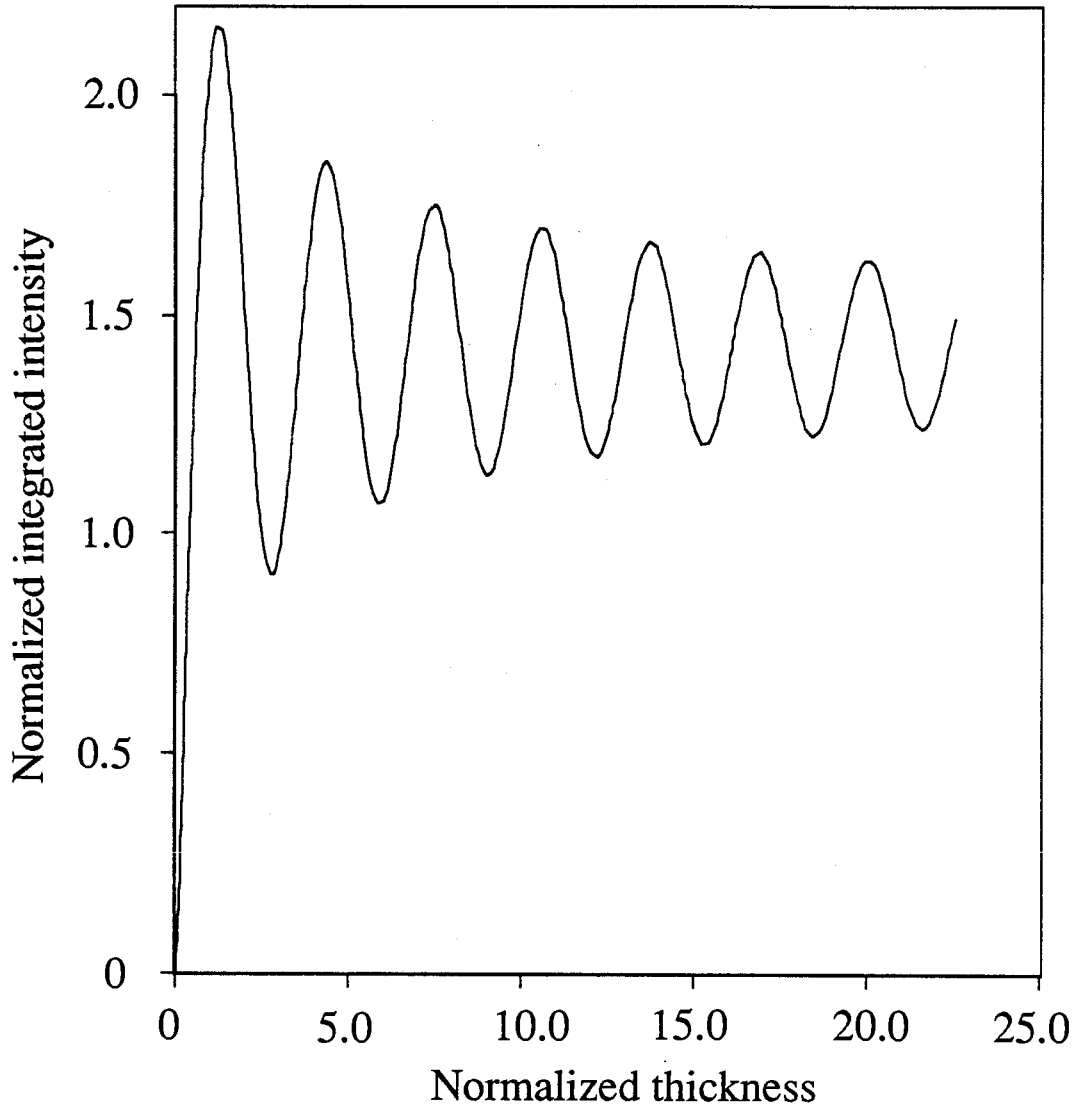
Figure 2.6:- A universal curve representing thickness oscillations (Pendellösung beats) in the Laue diffraction for a perfect crystal.

incoming neutrons throughout the integrated intensity calculation. If the portion of incident beam hitting the sample changes during the process of rotating the crystal sample in order to examine the different Laue transmission geometries, one would have a different value of the constant C for different reflections.

2.5   Experimental methods

The experiments were carried out using neutrons (2-5x10^{11} thermal neutrons/ cm^2/sec source flux, depending upon how much the proton beam effectiveness is decreased in the isotope production facility) from the TNF (Thermal Neutron Facility) at TRIUMF. The experimental set up described below is shown in Fig. 2.7.   The cross-section of the thermal neutron beam from the D_2O moderator is rectangular with dimensions 5 cm x 20 cm. The beam is monochromated by 90° scattering from the (422) reflection from stacks of silicon wafers (7.5 cm diameter) which have been specially treated to produce high reflectivity. This monochromator set up produces neutrons of wavelength $\approx$ 1.57 A^o. A cadmium slit of width ~ 6mm x 20mm was placed just in front of the sample, 5 m from the monochromating crystals. The sample crystal was placed on a special sample holder which was mounted on the spectrometer table. The special sample holder allows one to scan the crystal from one end to the other using a stepping motor. With this system, one can rotate the crystal on the table in order to study the asymmetric Laue and Bragg geometries as well as the symmetric cases. This sample holder is also specially designed for bending the crystal in a unique manner. Further details are given in chapter 4. The diffracted beam is detected by a set of ^{3}He detectors (25 mm diameter by 150 mm) which are placed at a distance of 1 m from the sample. The detector collects neutrons over a range of 1.75^o. Actually, there are four detectors side by side in our experimental set up. All of the diffracted neutrons hit one detector while the other three detectors count the background. These detectors are coupled to a Tennelec electronic counting system. All experimental data are collected using an IMS computer which also controls the experiment via stepping motors.

^{3}He detectors

Si crystal

1 m

Cd slit
(~6 mm)

Crystal

A special sample holder
system

5 m

Neutrons from TNF

5cm

Monochromator
crystal stack
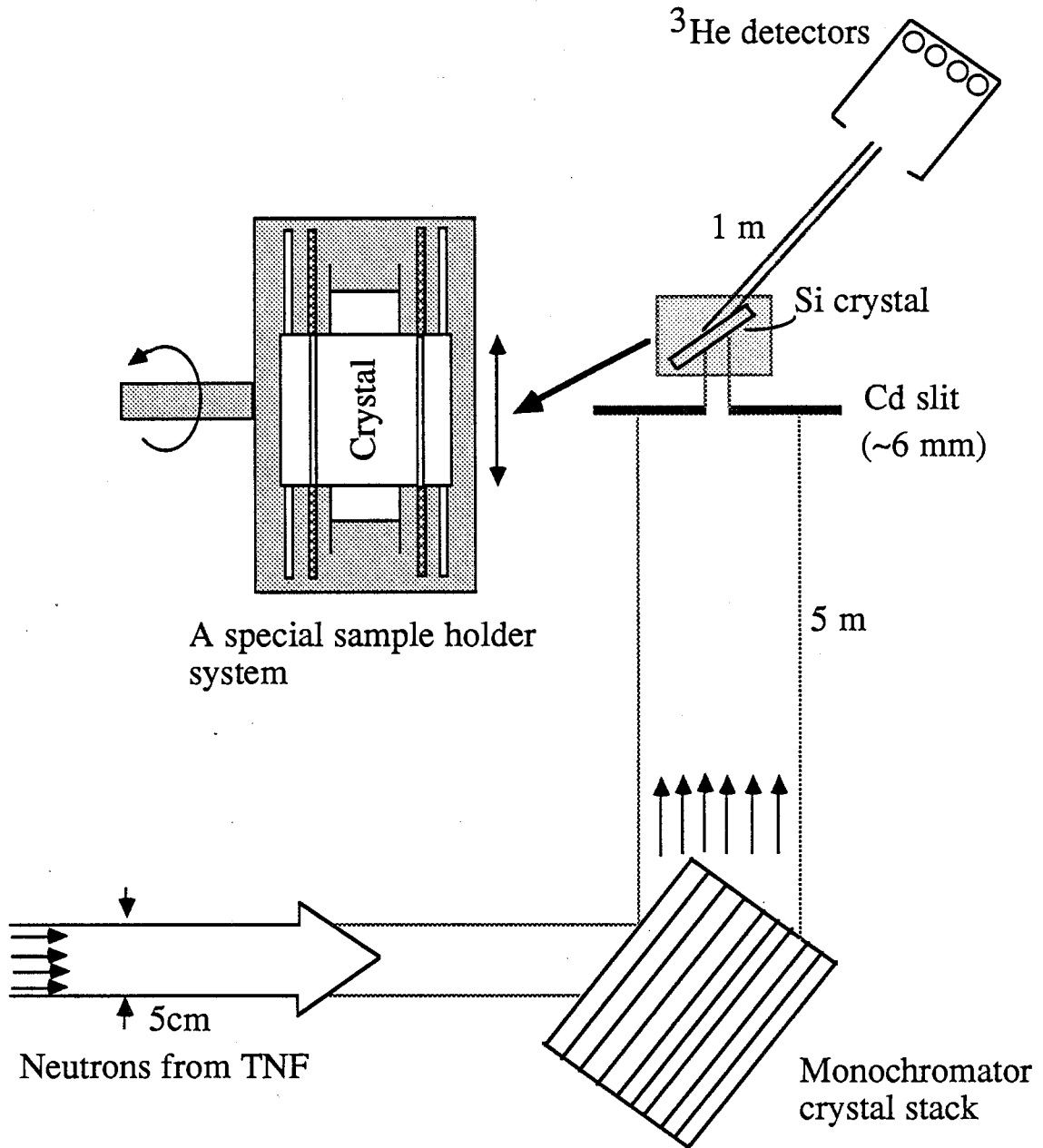
Figure 2.7:- A schematic diagram of the neutron diffraction apparatus.

A wedge shaped sample was prepared from a dislocation free silicon crystal, the surface of which was nearly parallel to the (400) direction (004 cut crystal). The Si crystal was slowly lowered into a bath of planer etch (75% HNO_3, 18% Acetic acid and 7% HF) at a speed of ($\pi/2$)$''$/hr. The bath was stirred every half an hour during the etching. After the first etch, the thickness of the crystal was measured at different positions along the translational axis. The thickness of the crystal at the thicker end was 710 μm and at the thinner end was 480 μm. After neutron studies, the thickness of the crystal was further decreased by successive etchings. The uniform etch was repeated until the thin edge was no longer there. The variation of thickness was approximately the same along the translational axis of the crystal after each etching. The etching is not completely uniform, so that there are variations of 5 μm at most in thickness across the length (2cm) of the slit. After each etching the tapered crystal was scanned from one end to the other by moving it over the Cd slit (6mm width) placed just below the sample mount. The spectrometer was set to study the (400) reflection (symmetric Laue case) from the Si crystal.

In another set of experiments a (111) cut silicon crystal was used. The crystal was etched as for the above (004) cut crystal except that the edges of the crystal were masked to prevent etching. This made the etched wafer easier to handle and mount. Only the etched region was scanned by the slit. Using this sample, the symmetric Laue reflection ($4\bar{2}\bar{2}$) and asymmetric reflections ($1\bar{1}\bar{1}$), ($3\bar{1}\bar{1}$) and (400) were studied. In the second set of experiments, the crystal was etched only once.

2.6   Results and Discussion

The experimental curve showing the integrated intensity as a function of thickness for the (400) symmetric Laue reflection is shown in Fig. 2.8. First we have measured a rocking curve for each particular thickness of the crystal and the integrated intensity was calculated by integrating the intensity over the rocking curve. The neutron flux in our system is low, so that the measurement of each rocking curve took about an hour. The
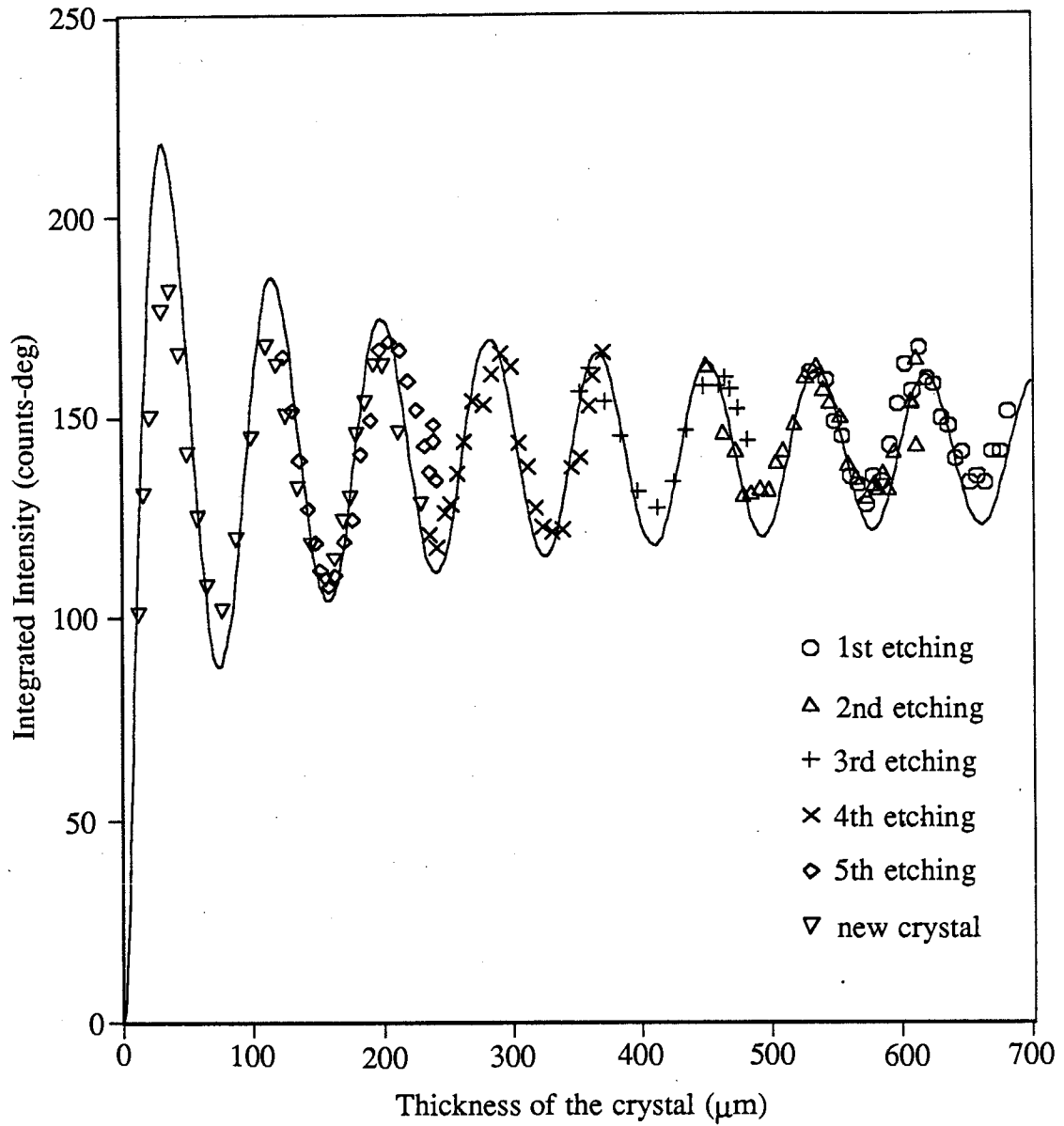
Figure 2.8:- Integrated intensity measured experimentally as a function of thickness of the crystal for (400) symmetric Laue reflection. The solid line is the fitted curve using all experimental points (using the curve fitting program, MINUIT).

crystal was translated in 3mm steps across the 6mm wide slit and rocking curve measurements were made at each position. Similar measurements were made after each etching.

From the universal curve of thickness oscillation, we can obtain a theoretical curve (without any correction for the experimental situation) of integrated intensity as a function of thickness of the crystal by knowing the scaling factors for the crystal thickness $f(\theta_B, \alpha)$ and the integrated intensity $g(\theta_B, \alpha)$. These scaling factors are given by

$$f(\theta_B, \alpha) = \frac{1}{\sqrt{\varepsilon}} \qquad (2.31a)$$

and

$$g(\theta_B, \alpha) = \frac{4\,\varepsilon^{3/2} \cos(\theta_B + \alpha)\,C}{v_{-G}^2 \sin\theta_B \cos\alpha}, \qquad (2.31b)$$

The values of the scaling factors are calculated for the silicon (400) symmetric Laue reflection for neutrons with a wavelength of 1.57 A°. The important parameter involved in the calculation of scaling factors is the crystal structure factor per unit cell F_{hkl}. It is related to the scattering amplitudes of the atoms contributing to the (hkl) reflection and to the Debye Waller temperature factor for the particular reflection. For the (400) silicon reflection, $F_{400} = 8\,b\,e^{-W}$ with b (= 4.1534×10^{-15}m) being the coherent-nuclear scattering amplitude per atom. The other parameter involved in the calculation of the scaling factor of the integrated intensity is C. For the calculation of C, we make the following assumption for the incoming beam profile. The incident beam profile is described by

$$\Phi_O(K_{OZ}^{*A}) = 1 \quad \text{for } |\Delta K| \le 1\% \text{ of } (K_{OZ}^{*A})_M$$

$$= 0 \quad \text{otherwise.}$$

where $K_{OZ}^{*A} = (K_{OZ}^{*A})_M + \Delta K$ and $(K_{OZ}^{*A})_M$ is the value of K_{OZ}^{*A} at the exact Bragg condition for $k_O = 4 \times 10^{10} m^{-1}$ ($\lambda = 1.57$ A°). With this assumption the value of C is equal to $6.942 \times 10^{29} (m^{-3})$ for the (400) symmetric Laue reflection. The calculated values of the scaling factors are $2.66 \times 10^{-5} (m)$ and $3.457 \times 10^{13} (m^{-2})$ for the crystal thickness and for the integrated intensity using the above parameters.

Next we will consider the corrections for the experimental situation. During the experiment we have placed a 6 mm wide Cd slit across the incoming beam. So one has to consider the effects of the slit in the intensity calculation. However, there won't be any correction in the total integrated intensity by introducing the slit across the incident beam. Now we will justify this statement.

We consider the geometry as shown in Fig. 2.9. Let W_O (=2a) be the width of the slit AB. The incoming neutrons impinge on the entrance surface of the crystal along a strip A'B' of width W_i { = $2a/\cos(\theta - \alpha) \approx 2a/\cos(\theta_B - \alpha)$} due to the presence of the slit AB. The origin is chosen to be at the center of A'B'. By introducing the slit AB across the incident beam, we will get non-zero wave fields in the segment CF at the lower surface of the crystal. The width of the segment CF (W) is related to the width of the strip A'B' (W_i) and the thickness of the crystal by

$$W = W_i + t \{ \tan(\theta_B^* - \alpha) + \tan(\theta_B^* + \alpha) \} \tag{2.32}$$

As we see from Fig. 2.9, any point in the region DE receives the same neutron flux as it would if the slit were infinitely wide, i.e. the points in the region DE covers a complete inverse Borrmann triangle. At the same time, the points in the regions CD and EF receive only a part of the plane wave intensity. Therefore the wave field is constant on the segment DE and is found as the solution of the ordinary dynamic problem (Plane wave type approximation). The width of the segment DE (W_d) is given by
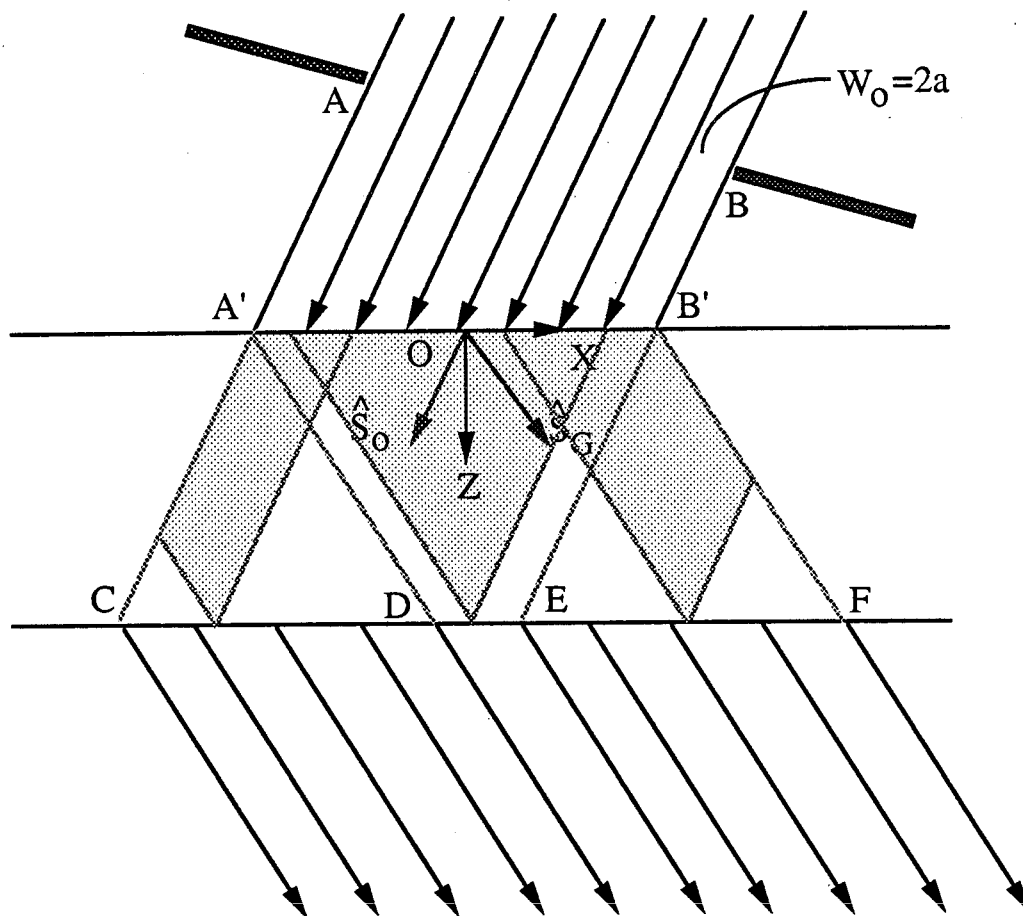
Figure 2.9:- This diagram shows the cross-sectional area of incident and of diffracted beams at the entrance and the exit surface of the crystal. A slit (AB) of width W_O (=2a) is introduced across the incident beam. The origin is chosen at the center of A'B'.

$$W_d = W_i - t \{ \tan (\theta_B^* - \alpha) + \tan (\theta_B^* + \alpha) \} \qquad (2.33)$$

The intensity distribution in the regions CD and EF can be calculated by integrating the point source type solutions over a part of the Borrmann triangle with the appropriate relative phases to satisfy the boundary conditions of an incident plane wave [13]. This calculation is extensive and difficult. Furthermore, the width of the regions CD and EF are small compared to DE in our experimental set up {slit width (6 mm) and the crystal thickness $(0 - 700 \ \mu m)$}. In the first approximation, one can assume that the integrated intensity linearly decreases in the regions CD and EF from the plane wave type solution to zero as shown as in Fig. 2.10. Here the plane wave type solution is normalized to 1. The total integrated intensity is given by the area of trapezoid C'D'E'F' which is equal to W_i (constant for a particular slit width and a particular reflection).

The other correction for the experimental situation is due to the variation in thickness across the width of the slit. The average variation is about 10 μm. This correction can be made by averaging the integrated intensity over the variation in thickness across the slit. The experimental results are compared with the theoretical results and shown in Fig. 2.11. The normalization factor for the theoretical curve was calculated by equating the area under the experimental and theoretical curves. The experimental results agree rather well with the dynamical theory prediction.

The asymmetric reflection results are tabulated in Table 2.1. The period of oscillations calculated experimentally agree very well with the theoretical predictions.

In the extreme asymmetric cases, the conventional dynamical theory starts to fail. The detailed calculation in these cases are given in the next chapter.
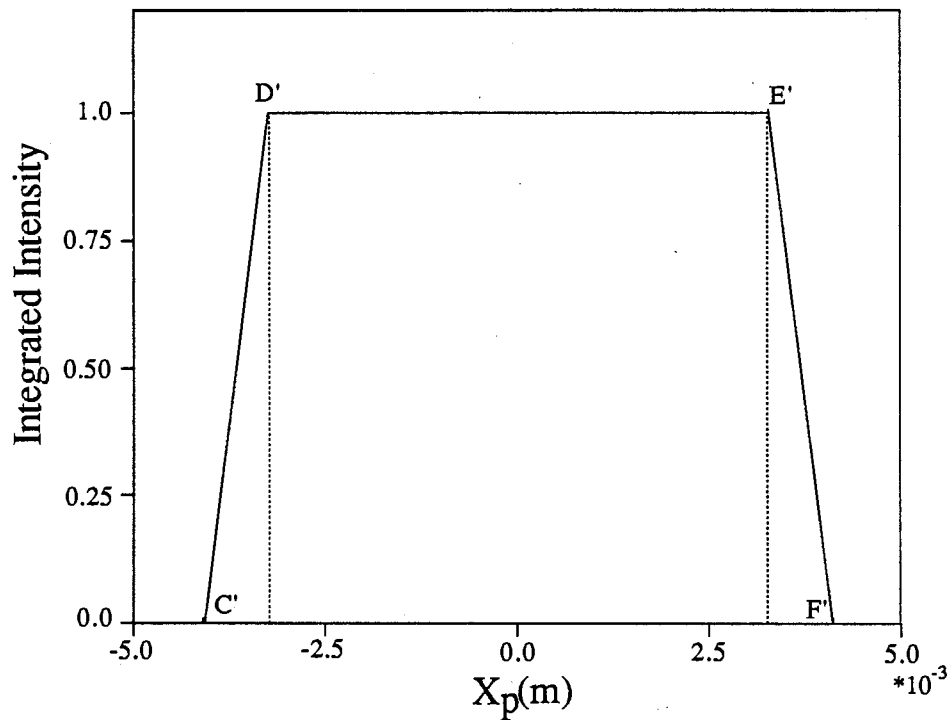
Figure 2.10:- This diagram illustrates the integrated intensity as a function of position at the exit surface of the crystal. The integrated intensity in the segment DE (plane wave type solution) is normalized to 1.

Table 2.1:- Comparison of experimental and theoretical results.

Reflection (111) cut wafers	α (deg.)	Period of oscillation (μm)	
		Theory	Experiment
($4\overline{2}\overline{2}$)(symmetric Laue case)	0	73.6	72.2 ± 0.3
($3\overline{1}\overline{1}$)(asymmetric Laue case)	10.025	120.6	119.5 ± 0.5
($1\overline{1}\overline{1}$) (" ")	19.471	123.6	124.8 ± 0.6
(400) (" ")	35.264	58.3	57.2 ± 0.3
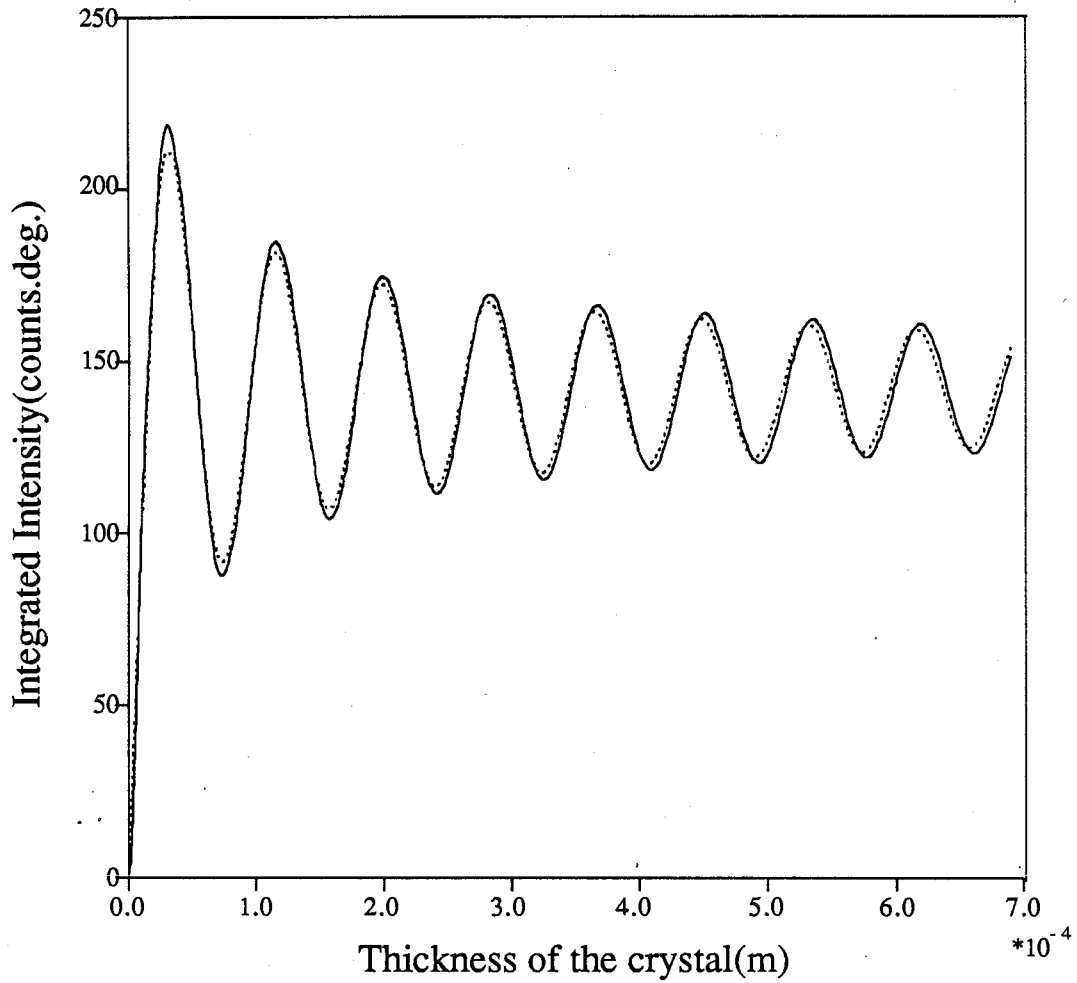
Figure 2.11:- Integrated intensity versus thickness of the crystal for (400) symmetric Laue
transmission geometry. The solid line represents the fitted experimental
curve (see Fig. 2.8) with the theory including the correction for the thickness
variation across the width of the slit. The dotted line is the theory
normalized to the experimental values.

CHAPTER 3
EXTENDED THEORY OF DIFFRACTION

3.1   Introduction

The conventional dynamical theory of neutron diffraction, which works very well in both symmetric and non extreme asymmetric Laue and Bragg cases, is not valid in extreme asymmetric cases of Laue and Bragg geometries. In the conventional theory, the dispersion surface is approximated to hyperboloids and the asymptotes of the dispersion surfaces are straight lines. In general, the dispersion surface is described by an equation of the fourth order. This fourth order equation can be reduced to a second order equation in symmetric and non extreme asymmetric Laue and Bragg cases, because the distance between the Laue point and only two of the four tie points is small. Therefore, only the wave field corresponding to these two tie points have considerable amplitudes and only they have to be known accurately. Note that the wave field corresponding to each tie point consists of two waves, one in the incident direction and the other in the diffracted direction. However, in the extreme asymmetric cases, the distance between the Laue point and at least three tie points is small and three wave fields associated with these three tie points become important. In addition, there are four waves appearing out side the crystal (besides the incident wave) instead of two in the symmetric and non extreme asymmetric cases. They are the transmitted wave, the Bragg diffracted wave and the mirror reflections of the incident and of the diffracted wave (specular reflected wave and specular diffracted wave).

There are four possible extreme asymmetric cases, depending on which beam (incident or diffracted beam) makes a small angle with the crystal surface and whether the geometry is Laue or Bragg. These extreme asymmetric cases of x-ray diffraction were studied extensively using some approximations by different groups. Kishino and Kohra [14], Brümmer et. al. [15, 16] and Zeilinger and Beatty [17] treated an extreme asymmetric

Bragg case in which the angle between the incident beam and the crystal surface is small. Kishino [18] and Benyńska [19] investigated the Bragg case with a small angle between the crystal surface and their diffracted beam. The diffraction patterns in extremely asymmetric Laue cases were studied in the papers by Kishino et. al. [20], Benyńska [19,21] and Härtwig [22,23].

In this chapter, four extreme asymmetric cases of neutron diffraction are investigated. In these cases, at most three tie points are close to the Laue point. One tie point is always far away from the Laue point. Therefore one can use the asymptotic value for the wave vector corresponding to this tie point. In addition, the amplitudes of the internal wave field associated with this tie point are extremely small. With this assumption, we can reduce the fourth order equation of dispersion to a cubic equation. The solution of a cubic equation is straight forward. The solutions of this cubic equation will give accurate values of the wave vectors associated with the three tie points. Furthermore, either the specular reflected wave or the specular diffracted wave will have a considerable amplitude in the extreme asymmetric cases depending on which beam, either the incident beam or the diffracted beam makes, a small angle with the crystal surface. The unknown internal and external wave amplitudes can be calculated by applying the boundary conditions at the upper and lower surfaces of the crystal. The results are discussed in this chapter in great detail for all extreme asymmetric cases. The results are also compared with the conventional theory.

3.2 Theoretical formulation

We consider the diffraction geometry schematically shown in Fig. 3.1, for the Laue case. Diffraction takes place from the lattice planes (hkl) making an angle α with the inward crystal normal. In this particular case, the angle between the incident beam and the crystal surface is small (comparable to the critical angle of specular reflection θ_c). Note that, theoretically one can obtain the other extreme asymmetric cases by changing the value
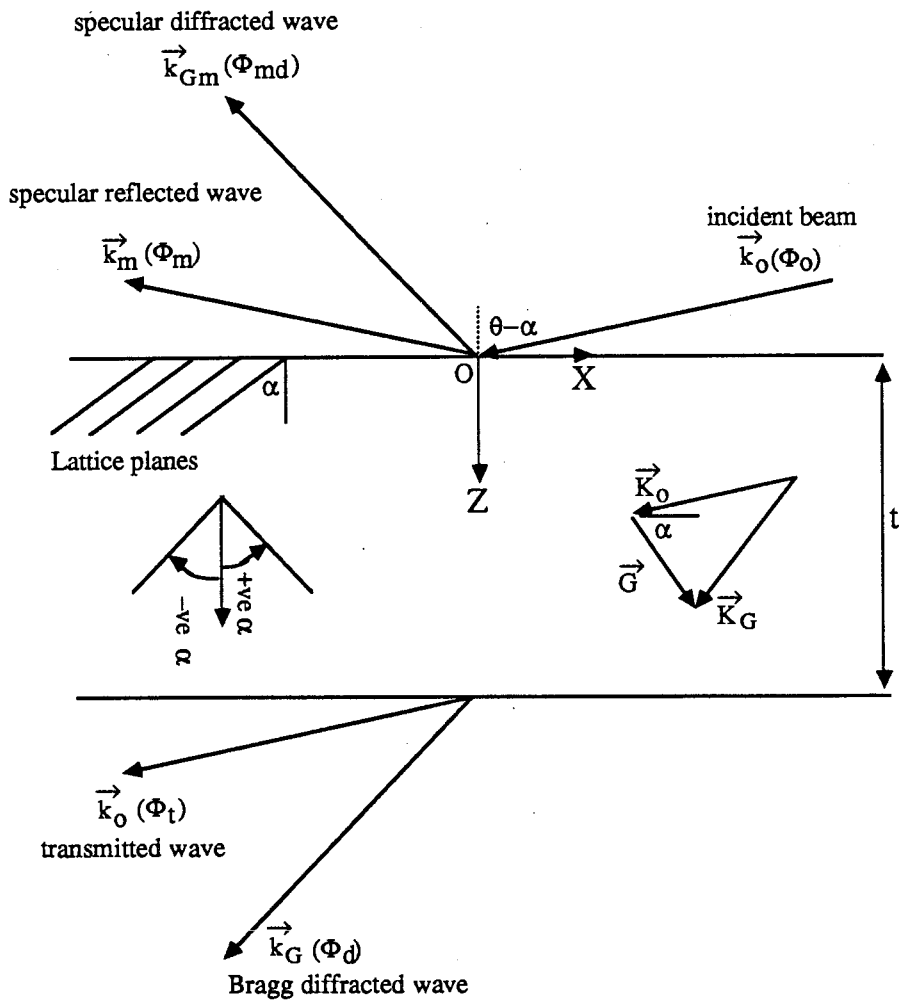
Figure 3.1: A schematic representation of the extreme asymmetric Laue case in which the angle between the incident beam and the crystal surface is small. $\Phi_0(\vec{k_0})$, Φ_t $(\vec{k_0})$, $\Phi_d(\vec{k_G})$, $\Phi_m(\vec{k_m})$ and $\Phi_{md}(\vec{k_{Gm}})$ are the incident, transmitted, Bragg diffracted, specular reflected and specular diffracted wave amplitudes (wave vectors) respectively. The thickness of the crystal is t.

of α. The dispersion surface corresponding to this extreme asymmetric Laue case is shown in Fig. 1.7 (see chapter 1). The fourth order dispersion relation

$$(K_{oz} - K_{oz}^{*A})\,(K_{oz} - K_{oz}^{*B})\,(K_{oz} - K_{oz}^{*C})\,(K_{oz} - K_{oz}^{*D}) = v_G v_{-G} \qquad (3.1)$$

can be approximated to the cubic equation of the form

$$(K_{oz} - K_{oz}^{*A})\,(K_{oz} - K_{oz}^{*B})\,(K_{oz} - K_{oz}^{*C}) \approx \frac{v_G v_{-G}}{(K_{oz}^{*C} - K_{oz}^{*D})}, \qquad (3.2)$$

where K_{oz}^{*A}, K_{oz}^{*B}, K_{oz}^{*C} and K_{oz}^{*D} are given by eqs. (1.22). Here, the tie points A, B and C are closer to the Laue point and the tie point D is far away from the Laue Point. Note that the values of K_{oz}^{*A}, K_{oz}^{*B} and K_{oz}^{*C} are nearly equal to each other. The right hand side of the eq. (3.2) was obtained by replacing K_{oz} by K_{oz}^{*C} (in the term $(K_{oz} - K_{oz}^{*D})$ of eq. (3.1)) rather than K_{oz}^{*A} or K_{oz}^{*B} because $(K_{oz}^{*C} - K_{oz}^{*D})$ will yield the simplest form. The solutions of the eq. (3.2) $K_{oz}^{A,B,C}$ together with $K_{ox}^{A,B,C} = k_{ox}$ determine the internal wave vectors corresponding to the tie points A, B and C. The fourth internal wave vector corresponding to the tie point D can be approximated by the asymptotic values, i.e. ($K_{oz}^{D} = K_{oz}^{*D}$, $K_{ox}^{D} = k_{ox}$).

The total wave inside the crystal consists of the coherent superposition of eight plane waves and is given by eq. (1.21). Waves in the vacuum (outside the crystal) are represented as

$$\Psi_U(\vec{r}) = \Phi_0\, e^{i\,\vec{k_o}\cdot\vec{r}} + \Phi_m\, e^{i\,\vec{k_m}\cdot\vec{r}} + \Phi_{md}\, e^{i\,\vec{k_{Gm}}\cdot\vec{r}} \qquad (3.3a)$$

and

$$\Psi_L(\vec{r}) = \Phi_t\, e^{i\,\vec{k_o}\cdot\vec{r}} + \Phi_d\, e^{i\,\vec{k_G}\cdot\vec{r}} \qquad (3.3b)$$

at the upper and lower surfaces of the crystal. The wave vectors of the vacuum waves (transmitted, Bragg diffracted, specular reflected and specular diffracted waves) are calculated in chapter 1 and are given by eqs. (1.5) and (1.8).

3.3 Boundary conditions

Waves in the vacuum and in the crystal must satisfy the following two boundary conditions at the boundaries of the crystal. The boundary conditions are continuity of the waves and continuity of the gradients of the waves normal to the surface. By applying these boundary conditions at the upper surface of the crystal, one obtains

$$\Phi_o + \Phi_m = \sum_{j=A,B,C,D} \Psi_o^j \quad , \tag{3.4a}$$

$$\Phi_{md} = \sum_{j=A,B,C,D} \Psi_G^j \quad , \tag{3.4b}$$

$$k_{oz}\Phi_o + k_{mz}\Phi_m = \sum_{j=A,B,C,D} K_{oz}^j \Psi_o^j \tag{3.4c}$$

and

$$k_{Gmz}\Phi_{md} = \sum_{j=A,B,C,D} K_{Gz}^j \Psi_G^j . \tag{3.4d}$$

At the lower surface of the crystal, one obtains

$$\Phi_t e^{ik_{oz}t} = \sum_{j=A,B,C,D} \Psi_o^j e^{iK_{oz}^j t} \quad , \tag{3.5a}$$

$$\Phi_d e^{ik_{Gz}t} = \sum_{j=A,B,C,D} \Psi_G^j e^{iK_{Gz}^j t} \, , \qquad (3.5b)$$

$$k_{oz}\Phi_t e^{ik_{oz}t} = \sum_{j=A,B,C,D} K_{oz}^j \Psi_o^j e^{iK_{oz}^j t} \qquad (3.5c)$$

and

$$k_{Gz}\Phi_d e^{ik_{Gz}t} = \sum_{j=A,B,C,D} K_{Gz}^j \Psi_G^j e^{iK_{Gz}^j t} \, . \qquad (3.5d)$$

Here $\vec{K}_G = \vec{K}_o + \vec{G}$.

In addition we know the ratio of internal wave amplitudes from eq. (1.18a), i.e.

$$\frac{\Psi_o^j}{\Psi_G^j} = \frac{v_{-G}}{(k_{oz}^2 - v_o - K_{oz}^{j\,2})} \qquad (3.6)$$

where $j \equiv$ A, B, C, D

From eqs. (3.4), (3.5) and (3.6), it is possible to calculate the amplitudes of all the waves present inside and outside the crystal. For the geometry as shown in Fig. 3.1, we can neglect the amplitudes (Ψ_o^D and Ψ_G^D) of the internal wave field associated with the tie point D and the amplitude of the specular diffracted wave Φ_{md}. For simplicity we will take them to be zero. In this particular geometry, the z component of the incident wave vector (k_{oz}) is small. In addition, the difference between the z component of the internal wave vectors $K_{oz}^{A,B,C}$ (corresponding to the internal waves in the incident direction) and k_{oz} is comparable to the value of k_{oz}. However, the values of $K_{Gz}^{A,B,C}$ are approximately equal to k_{Gz} (z component of the Bragg diffracted wave vector) and to $|k_{Gmz}|$. Under these conditions, the eqs. (3.4d) and (3.5d) become equivalent (approximately) to the eqs. (3.4b) and (3.5b) respectively. Using the equations (3.4a, b, c), (3.5a, b, c) and (3.6), one can

calculate the internal and the external wave amplitudes. (note:- In applying the boundary conditions at the upper surface of the crystal, some internal wave fields corresponding to different tie points can be excluded depending on the experimental situation. For example if the width of the incident beam is narrow and the thickness of the crystal is large enough, the incident wave will not interfere with the waves diffracted at the lower surface of the crystal. Under these conditions, one can exclude the internal wave fields corresponding to the tie points B and D in applying the boundary conditions at the upper surface of the crystal.) We also calculate the intensity of the various waves present outside the crystal in the four extreme asymmetric cases. We extract the different regions from the dispersion surface and corresponding intensity profiles are analyzed. In order to visualize the problem geometrically, we keep the energy of the incident beam constant (k_O is constant). We study the intensity profile only as a function of incident angle. If we also vary the value of k_O, we will get a series of dispersion surfaces. This will make the problem more difficult. Furthermore, we cannot find a single variable (some function of k_O and $\theta-\alpha$) which better describes the intensity profiles, as we found in the conventional theory of diffraction. Here, most of the results are obtained using numerical calculations.

3.4   The extreme cases

3.4.1   Extreme asymmetric Laue case where the angle between the incident beam and the crystal surface is small

In this extreme asymmetric case, there are two possible situations. They are illustrated in Fig. 3.2(a) and (b). In the first situation, we distinguish two different angular ranges of diffraction. In the region 1, the surface normal n_1 intersects the dispersion surface in four real points. The tie points C_1 and D_1 lie on the α-branch while the other two tie points A_1 and B_1 lie on the β-branch. The tie point D_1 is not shown in Fig. 3.2(a) because it is far away from the Laue point L. In the region 2, only two tie points C_2 and

D_2 lie in the real k-space (both lie on the α-branch), i.e. the internal wave vectors corresponding to the tie points A and B are complex. This is the range for total external reflection. The border of these two regions lies at $(\theta_B + \Delta\theta - \alpha) = 90 - \theta_C$, where θ_C is the critical angle of the total external reflection. The approximate condition for the criticality can be written as (see Fig. 3.3)

$$k_{ox} \geq \sqrt{k_o^2 - v_o}$$

i.e.
$$k_{ox}^2 \geq k_{ox}^2 + k_{oz}^2 - v_o$$

$$k_{oz}^2 \leq v_o$$

$$k_o^2 \cos^2(\theta_B + \Delta\theta - \alpha) \leq v_o \qquad (3.7)$$

This condition was obtained by using the asymptotic forms of the dispersion surfaces only. From eq. (3.7) we will get,

$$(\Delta\theta)_{app}^{cL} = \cos^{-1}\left(\frac{\sqrt{v_o}}{k_o}\right) + \alpha - \theta_B \qquad (3.8)$$

Where $(\Delta\theta)_{app}^{cL}$ is the approximate misset angle corresponding to the border of the critical region. The accurate value of the misset angle corresponding to the border of the critical region { $(\Delta\theta)_{acc}^{cL}$ } can be calculated from the fact that the wave vectors corresponding to the tie points A and B (on the β-branch) change from the real value to complex, i.e. the surface normal becomes tangent to the β-branch of the dispersion surface. The value of $(\Delta\theta)_{acc}^{cL}$ can be calculated mathematically from eq. 3.2 using the condition that all the roots

(a)

(b)
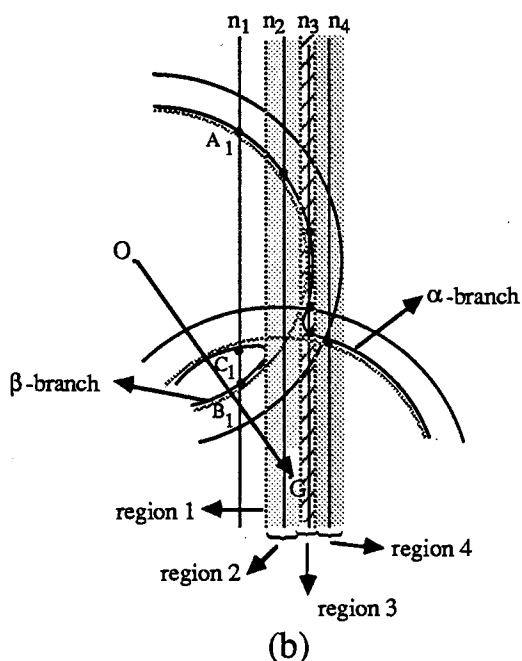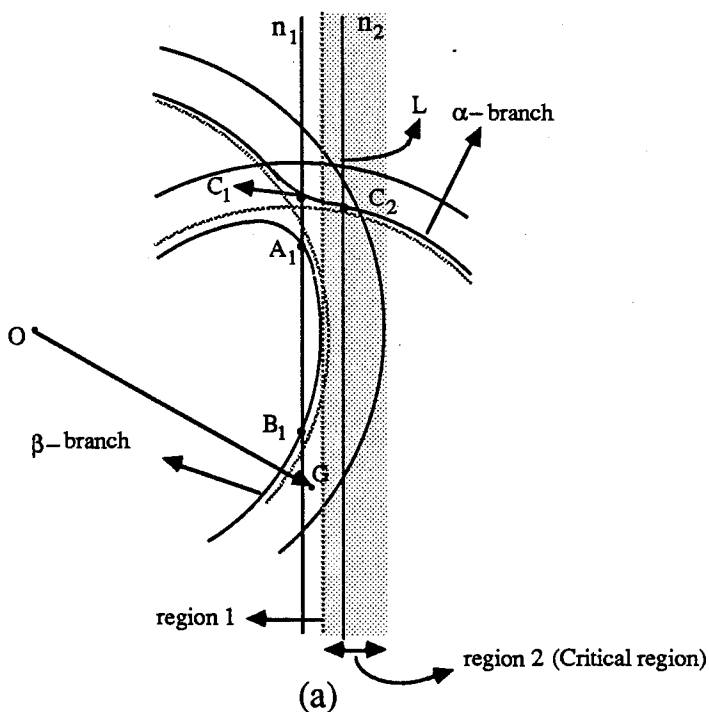
Figure 3.2: Dispersion surfaces in the extreme asymmetric Laue case in which the incident

beam makes a small angle on the crystal surface.

(a) Two distinctly different angular ranges of diffraction are observed.

(b) Four different angular ranges of diffraction are observed.

The tie point D is far away from the Laue point L and not shown in this

diagram.
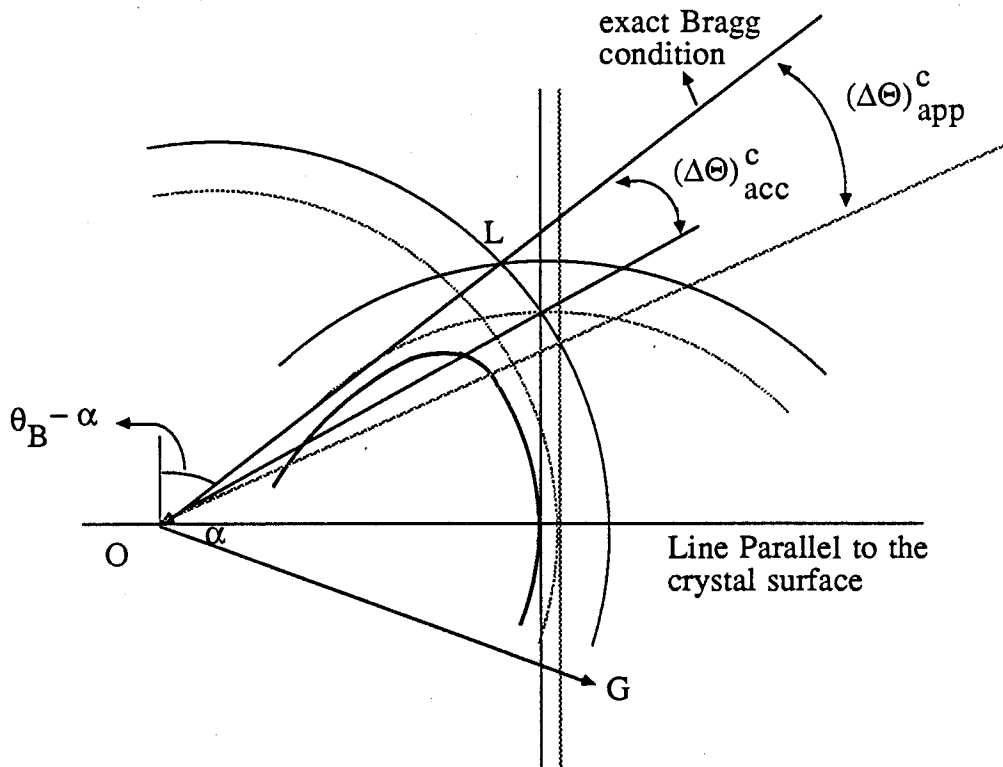
Figure 3.3: Representation of total external reflection explaining the approximate (using the asymptotic circles) and the accurate (using the β-branch of the dispersion surface) conditions.

of that cubic equation (eq. 3.2) have to be real and at least two are equal. $(\Delta\theta)^{cL}_{app}$, $(\Delta\theta)^{cL}_{acc}$ and the difference between these two values $\{(\Delta\theta)^{cL}_{app} - (\Delta\theta)^{cL}_{acc}\}$ are plotted against $(\theta_B - \alpha)$ in Fig. 3.4.

In the second situation {Fig. 3.2(b)}, we distinguish four different angular regions of diffraction. In the region 1, we excite four real tie points in a same way as in the region 1 of the first situation. In the region 2, we excite only two real tie points (both lie on the α-branch). If we decrease the angle of incidence, we are in a situation such that the surface normal n_3 again cut the dispersion surface in four real points (region 3). These four tie points are now arranged on the α-branch of the dispersion surface. We excite only two real tie points in the region 4.

In Fig. 3.2(b), the incident beam corresponding to the exact Bragg condition would have to be inside the crystal, i.e. $\theta_B - \alpha > 90°$. However, the incident beams which produce the four different angular ranges of diffraction {see Fig. 3.2(b)} have finite misset angles and can be outside the crystal surface, making small angles with the crystal surface. It is clear that these two situations {Fig. 3.2(a) & (b)} are well separated by a condition in which the surface normal becomes tangent to the α-branch of the dispersion surface at the inflection point of that branch. For a particular value of G, this condition is determined by the values of k_o and α, i.e. if we fixed the orientation of the reflecting planes with respect to the inward surface normal (α), the condition will occur at a particular value of k_o (k_o^L) or if we fixed k_o, the condition will occur at a particular value of α (α_T^L). Note that this condition occurs only when $\theta_B - \alpha > 90°$. We will get either the first or the second situation depending upon the value of k_o (α) which is slightly greater than or less than k_o^L (α_T^L) for the fixed values of α (k_o) and G.

In this particular extreme asymmetric case, the amplitude of the specular reflected
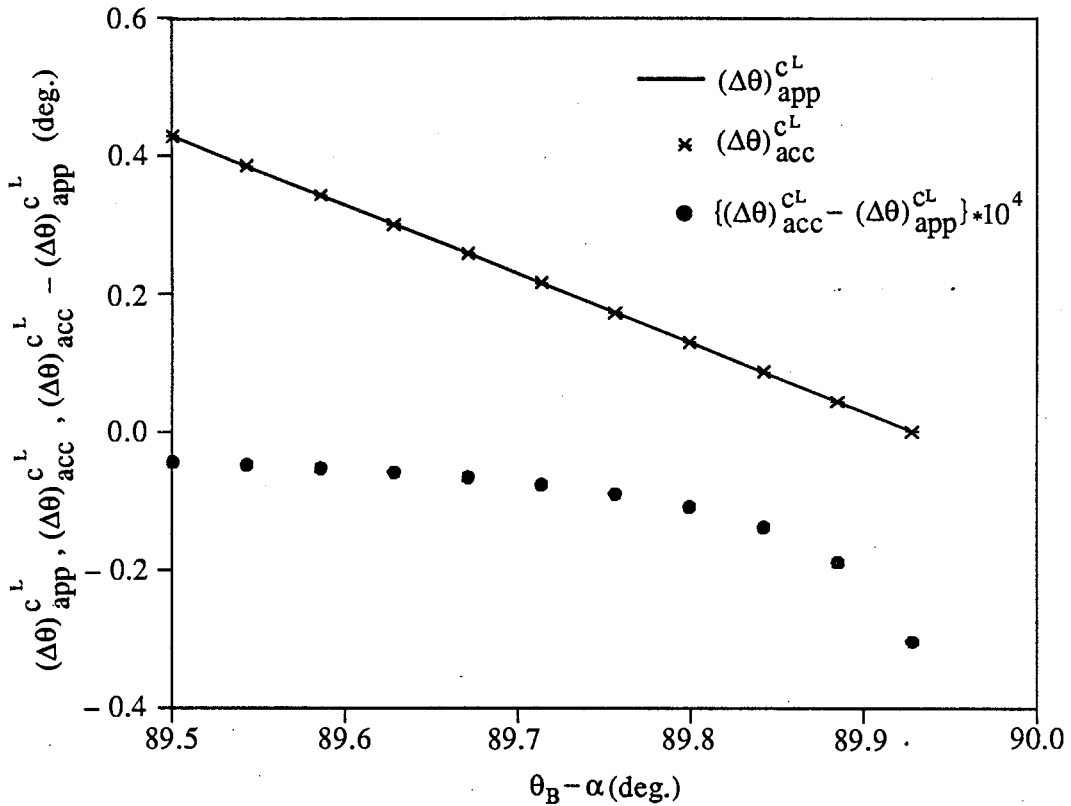
Figure 3.4: Misset angle corresponding to the border of the critical region calculated using the approximate condition [$(\Delta\theta)^{c_L}_{app}$], the accurate condition [$(\Delta\theta)^{c_L}_{acc}$] and the difference $\{(\Delta\theta)^{c_L}_{app} - (\Delta\theta)^{c_L}_{acc}\}$ (x10^4) for different values of (θ_B - α). Here we keep the external Bragg angle θ_B corresponding to the (220) Si reflection a constant and rotate the reflecting planes with respect to the inward crystal surface normal (allowing the value of α to change). This corresponds to recutting the crystal, but that is an experimental difficulty that we overlook here where we are free to change the value of α.

wave has a considerable value. As we mentioned earlier, one can neglect the amplitudes of the internal wave field associated with the tie point D and the amplitude of the specular diffracted wave in this case. With these assumptions, we have calculated the intensity of the Bragg diffracted wave (at the lower surface of the crystal) and of the specular reflected wave (at the upper surface of the crystal) numerically using the eqs. (3.2), (3.4a, b and c), (3.5a, b and c) and (3.6) as a function of misset angle in both situations. The results obtained for the first situation are shown in Fig. 3.5(a) and (b). Figures 3.5(c) and (d) show the results of the second situation. The numerical calculations are made for the (220) Si reflection. The wavelength of the incoming neutrons is $1.57A^{\circ}$. In the first situation, the Bragg reflecting atomic planes make an angle α with the inward surface normal which satisfies $(\theta_B - \alpha) = 89.90^{\circ}$. In the second situation, $(\theta_B - \alpha) = 90.10^{\circ}$. The width of the region 2 in the second situation is too small to show in Fig. 3.5(c) and (d). The intensity of the Bragg diffracted wave at the lower surface of the crystal is compared with the results obtained from the conventional treatment. From Fig. 3.5(a) and (c), it is obvious that the diffraction occurs even at an angle comparable to the critical angle of total external reflection, although it is weak in intensity. Here specular reflection occurs simultaneously and its intensity increases rapidly as the incident angle approaches the condition for the total external reflection.

We also calculated the value of the deviation from the Bragg law (angle between the position of maximum of the diffracted intensity and the geometrical exact Bragg position for the incident beam) and the full width at half maximum (FWHM) of the envelope of the diffraction pattern using numerical calculations. For the extreme asymmetric Bragg cases, Rustichelli [24] has derived expressions for the deviation from the Bragg law and for the width of the Darwin plateau of the diffraction patterns which are more precise than the conventional expressions. One could modify these expressions for the extreme asymmetric Laue cases. In deriving these expressions, the asymptotic forms of the dispersion surface
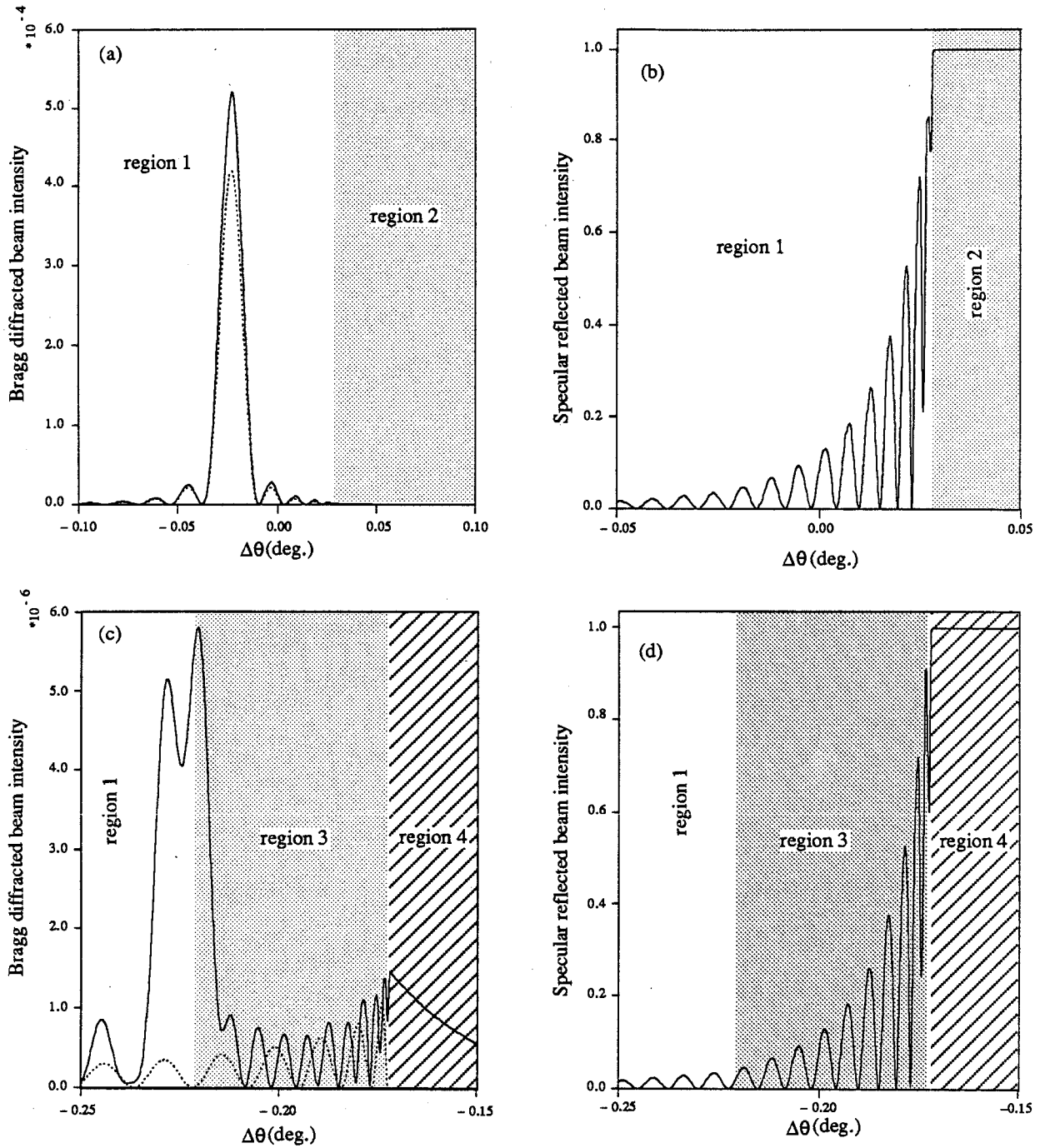
Figure 3.5: Intensities of the Bragg diffracted wave at the exit surface {(a) and (c)} and of the specular reflected wave at the entrance surface {(b) and (d)} of the crystal as a function of misset angle ($\Delta\theta$) for the situations illustrated in Fig. 3.2(a) [$(\theta_B - \alpha) = 89.9°$] and (b)[$(\theta_B - \alpha) = 90.1°$] respectively. In both situations λ =1.57A° and t = 0.5μm. The dotted line shows the intensity of the Bragg diffracted wave estimated using the conventional theory.

and the incidence circle are actual circles and not straight lines as in the conventional theory. The expressions for the deviation from the Bragg law $\Delta\theta_i^{acc}$ and for the FWHM of the envelope of the diffraction pattern $\Delta\theta_w^{acc}$ are

$$\Delta\theta_i^{acc} = \frac{\gamma_1 - \sqrt{\gamma_1^2 - \frac{v_O}{k_O^2 \sin 2\theta_B}\gamma_1\left(1 - \frac{\gamma_2}{\gamma_1}\right)\sqrt{1 - \gamma_1^2}}}{\sqrt{1 - \gamma_1^2}} \qquad (3.9a)$$

and

$$\Delta\theta_w^{acc} = \frac{\gamma_1}{\sqrt{\gamma_1^2 - \frac{v_O}{k_O^2 \sin 2\theta_B}\gamma_1\left(1 - \frac{\gamma_2}{\gamma_1}\right)\sqrt{1 - \gamma_1^2}}} \cdot \frac{2 v_G}{k_O^2 \sin 2\theta_B}\sqrt{\frac{\gamma_2}{\gamma_1}}, \qquad (3.9b)$$

where $\gamma_1 = \cos(\theta_B - \alpha)$ and $\gamma_2 = \cos(\theta_B + \alpha)$ (see appendix 5).

These results are compared with the conventional theory predictions, according to which, the deviation from the Bragg law ($\Delta\theta_i^c$) and FWHM of the Lorentzian envelope ($\Delta\theta_w^c$) are given by the following formulas:

$$\Delta\theta_i^c = \frac{v_O}{k_O^2 \sin 2\theta_B}\left(1 - \frac{\gamma_2}{\gamma_1}\right) \qquad (3.10a)$$

and

$$\Delta\theta_w^c = \frac{2 v_G}{k_O^2 \sin 2\theta_B}\sqrt{\frac{\gamma_2}{\gamma_1}}. \qquad (3.10b)$$

When $\gamma_1 \to 0$ (incident angle $(\theta_B - \alpha) \to 90°$), conventional expressions give $\Delta\theta_i^c \to -\infty$

and $\Delta\theta_w^c \to \infty.$ Rustichelli's modified expressions give $\Delta\theta_i^{acc} \to -\sqrt{\dfrac{v_0}{k_0^2}}$ and

$\Delta\theta_w^{acc} \to 0$ as $\gamma_1 \to 0$. We see that the conventional expressions start to fail as γ_1

approaches to zero. Results obtained from these three approaches are graphically shown in

Figs. 3.6(A) and (B). The numerical values calculated using the present theory (extended

theory) agree with Rustichelli's curves representing the deviation from the Bragg law and

the FWHM of the envelope of the diffraction pattern.

3.4.2   *Extreme asymmetric Laue case where the angle between the Bragg diffracted beam and the crystal surface is small*

In this extreme asymmetric Laue case, it is possible to distinguish three different

angular ranges of diffraction (see Fig. 3.7). In the range 1, the surface normal n_1 intersects

the dispersion surface in four real points; C_1 and B_1 lie on the α–branch, A_1 and D_1 lie on

the β–branch. Here the tie point B_1 is far away from the Laue point L and it is not shown

in Fig. 3.7. In the range 2, only two tie points A_2 and B_2 (both on the α–branch) lie in the

real k-space. In the range 3, the tie points A_3 and B_3 lie in the real k-space. In addition,

k_{Gz} and k_{Gmz} (z components of the wave vectors of the Bragg diffracted and of the

specular diffracted waves) are purely imaginary in this region, i.e. the phenomenon of total

internal reflection of the diffracted wave occurs.

The approximate misset angle corresponding to the border of the regions 1 and 2

$[(\Delta\theta)_\beta^{app}]$ can be calculated from the following condition:

$$K_{0z}^{*C} = K_{0z}^{*D} = -G_z, \qquad \text{(see Fig 3.8)}$$

i.e. $\qquad k_{0z}^2 - v_0 - (G_x^2 + 2\,k_{0x}\,G_x) = 0$
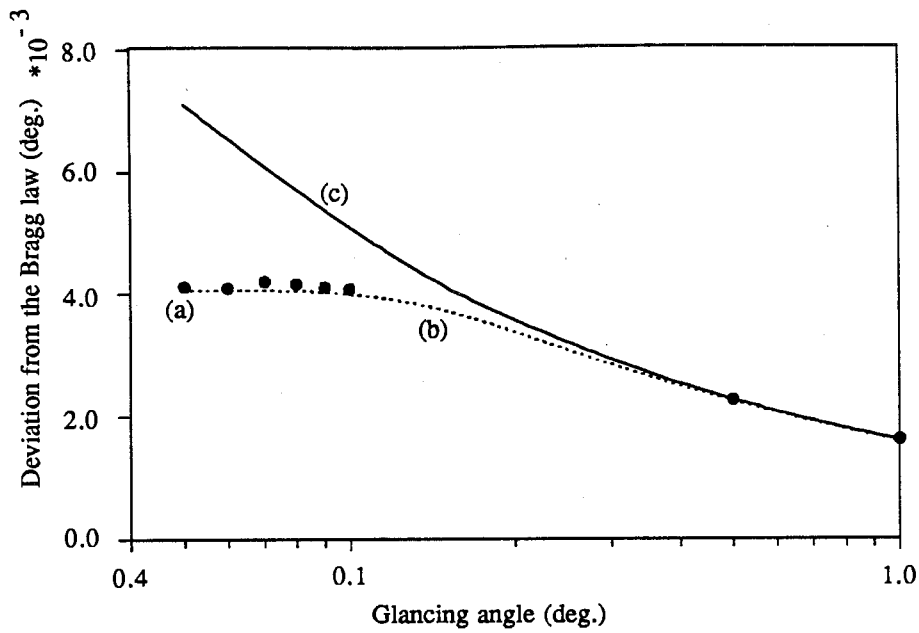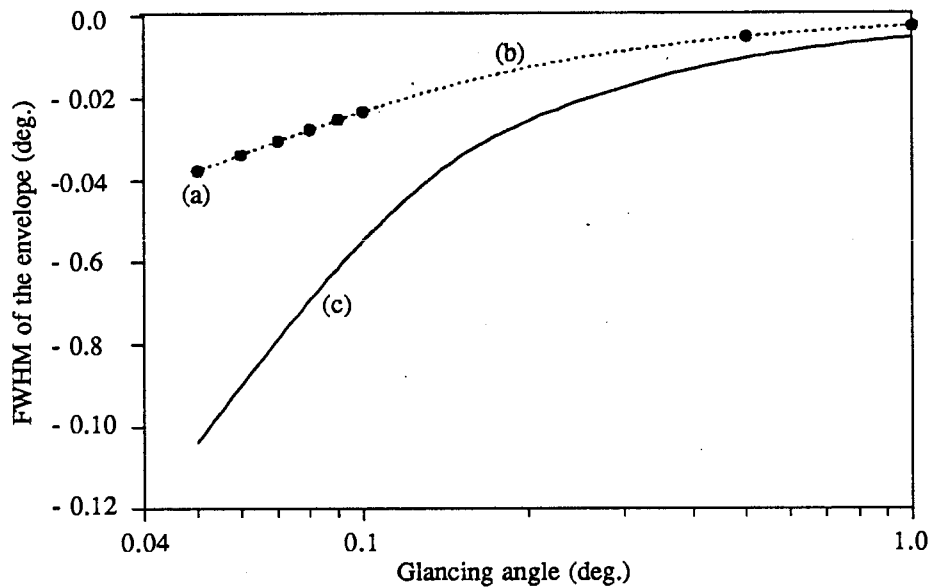
Figure 3.6: (A) The deviation from the Bragg law $\Delta\theta_1$

(B) FWHM of the envelope of the diffraction pattern
for the (220) asymmetric Si reflection as a function of glancing angle (the angle
between the crystal surface and the incident beam which satisfies the external
exact Bragg condition).

(a) according to the extended theory (●) (b) according to Rustichelli's
formulation (c) according to the conventional theory.

$$k_0^2 \cos^2(\theta - \alpha) - v_0 - 4 k_0^2 \sin^2 \theta_B \cos^2 \alpha + 2 k_0 \sin(\theta - \alpha) . 2 k_0 \sin \theta_B \cos \alpha = 0$$

$$k_0^2 - k_0^2 \sin^2(\theta - \alpha) + 4 k_0^2 \sin(\theta - \alpha) . \sin \theta_B \cos \alpha - v_0 - 4 k_0^2 \sin^2 \theta_B \cos^2 \alpha = 0$$

$$\sin^2(\theta - \alpha) - (4 \sin \theta_B \cos \alpha) \sin(\theta - \alpha) + 4 \sin^2 \theta_B \cos^2 \alpha + \frac{v_0}{k_0^2} - 1 = 0$$

$$\sin(\theta - \alpha) = 2 \sin \theta_B \cos \alpha \pm \sqrt{1 - \frac{v_0}{k_0^2}}$$

$$\sin(\theta - \alpha) = 2 \sin \theta_B \cos \alpha - \sqrt{1 - \frac{v_0}{k_0^2}} .$$

Here we eliminate the solution with (+) sign by physical considerations. The approximate misset angle is given by

$$(\Delta\theta)_\beta^{app} = \beta_1 + \alpha - \theta_B , \qquad (3.11a)$$

where $\beta_1 = \sin^{-1}\left\{ 2 \sin \theta_B \cos \alpha - \sqrt{1 - \frac{v_0}{k_0^2}} \right\} . \qquad (3.11b)$

The accurate value of misset angle corresponding to this border $(\Delta\theta)_\beta^{acc}$ can be calculated using the fact that the surface normal becomes tangent to the β–branch of the dispersion surface. Since only the tie points C, A and D are close to the Laue point in this case, one could reduce the fourth order dispersion relation to the cubic equation of the form

$$(K_{oz} - K_{oz}^{*A})(K_{oz} - K_{oz}^{*C})(K_{oz} - K_{oz}^{*D}) \approx \frac{v_G v_{-G}}{(K_{oz}^{*A} - K_{oz}^{*B})} .$$
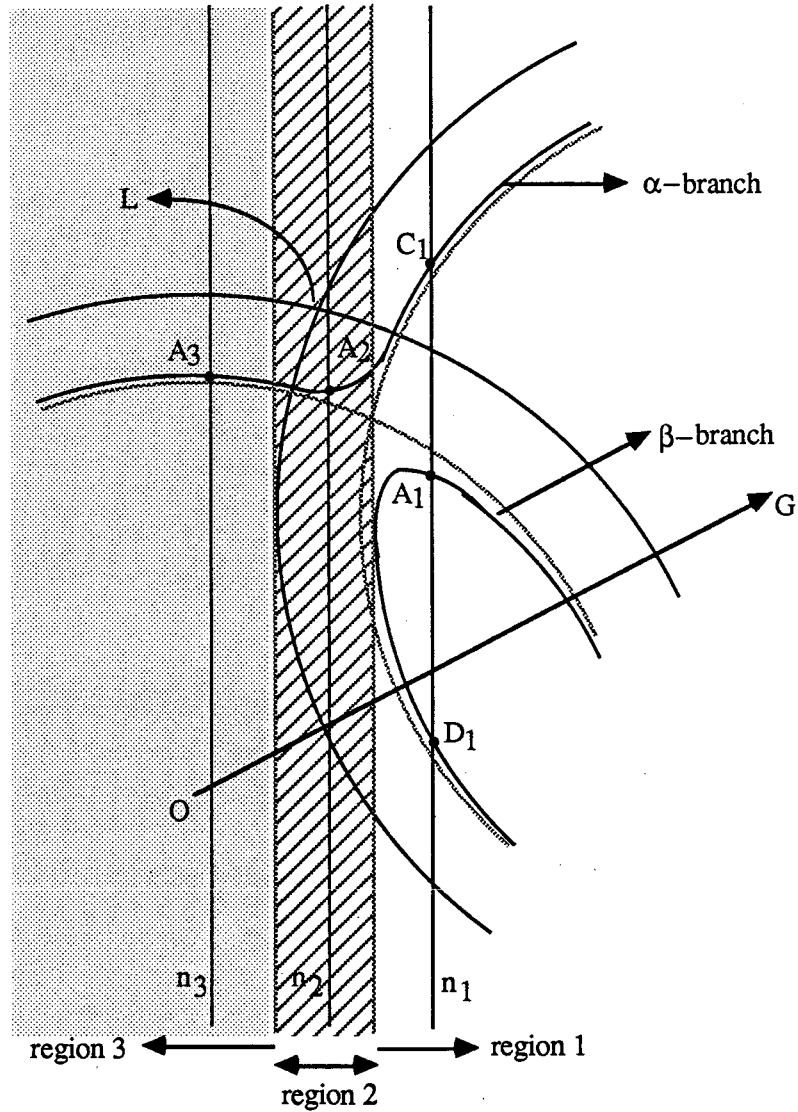
Figure 3.7: Dispersion surface in the extreme asymmetric Laue case in which the Bragg diffracted beam makes a small angle with the crystal surface. The surface normals n_1, n_2 and n_3 lie in the diffraction regions 1, 2 and 3 respectively.
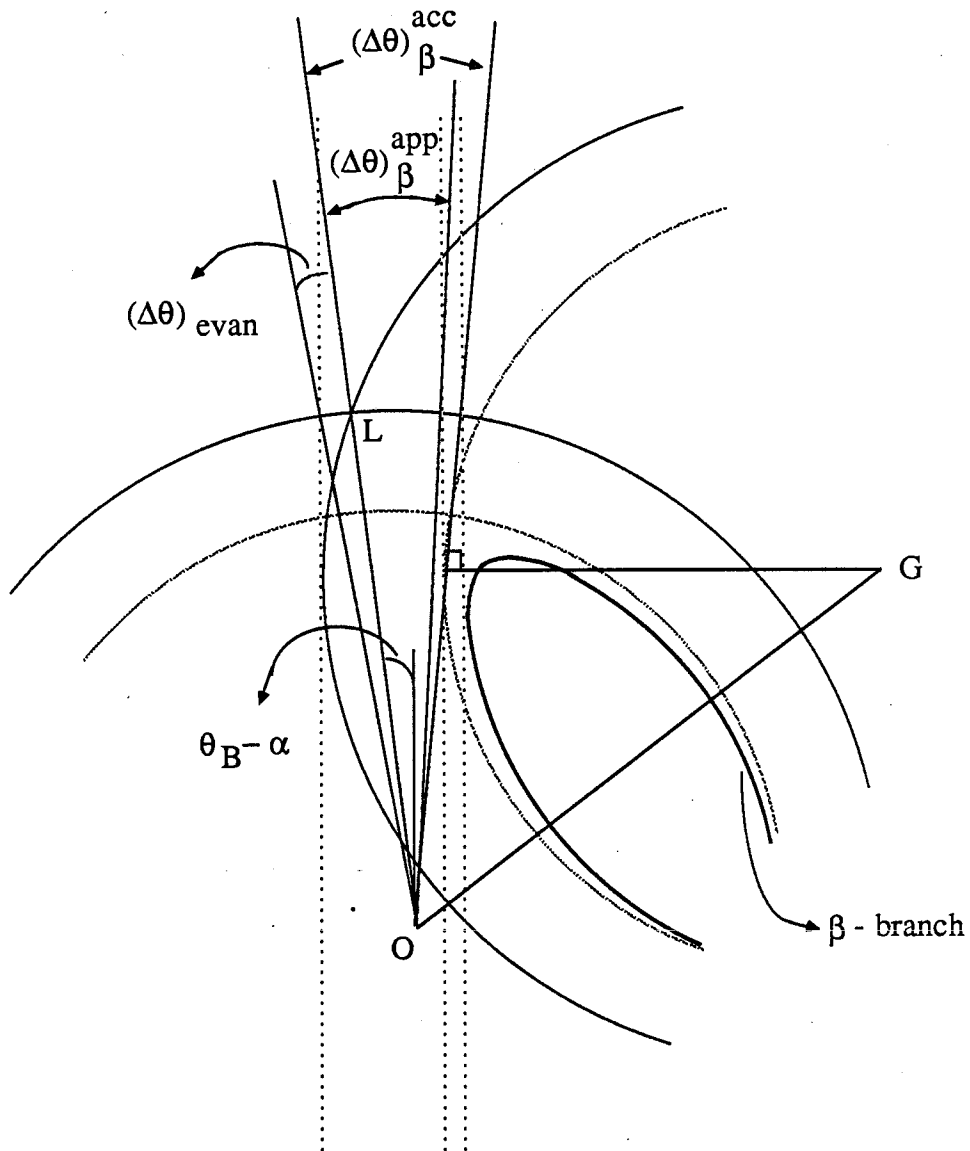
Figure 3.8: Situation explaining the formation of evanescent surface diffracted waves. The border of the regions 1 and 2 is also shown using asymptotic circles (approximate condition) and using the β-branch of the dispersion surface (accurate condition).

Mathematically the solutions of the above cubic equation are real and at least two have to be equal at the misset angle of value $(\Delta\theta)_\beta^{acc}$.

The border of the regions 2 and 3 can be calculated from the condition that the Bragg diffracted and the specular diffracted waves become evanescent (k_{Gz} and k_{Gmz} become imaginary quantities). This situation can be expressed mathematically as

$$(k_{ox} + G_x) \geq k_o , \quad \text{(see Fig. 1.3)}$$

$$\text{i.e.} \quad G \cos \alpha - k_o \sin (\theta - \alpha) \geq k_o$$

$$\Delta\theta \leq \beta_2 + \alpha - \theta_B , \tag{3.12}$$

where $\theta = \theta_B + \Delta\theta$ and $\beta_2 = \sin^{-1} (2 \sin \theta_B \cos \alpha - 1)$.

Therefore, the misset angle corresponding to the border of the regions 2 and 3 $(\Delta\theta)_{evan}$ is given by

$$(\Delta\theta)_{evan} = \beta_2 + \alpha - \theta_B \tag{3.13}$$

$(\Delta\theta)_{evan}$, $(\Delta\theta)_\beta^{app}$ and $(\Delta\theta)_\beta^{acc}$ are plotted against $(\theta_B + \alpha)$ in Fig. 3.9.

The amplitudes of the specular reflected wave and of the internal wave field associated with the tie point B are negligible in this extreme asymmetric Laue case. We will take them to be zero. However, the amplitude of the specular diffracted wave becomes large. In this extreme case, the eqs. (3.4c) and (3.5c) become equivalent (approximately) to the eqs. (3.4a) and (3.5a) respectively (Same kind of argument given for the case 1 is valid. The only difference is that the value of k_{Gz} is small instead of k_{oz} in the case 1. Therefore, one can assume that the values of $K_{oz}^{A,C,D}$ are approximately equal to k_{oz}.).
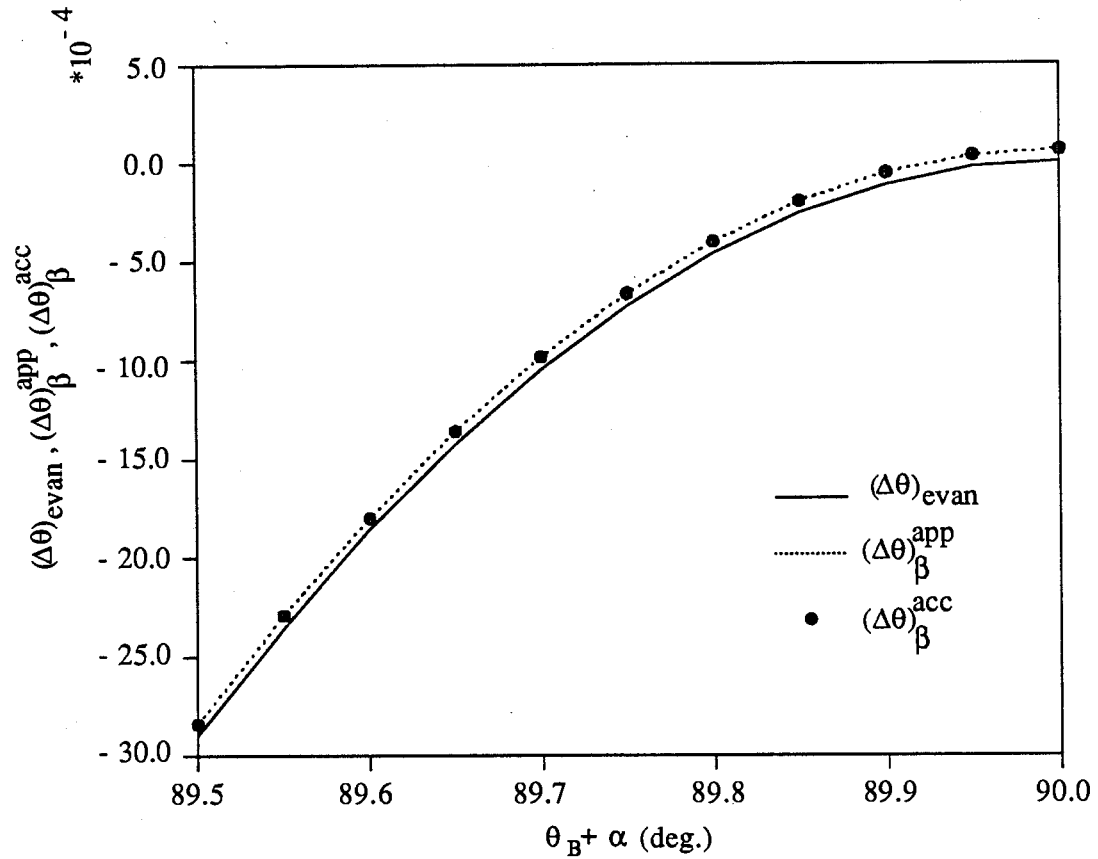
Figure 3.9: Misset angles corresponding to the formation of evanescent surface diffracted waves [$(\Delta\theta)_{evan}$] and corresponding to the border of the regions 1 and 2 calculated using the approximate condition [$(\Delta\theta)_{\beta}^{app}$] and using the accurate condition [$(\Delta\theta)_{\beta}^{acc}$] are plotted for different values of ($\theta_B + \alpha$).

Using the equations (3.4a, b, d), (3.5a, b, d) and (3.6), we have calculated all the unknown internal and external wave amplitudes. Note that the cubic equation which gives the z components of the important internal wave vectors associated with the tie points C, A and D (closer to the Laue point L) is of the form

$$(K_{OZ} - K_{OZ}^{*A})(K_{OZ} - K_{OZ}^{*C})(K_{OZ} - K_{OZ}^{*D}) \approx \frac{v_G v_{-G}}{(K_{OZ}^{*A} - K_{OZ}^{*B})} \qquad (3.14)$$

in this extreme case. The intensities of the Bragg diffracted wave (at the lower surface of the crystal) and of the specular diffracted wave (at the upper surface of the crystal) are shown in Fig. 3.10(a) and (b) as a function of misset angle. The calculations were made for the (220) Si reflection where the atomic planes make an angle α with the inward surface normal such that $(\theta_B + \alpha) = 89.75°$. In the region 3, the diffracted waves outside the crystal are propagated along the crystal surfaces because the normal component of the wave vectors are purely imaginary. Therefore the wave function of the Bragg diffracted wave at the exit surface of the crystal is of the form $\Phi_d e^{i(i.k_{Gz})t} e^{ik_{ox}x} (= \Phi_d e^{-k_{Gz}t} . e^{ik_{ox}x})$. Note that, the amplitude of this wave is equal to $\Phi_{Gd} e^{-k_{Gz}t}$. Therefore, the intensities of the diffracted waves outside the crystal are exponentially attenuated in this region as expected.

3.4.3 Extreme asymmetric Bragg case where the angle between the Bragg diffracted beam and the crystal surface is small

The dispersion surface corresponding to this extreme case is shown in Fig. 3.11. In Fig. 3.11, we distinguish five possible different angular ranges of diffraction. The surface normals are denoted by n_1, n_2, n_3, n_4 and n_5 in these five different regions. In the region 1, the surface normal n_1 intersects the dispersion surface in four real points; C_1 and B_1 lie on the α-branch, A_1 and D_1 lie on the β-branch (note that the tie point B_1 is far away from
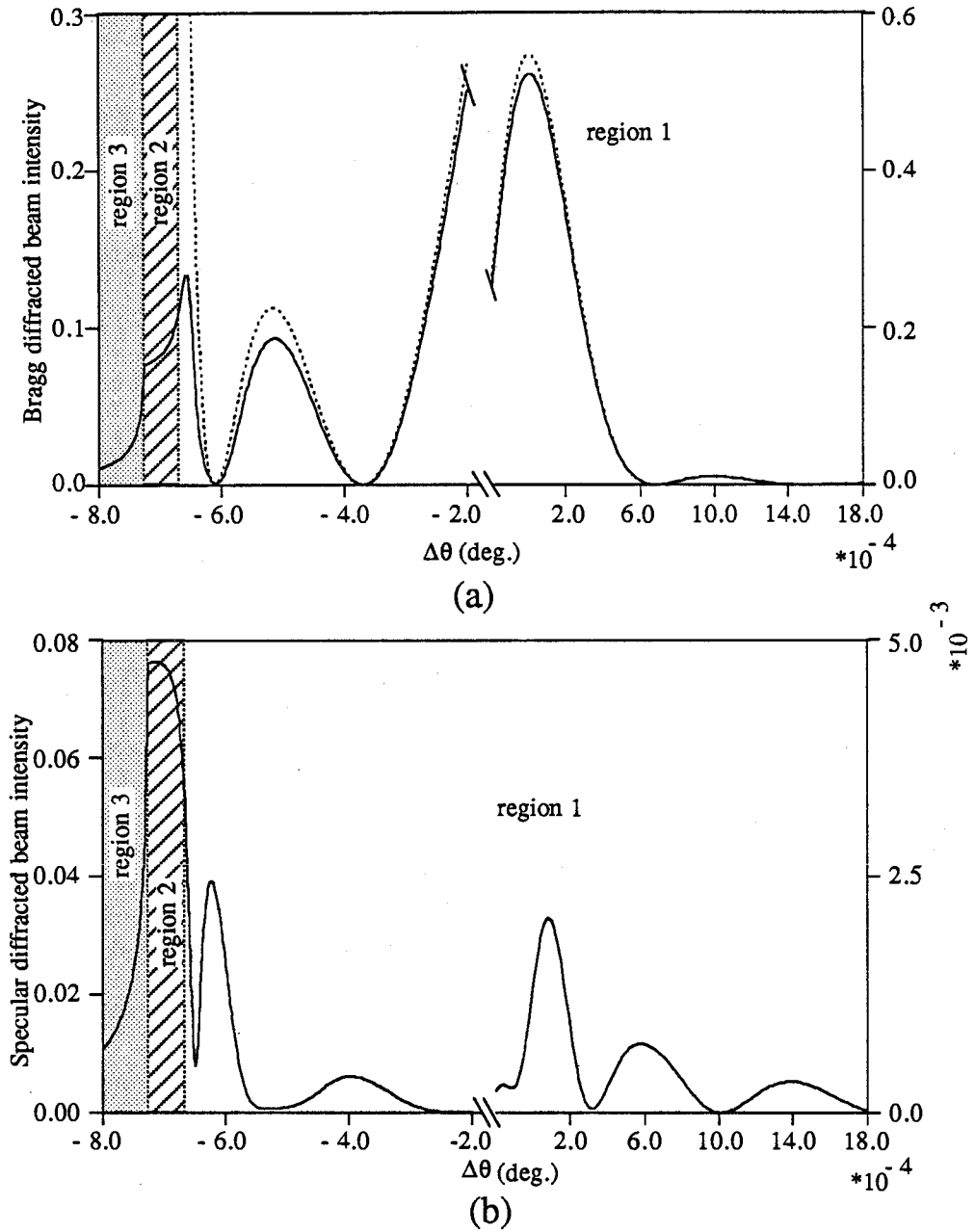
Figure 3.10: Intensity of the Bragg diffracted wave (a) and of the specular diffracted wave (b) as a function of $\Delta\theta$; $(\theta_B + \alpha) = 89.75°$, $t = 0.1\mu m$, $\Phi_0 = 1$. The dotted line shows the Bragg diffracted beam intensity estimated from the conventional theory.

the Laue point L and it is not shown in Fig. 3.11). In the region 2, the surface normal n_2 intersects the dispersion surface only at two real points C_2 and B_2 (both lie on the α-branch). Again in the region 3, the surface normal n_3 intersects the dispersion surface in four real points, but all four tie points lie on the α-branch of the dispersion surface. In the region 4, the surface normal n_4 intersects the dispersion surface only at two real points A_4 and B_4. In the region 5, the tie points A_5 and B_5 only lie in the real k-space, but the normal components of the wave vectors of the Bragg diffracted wave and of the specular diffracted wave become imaginary. Therefore the phenomenon of total internal reflection for the diffracted wave occurs.

Misset angles corresponding to the borders of the different diffraction regions are calculated and are shown in Fig. 3.12(a) and (b) as a function of $(\theta_B + \alpha)$. Misset angles corresponding to the borders of regions 1 and 2 and of regions 2 and 3 are calculated accurately using the fact that the surface normals become tangent to β-branch and α-branch of the dispersion surface respectively. These misset angles are denoted by $\Delta\theta^\beta$ and $\Delta\theta^\alpha$. Note that there are no approximate values for $\Delta\theta^\beta$ and $\Delta\theta^\alpha$ using asymptotic circles. In the region 2, the internal wave vectors corresponding to the tie points A and D are complex. The width of this region is also known as width of the Darwin plateau. The misset angle associated with the border of the regions 3 and 4 [$(\Delta\theta)_\alpha^{acc}$] is also calculated using the condition that the surface normal again becomes tangent to α-branch of the dispersion surface. The approximate value of this misset angle [$(\Delta\theta)_\alpha^{app}$] can be calculated using the asymptotic circles and is given by

$$(\Delta\theta)_\alpha^{app} = \beta_1 + \alpha - \theta_B$$

where $\beta_1 = \sin^{-1}\left\{ 2\sin\theta_B \cos\alpha - \sqrt{1 - \frac{v_o}{k_o^2}} \right\}$
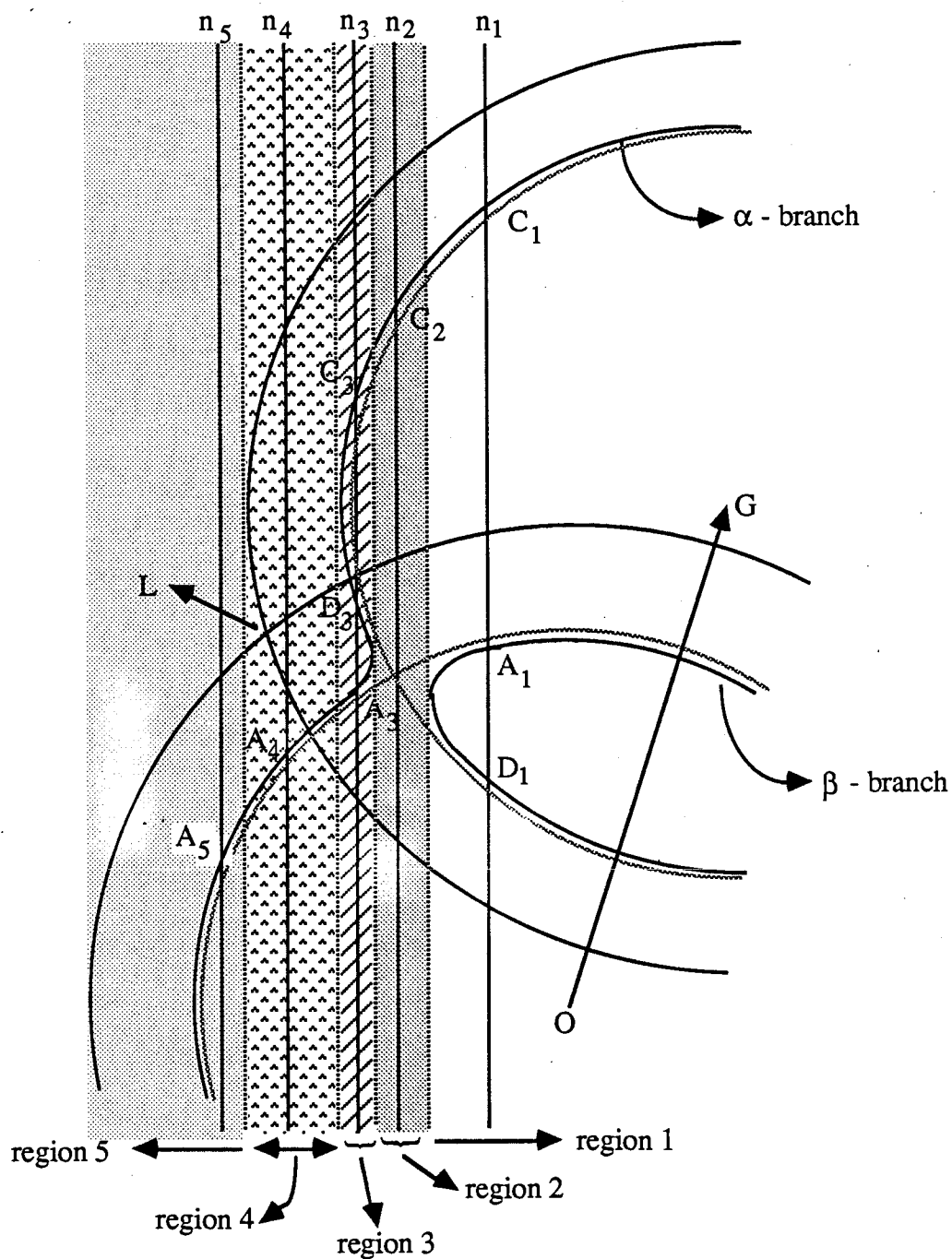
Figure 3.11: Dispersion surface in the extreme asymmetric Bragg case in which the Bragg diffracted beam makes a small angle with the crystal surface. The surface normals n_1, n_2, n_3, n_4 and n_5 lie in the diffraction regions 1, 2, 3, 4 and 5 respectively.

The misset angle corresponding to the border of the regions 4 and 5 [$(\Delta\theta)_{evan}$] is given by eq. (3.13).

As we see from Fig. 3.11, the tie points C, A and D are closer to the Laue point L and the internal wave fields corresponding to these tie points have to be taken into account. The amplitudes of the fourth internal wave field associated with the tie point B which is far away from the Laue point L, are extremely small and therefore this wave field may be neglected. Furthermore the amplitude of the specular reflected can also be neglected in this extreme case. Under these conditions, the eqs. (3.4c) and (3.5c) obtained from the boundary conditions, become equivalent (approximately) to eqs. (3.4a) and (3.5a) as for the case 2. Note that the internal wave vectors associated with the tie points C, A and D can be calculated from eq. (3.14). We have calculated the intensity of the diffracted waves present at the upper and lower surfaces of the crystal using the boundary conditions and the ratio of internal wave amplitudes. The results which covers all five different angular ranges of diffraction are shown in Fig. 3.13(a) and (b). The intensity of the Bragg diffracted wave at the entrance surface of the crystal is compared with the results obtained from the conventional treatment. The calculations were made for the (220) Si reflection in which the atomic planes make an angle α with the inward surface normal, satisfies the condition (θ_B + α) = 90.25°. The intensity of the diffracted waves outside the crystal are exponentially attenuated in the region 5 where the total internal reflection for the diffracted wave occurs.

The difference between the case 2 (section 3.4.2) and the case 3 (section 3.4.3) is the number of possible different angular ranges of diffraction. In the case 2, there are only three possible angular ranges of diffraction while there are five in the case 3. These two cases are well separated by a situation where the surface normal cuts the α-branch of the dispersion surface at four real points and three (which are closer to the Laue point L) out of four tie points have to coincide each other, i.e. the surface normal has to be tangent to the
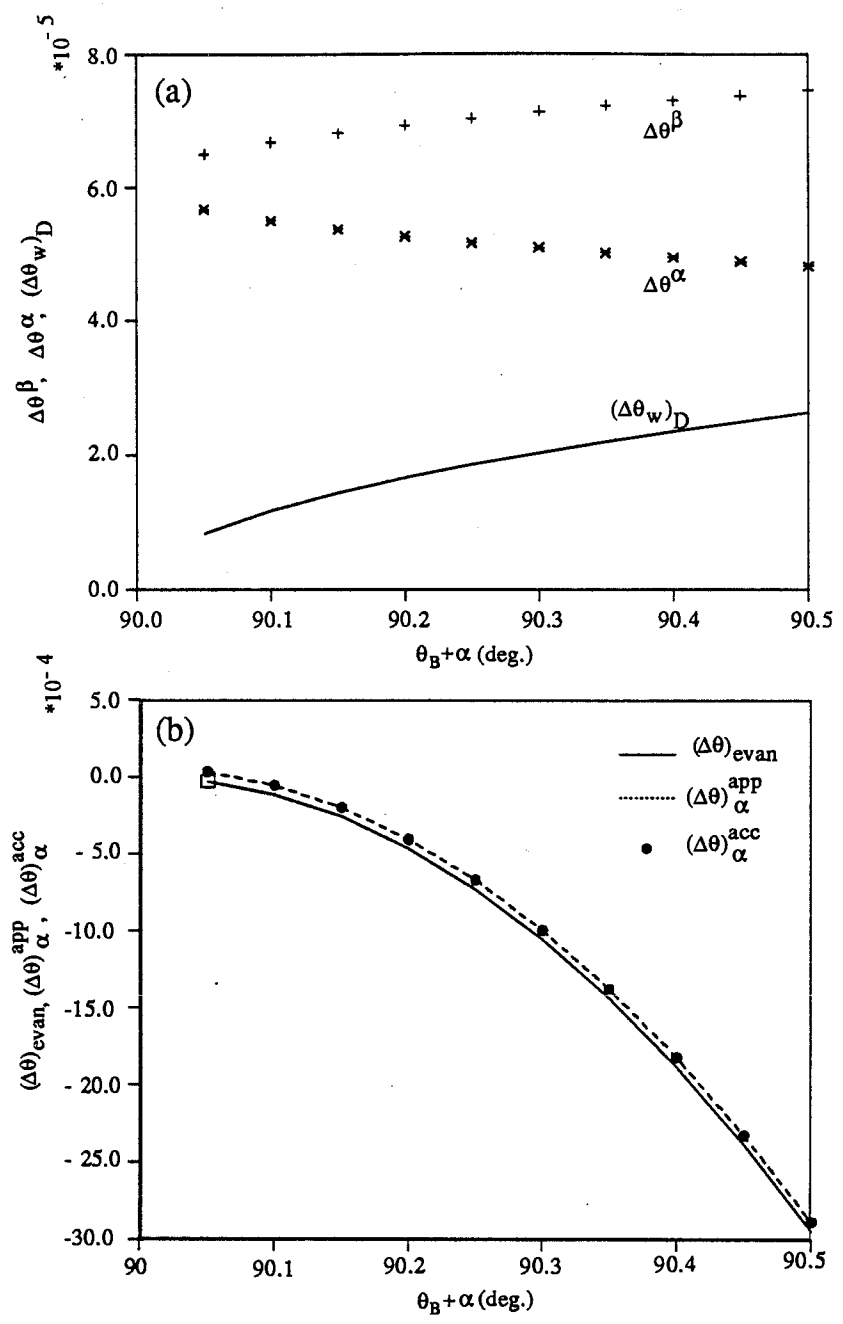
Figure 3.12: (a) Misset angles corresponding to the borders of the regions 1 and 2 $(\Delta\theta^\beta)$ and of the regions 2 and 3 $(\Delta\theta^\alpha)$ and width of the Darwin plateau $[(\Delta\theta_w)_D]$ as a function of $(\theta_B + \alpha)$.

(b) Misset angles corresponding to the borders of the regions 3 and 4 calculated using the approximate condition $[(\Delta\theta)_\alpha^{app}]$ and using the accurate condition $[(\Delta\theta)_\alpha^{acc}]$ and of the regions 4 and 5 $[(\Delta\theta)_{evan}]$ as a function of $(\theta_B + \alpha)$.
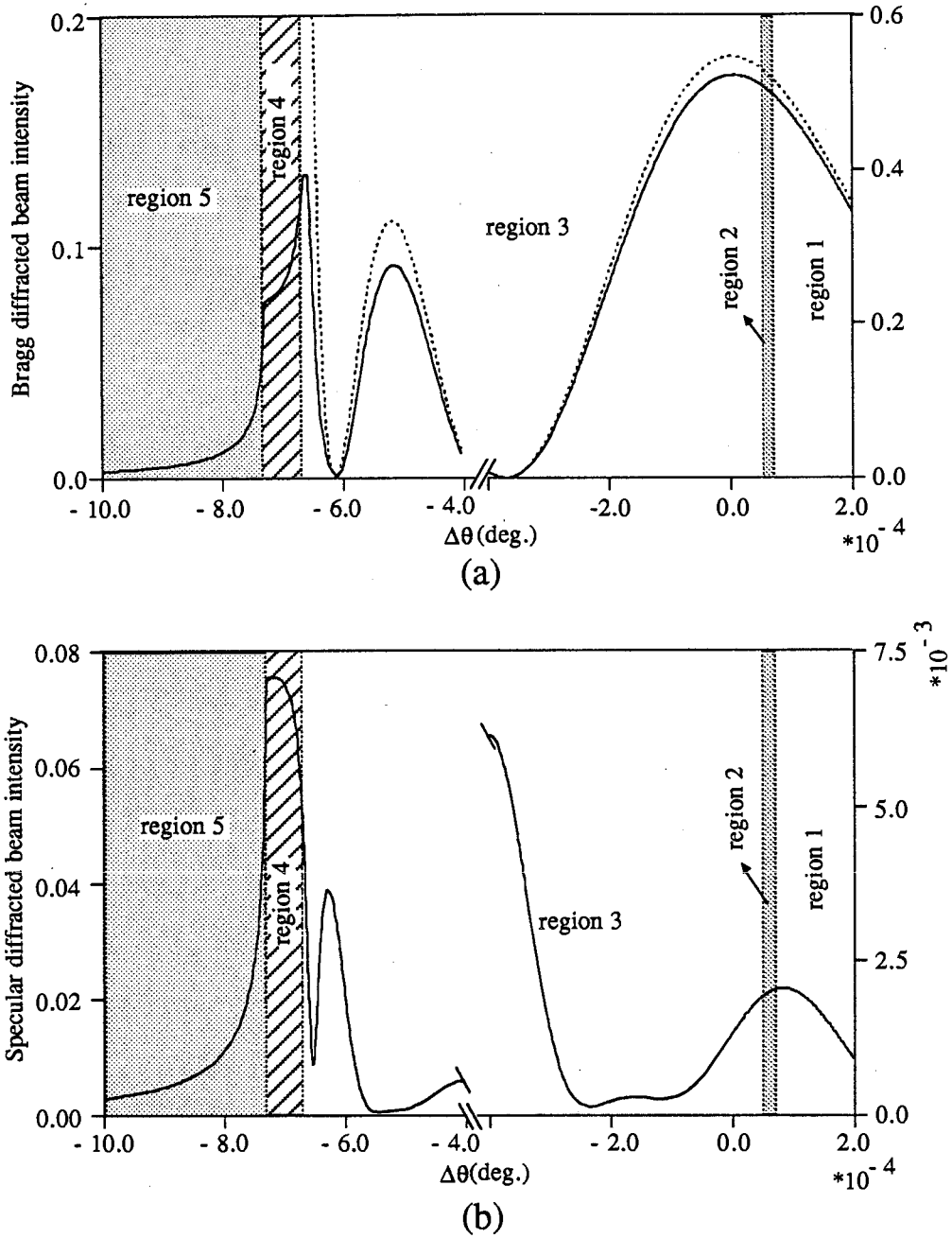
Figure 3.13: Intensity of the Bragg diffracted wave (a) and of the specular diffracted wave (b) as a function of $\Delta\theta$; $(\theta_B + \alpha) = 90.25°$, $t = 0.1\mu m$, $\Phi_O = 1$. The dotted line shows the Bragg diffracted beam intensity estimated from the conventional theory.

α-branch of the dispersion surface at the inflection point of that branch. This situation can be expressed mathematically by the condition that the solutions of the cubic equation (eq. 3.14) are real and also equal to each other. This situation occurs at a particular value of α (α_T^{LB}) for fixed k_O and G or at a particular value of k_O (k_O^{LB}) for fixed values of α and G. If we fixed the value of k_O and G, we will get the extreme asymmetric cases like either case 2 or case 3 depending upon the value of α which is slightly less than or greater than α_T^{LB}. Similarly, we will get the extreme asymmetric cases like either case 2 or case 3 depending upon the value of k_O which is slightly greater than or less than k_O^{LB} for fixed values of α and G.

3.4.4 *Extreme asymmetric Bragg case in which the incident beam makes a small angle with the crystal surface*

In this extreme case, there are two possible situations as shown as in Fig. 3.14(a) and (b). In the first situation (Fig. 3.14(a)), we have distinguished four different regions of diffraction. In the region 1, the surface normal n_1 cuts the dispersion surface in four real tie points (A and D lie on the β-branch while C and B lie on the α-branch) and therefore four wave fields associated with these tie points are excited inside the crystal. The surface normal n_2 cuts the dispersion surface in only two real tie points (both lie on the α-branch) in the region 2. This is also known as Darwin plateau region. In the region 3, we have again four real tie points, but now they are arranged on the α-branch of the dispersion surface. Again we have only two real tie points in the region 4. This region is known as the critical region.

The misset angles associated with the borders of the regions 1 and 2 ($\Delta\theta^\beta$) and the regions 2 and 3 ($\Delta\theta^\alpha$) are calculated using the fact that the surface normals become tangent to β-branch and α-branch of the dispersion surface respectively. The width of the Darwin plateau (width of the region 2) is given by
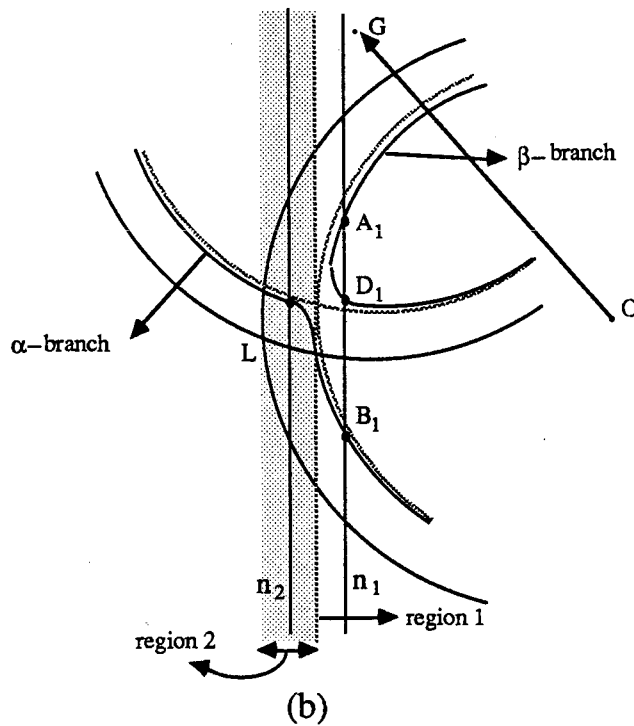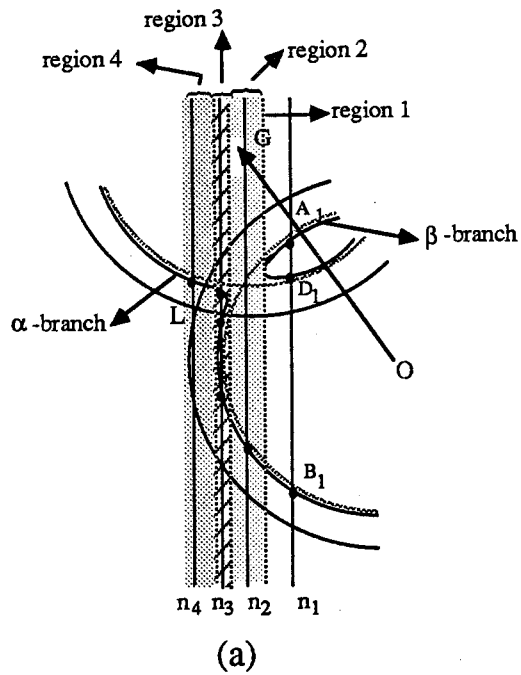
Figure 3.14: Dispersion surfaces in the extreme asymmetric Bragg case in which the incident neutrons at grazing angles on the crystal surface.

(a) Four distinctly different angular ranges of diffraction are observed.

(b) Only two different regions of diffraction are observed.

$$(\Delta\theta_w)_D = \Delta\theta^\beta - \Delta\theta^\alpha. \tag{3.15}$$

The border of the regions 3 and 4 gives the condition for the total external reflection. The misset angle corresponding to this condition $[(\Delta\theta)^{C\ B}_{acc}]$ can be calculated from the fact that the surface normal becomes tangent again to the α-branch of the dispersion surface. The approximate value $[(\Delta\theta)^{C\ B}_{app}]$ can be obtained using the asymptotic circles and is given by

$$[(\Delta\theta)^{C\ B}_{app}] = -\cos^{-1}\left(\frac{\sqrt{v_0}}{k_0}\right) + \alpha - \theta_B. \tag{3.16}$$

In order to calculate the misset angles corresponding to the borders of the different angular ranges of diffraction, we have to know the equation of the dispersion surface. In this extreme case, the tie points A, B and D are close to the Laue point L and the tie point C is far away. Therefore one could reduce the fourth order equation of the dispersion surface to a cubic equation of the form

$$(K_{oz} - K_{oz}^{*A})\,(K_{oz} - K_{oz}^{*B})\,(K_{oz} - K_{oz}^{*D}) \approx \frac{v_G v_{-G}}{(K_{oz}^{*D} - K_{oz}^{*C})} \tag{3.17}$$

with $K_{ox}^{A,B,D} = k_{ox}$.

The misset angles corresponding to the borders of the different diffraction regions and width of the Darwin plateau are shown in Fig. 3.15(a) and (b) as a function of $(\theta_B-\alpha)$.

In the second situation (Fig. 3.14(b)), we observed only two different regions of diffraction. In the region 1, we excite four real tie points in a same way as in the region 1 of the first situation. If we decrease the angle of incidence, the surface normal (n_2) enters into a region (region 2) where only two real tie points are excited. A further reduction of incident angle will never result in a situation such as the region 3 in Fig. 3.14(a) where four

real tie points are excited and all four tie points lie on the α-branch of the dispersion surface.

This second situation occurs at shorter wavelengths (at larger values of k_O) as compared to the first situation if we keep the orientation of the reflecting lattice planes with respect to the inward surface normal (α) unchanged. If we fixed the values of k_O and G, this case can be obtained at larger values of α compared to the first situation. These two cases are well separated by a condition in which the surface normal becomes tangent to the α-branch of the dispersion surface at the inflection point. This condition occurs at a particular value of k_O (k_O^B) for fixed values of G and α, or at a particular value of α (α_T^B) for fixed k_O and G. We will get either the first or the second situation depending upon the value of k_O (α) which is slightly less than or greater than k_O^B (α_T^B) for the fixed values of α (k_O) and G.

In this extreme case, the tie points D, A and B are close to the Laue point and the internal wave fields corresponding to these tie points have been taken into account in applying the boundary conditions. The amplitudes of the fourth internal wave fields associated with the tie point C (far away from the Laue point L) and the amplitude of the specular diffracted wave are extremely small. For simplicity, we take them to be zero. Under these conditions, the eqs. (3.4d) and (3.5d) become approximately equivalent to the eqs. (3.4b) and (3.5b) (same as the case 1). The internal wave vectors associated with the tie points A, B and D are given by the solutions of the cubic equation (3.17). We have calculated the intensity of the Bragg diffracted wave and of the specular reflected wave in both situations {illustrated in Fig. 3.14(a) and (b)} as a function of misset angle which covers all different angular ranges of diffraction. The results are shown in Fig. 3.16(a), (b), (c) and (d). For the first situation, the calculations were made for the (200) Si reflection of neutrons of wavelength 1.57 A^o. Here the reflecting planes makes an angle α
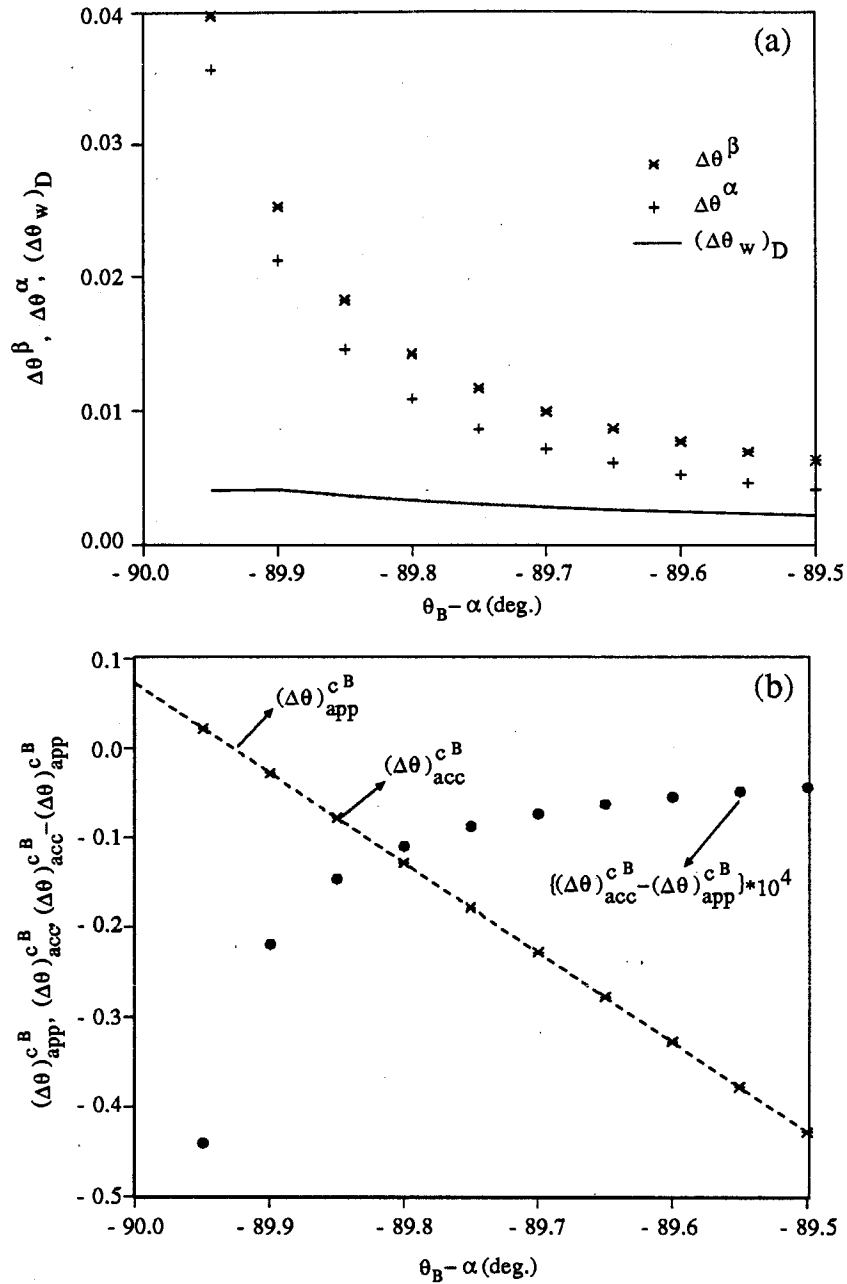
Figure 3.15: (a) Misset angles corresponding to the borders of the regions 1 and 2 $(\Delta\theta^{\beta})$ and of the regions 2 and 3 $(\Delta\theta^{\alpha})$ and width of the Darwin plateau $[(\Delta\theta_w)_D]$ as a function of $(\theta_B - \alpha)$.

(b) Misset angle corresponding to the border of the regions 3 and 4 calculated using the approximate condition [$(\Delta\theta)^{cB}_{app}$], the accurate condition [$(\Delta\theta)^{cB}_{acc}$] and the difference $\{(\Delta\theta)^{c}_{app} - (\Delta\theta)^{c}_{acc}\}(x10^4)$ as a function of $(\theta_B - \alpha)$.

The calculations were made for a fixed value of θ_B and by changing the value of α.

with the inward surface normal, which satisfies $\theta_B - \alpha = -89.9°$. In the second situation, we made the calculations for the same reflecting planes, but now $\theta_B - \alpha = -89.99°$. The intensity of the Bragg diffracted wave at the entrance surface of the crystal is compared with the results obtained from the conventional theory. From Fig. 3.16(a) and (c), it is obvious that the process of diffraction occurs at an angle comparable to the critical angle of total external reflection, but it is weak in intensity. The intensity of the specular reflected beam increases rapidly as the incident angle approaches to the condition for the total external reflection.

In this extreme case, the angular position of the Bragg peak (the position of maximum of the diffracted intensity) is strongly shifted from the geometrical exact Bragg position for the incident beam. The shift calculated using the conventional dynamical theory of diffraction is given by eq. (3.10a). This theory also predicts the width of the Darwin plateau {width of the region 2 in Fig. 3.14(a)} to be

$$(\Delta\theta_w)_D = \frac{2\,v_G}{k_O^2 \sin 2\theta_B} \sqrt{-\frac{\cos(\theta_B + \alpha)}{\cos(\theta_B - \alpha)}} \ . \qquad (3.18)$$

This expression was obtained using the fact that the internal wave vectors corresponding to the two important tie points were complex in the Darwin plateau region. Note that, the negative sign was introduced inside the square root sign in the expression (3.18) because $(\theta_B + \alpha)$ is greater than 90° in the Bragg geometry. This expression is similar to the FWHM of the Lorentzian envelope in the Laue case except for the negative sign. In deriving the conventional expressions, we approximated the asymptotic forms of the dispersion surface by straight lines. These results break down for grazing angles of incidence. Rustichelli[24] has derived more accurate expressions for the deviation from the Bragg law and for the width of the Darwin plateau from purely geometrical considerations using circles as the asymptotes
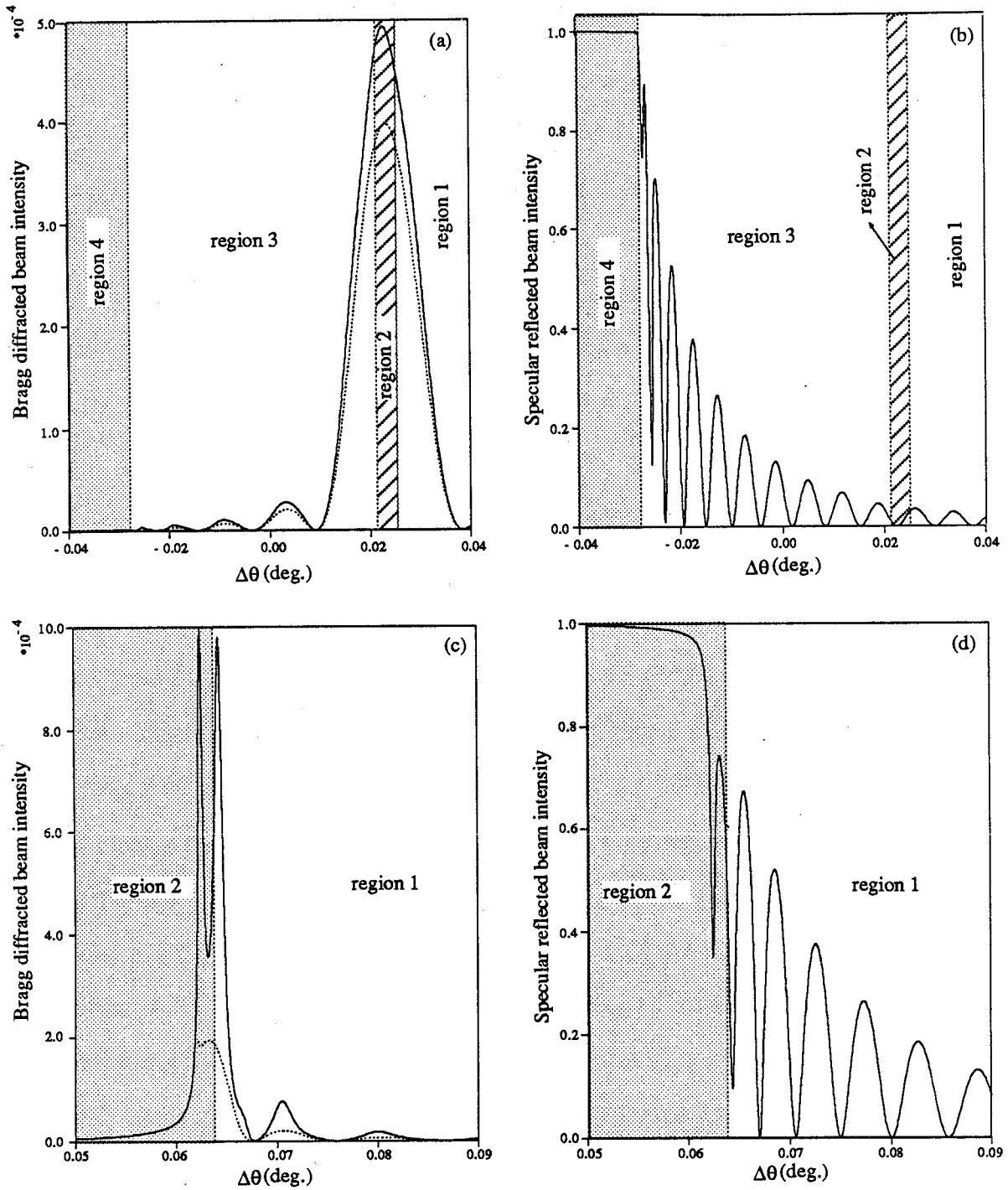
Figure 3.16: Intensities of the Bragg diffracted wave {(a) and (c)} and of the specular reflected wave {(b) and (d)} at the entrance surface of the crystal as a function of misset angle ($\Delta\theta$) for the situations illustrated in Fig. 3.14(a) [$(\theta_B - \alpha) = -89.9°$] and (b)[$(\theta_B - \alpha) = -89.99°$] respectively. In both situations $\lambda = 1.57$A° and t = 0.5μm. The dotted line shows the intensity of the Bragg diffracted wave estimated using the conventional theory.

for the dispersion surface. The expression are given by eqs. (3.9a) and (3.9b). (Note: In these expressions $\sqrt{1 - \gamma_I^2}$ must be replaced by $-\sqrt{1 - \gamma_I^2}$ because $\sin(\theta_B - \alpha)$ is negative in these extreme Bragg cases). The results obtained from the extended theory, Rustichelli's formulation and the conventional theory are compared in Fig. 3.17(A) and (B). Note that the deviation from the Bragg law was determined from the center of the Darwin plateau. Excellent agreement was found between the extended theory and Rustichelli's formulation.

3.5 Spatially Dependent Amplitude Approach

The conventional form of dynamical theory in the eikonal approach is not applicable in extreme asymmetric cases of neutron diffraction. Similarly, the reduced form of spatially dependent amplitude method (Takagi-Taupin approach) is also not applicable in extreme asymmetric cases. In this form, the second order derivatives are neglected and we kept only the first order derivatives which almost corresponds to the approximation of the form of dispersion surface in the conventional eikonal approach. However, one can solve the extreme asymmetric problem using the spatially dependent amplitude method. Here, the load line will intersect the dispersion surface in (a,b) space in four real points and at least three of them are closer to the origin. Therefore, the wave fields corresponding to these three points have considerable amplitudes and have to be taken into account in applying the boundary conditions. This approach is more or less same as the extended theory of eikonal approach discussed in this chapter. However, the coordinate system of the reciprocal space (a,b) is oblique which makes it difficult to visualize the problem geometrically. In addition, we have two variables (a and b) in the spatially dependent amplitude method instead of one variable (K_{Oz}) in the eikonal approach. Furthermore, the asymptotic values of a and b are not trivial. Because of these reasons, the spatially dependent amplitude approach becomes difficult in solving the extreme asymmetric problems.
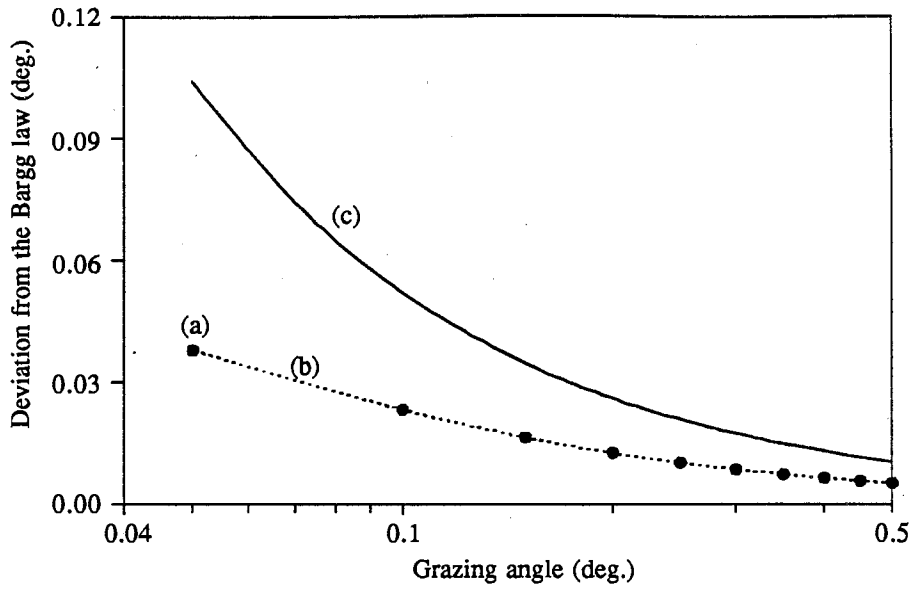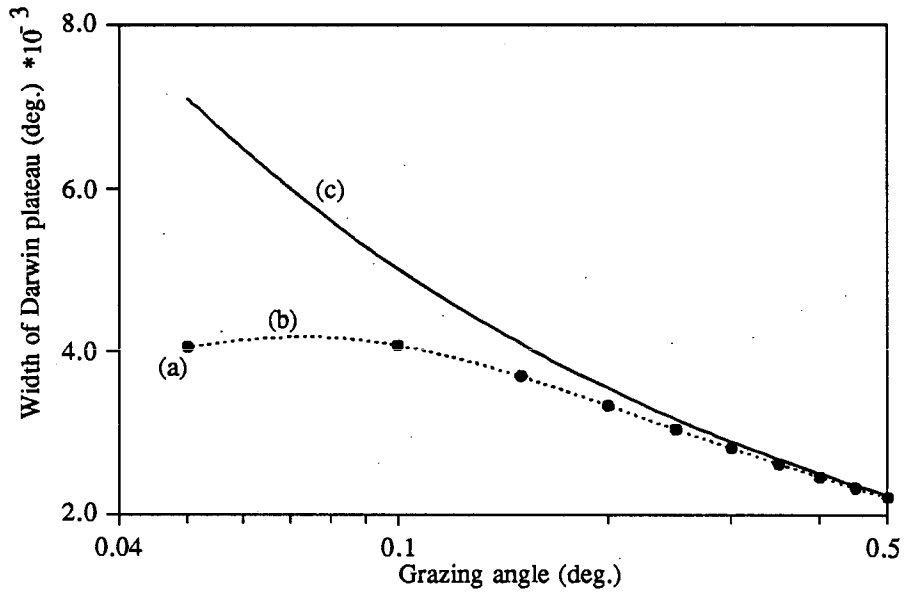
Figure 3.17: (A) The deviation from the Bragg law $\Delta\theta_i$

(B) Width of the Darwin plateau

for (220) asymmetric Si reflection as a function of glazing angle (the angle between the crystal surface and the incident beam which satisfies the external exact Bragg condition).

(a) according to the extended theory ($\bullet$) (b) according to Rustichelli's formulation (c) according to the conventional theory.

CHAPTER 4

DYNAMICAL THEORY OF DIFFRACTION FOR BENT CRYSTALS

4.1 Introduction

In the last three decades, diffraction phenomena in deformed crystals have been studied both theoretically and experimentally. The dynamical theory of x-ray diffraction from a bent crystal was first developed by Penning and Polder (1961)[25] and Kato (1964)[26]. They used the eikonal approximation and explained some experimental results. However, because of the strong restrictions associated with the conditions for the applicability of the eikonal approximation, this theory does not give the correct description of X-ray diffraction in strongly distorted crystal regions, nor near the edges of the Borrmann triangle.

A second approach of dynamical theory of diffraction for a distorted crystal was developed by Takagi (1962, 1969)[8] and Taupin [9]. This theory was developed purely based on wave-optical phenomena. So far, the Takagi-Taupin type equations have been solved exactly only for the case of a crystal with a uniform strain gradient [11 and references therein]. The analytical solutions of these equations are expressed in terms of confluent hypergeometric functions. The mathematical treatment of these functions is very complicated. However, the physical analysis of this solution is absolutely necessary to give an adequate explanation for the diffraction phenomenon in a homogeneously bent crystal. The wave field, which was obtained using the asymptotic forms of the confluent hypergeometric function, tends to results of kinematical theory as the strain gradient increases, and tends to the solution of the eikonal theory with decreasing strain gradient. Therefore, this approach can be used to explain the diffraction phenomenon from a crystal with a wide range of distortion.

We have modified the theory of x-ray diffraction from a homogeneously bent crystal based on the Takagi-Taupin equations to treat the neutron case. The details are given in this chapter. The complication of the mathematical treatment of confluent hypergeometric functions have been such that little use has been made in this approach by workers in this field. We have eliminated the mathematical obscurity by expressing the confluent hypergeometric function in terms of Chebyshev polynomials. This makes it possible to study the neutron diffraction phenomena from a homogeneously bent crystal numerically. We have chosen the type of homogeneous bending which was elaborated by Penning and Polder [25] as an example. Here we study the diffraction pattern (rocking curves) for different amplitudes of the strain gradient, integrated intensity as a function of curvature of bending, and dynamical thickness oscillations of integrated intensity in the Laue diffraction geometry. The results, computed numerically, are discussed in this chapter.

Elasticity theory adds more complications if theory is to be compared with experiments. The diffraction theory has been well established only in the case of a uniform strain gradient. In most experimental arrangements which were intended to produce uniform strain gradients, the strain gradient varies with the position. Yet, most of the researchers in this field have assumed the simplest form of displacement field which corresponds to the uniform strain gradient. The appropriate displacement field corresponding to the experimental arrangement can be found only by using elasticity theory. We have considered the bending of crystals by loading along two lines at each of two edges as an example. By using the conventional bending theory of thin crystal plates, we have found that higher order (> second order) terms of the coordinates of the position are necessary in order to specify the appropriate displacement field. These results indicate that the local radii of curvature vary position to position and even change sign. Either they can be calculated from the mid-surface displacements or can be measured experimentally. In diffraction theory, when we calculate the intensity of the diffracted beam at an arbitrary

point, only the strain field in the inverse Borrmann triangle associated with that point matters. The far strain fields won't come into the problem. The width of Borrmann triangles are very small compared to the length and width of crystal plates which we used in our experiments. Therefore one can assume that the strain gradient in any Borrmann triangle is uniform and they are determined by local radii of curvature. Now one can apply the solutions of diffraction theory as developed for the case of a uniform strain gradient to calculate the intensity of the diffracted beam at any point on the exit surface of the crystal. These remarks are discussed in detail in this chapter.

In most of our experiments we have exceeded the limits in which the conventional theory of bending can be applied, that is the displacements of the mid-surface become greater than the thickness of the crystal. In-plane forces (as a result of large curvature), which are neglected in the conventional bending theory, now have to be taken into account. This result in a pair of coupled non linear fourth order differential equations. There are no known non trivial solutions of these differential equations.

4.2 Solution to a uniform strain gradient problem using Takagi-Taupin equations

In the perfect crystal, the reduced neutron -nuclear interaction potential can be written as

$$v(\vec{r}\,) = v_0 + v_{\vec{G}}\ e^{i\,\vec{G}\cdot\vec{r}} + v_{-\vec{G}}\ e^{-i\,\vec{G}\cdot\vec{r}} \qquad (4.1)$$

Here we assume that the incident wave vector $\vec{k_0}$ is oriented very close to the exact Bragg condition for a particular reciprocal lattice vector $\vec{G}$. Therefore, the Fourier components of the potential corresponding to the other reciprocal lattice vectors are neglected.

Let $\vec{u}(\vec{r})$ be the displacement of the atom at $\vec{r}$ in a slightly distorted crystal and $\vec{r}_0$ be the position vector of the atom before the distortion which is now displaced to $\vec{r}$ during distortion. Thus the relation between $\vec{r}$ and $\vec{r}_0$ is given by

$$\vec{r} = \vec{r}_0 + \vec{u}(\vec{r}_0) \tag{4.2}$$

Note that, $\vec{u}(\vec{r})$ is a continuous function. If the distortion is slight (i.e. as long as the atoms within a single unit cell can be regarded as being uniformly displaced), the value of $v(\vec{r})$ in the distorted crystal can be mapped to the value of the reduced potential in the perfect crystal at the corresponding position $\vec{r}_0$, i.e.

$$v(\vec{r}) = v_0 + v_{\vec{G}}\, e^{i\vec{G}.\{\vec{r} - \vec{u}(\vec{r}_0)\}} + v_{-\vec{G}}\, e^{-i\vec{G}.\{\vec{r} - \vec{u}(\vec{r}_0)\}}$$

$$= v_0 + v_{\vec{G}}\, e^{-i\vec{G}.\vec{u}(\vec{r}_0)}\, e^{i\vec{G}.\vec{r}} + v_{-\vec{G}}\, e^{i\vec{G}.\vec{u}(\vec{r}_0)}\, e^{-i\vec{G}.\vec{r}} \tag{4.3}$$

In these equations, $\vec{G}$ is the reciprocal lattice vector for the undistorted crystal. In this approximation, the changes in Fourier coefficients and $\vec{G}$ on bending are neglected. The spatial frequency of the potential is modulated due to strain gradients. The effect of this variation in the potential on the internal wave function will be modeled using a single spatial frequency with amplitude modulation. Therefore, the wave function in a distorted crystal can be expressed by a sum of modulated waves

$$\Psi(\vec{r}) = \sum_{\vec{G}} \Psi_{\vec{G}}(\vec{r})\, e^{i(\vec{K}_0 + \vec{G}).\vec{r}} .$$

Under the same assumption as mentioned above, we anticipate the wave function to be of the form

$$\Psi(\vec{r}) = \Psi_0(\vec{r}) \, e^{i\vec{K}_0 \cdot \vec{r}} + \Psi_G(\vec{r}) \, e^{i\vec{K}_G \cdot \vec{r}} , \qquad (4.4)$$

where

$$\vec{K}_G = \vec{K}_0 + \vec{G} .$$

With the assumption that the amplitudes $\Psi_0(\vec{r})$ and $\Psi_G(\vec{r})$ are slowly varying functions of position, the terms $\nabla^2\Psi_0(\vec{r})$ and $\nabla^2\Psi_G(\vec{r})$ are small compared with terms proportional to $\Psi_0(\vec{r})$ and $\Psi_G(\vec{r})$ or their first derivatives and can be neglected. By substituting the reduced periodic potential given by eq. (4.3) and the above form of the wave function {eq. (4.4)} into the Schrödinger equation for the neutron {eq. (1.13)} and using the oblique coordinate system described in chapter 1, we will get the following coupled differential equations:

$$2\,i\,K\frac{\partial\Psi_0}{\partial s_0} = v_{-G} \, e^{\,i\vec{G}\cdot\vec{u}} \, \Psi_G \qquad (4.5a)$$

$$2\,i\,K\frac{\partial\Psi_G}{\partial s_G} = v_G \, e^{-\,i\vec{G}\cdot\vec{u}} \, \Psi_0 , \qquad (4.5b)$$

where K is the magnitude of the internal wave vector $\vec{K}_0$ and has the value $\sqrt{k_0^2 - v_0}$. These above equations (4.5a) and (4.5b) are the Takagi-Taupin type equations for a distorted crystal. These expressions are the same as the eqs. (1.41a & b) if $\vec{u}(\vec{r}) = 0$.

In the general case of a crystal with a uniform strain gradient, the function $\vec{G}\cdot\vec{u}$ is of the form

$$\vec{G}\cdot\vec{u} = 2\{ A\,s_0^2 + 2B\,s_0\,s_G + C\,s_G^2 \} + D\,s_0 + E\,s_G + F, \qquad (4.6)$$

Where A, B, C, D, E and F are constants. Note that the coordinate axes and $\vec{G}$ are in the same plane. (Note: The strain gradient is given by $\frac{d^2u}{dx^2}$ in the one dimensional case, where u is the displacement at an arbitrary point x. If $\frac{d^2u}{dx^2}$ is constant then u is of the form $ax^2 + bx + c$, where a, b and c are constants. This can be extended to the two dimensional case, i.e. the displacement field can be expressed in terms of a second order polynomial .) The constant term in the above expression represents the displacement of all atoms as a whole. The linear terms represent the change in lattice constant and would only lead to renomalization of the value of the Bragg angle.

By the substitutions:

$$\Psi_O = \tilde{\Psi}_O(s_O, s_G) \, e^{i\{2\,C\,s_G^2 + E\,s_G + \frac{F}{2}\}} \qquad (4.7a)$$

and

$$\Psi_G = \tilde{\Psi}_G(s_O, s_G) \, e^{-i\{2\,A\,s_O^2 + D\,s_O + \frac{F}{2}\}} \,, \qquad (4.7b)$$

the above coupled partial differential equations (4.5a) and (4.5b) reduce to

$$2\,i\,K\,e^{i\{2\,C\,s_G^2 + E\,s_G + \frac{F}{2}\}} \frac{\partial \tilde{\Psi}_O}{\partial s_O} = v_{-G}\, e^{i\vec{G}.\vec{u}}\, \tilde{\Psi}_G\, e^{-i\{2\,A\,s_O^2 + D\,s_O + \frac{F}{2}\}}$$

$$2\,i\,K\,\frac{\partial \tilde{\Psi}_O}{\partial s_O} = v_{-G}\, e^{i\vec{G}.\vec{u}}\, e^{-i\{2As_O^2 + 2Cs_G^2 + Ds_O + Es_G + F\}}\, \tilde{\Psi}_G$$

$$2\,i\,K\,\frac{\partial \tilde{\Psi}_O}{\partial s_O} = v_{-G}\, e^{i\vec{G}.\vec{u}}\, \tilde{\Psi}_G \qquad (4.8a)$$

and similarly

$$2\,i\,K\,\frac{\partial \tilde{\Psi}_G}{\partial s_G} = v_G\, e^{-i\vec{G}.\vec{u}}\, \tilde{\Psi}_O \,, \qquad (4.8b)$$

where $\quad \vec{G}.\vec{u} = 4\,B\,s_0\,s_G$. $\hspace{4cm}$ (4.8c)

By differentiating eq. (4.8a) with respect to s_G,

$$2\,i\,K\,\frac{\partial^2 \tilde{\Psi}_0}{\partial s_G \partial s_0} = v_{-G}\,e^{\,i\,\vec{G}.\vec{u}}\,\tilde{\Psi}_G \cdot i\frac{\partial}{\partial s_G}(\vec{G}.\vec{u}) + v_{-G}\,e^{\,i\,\vec{G}.\vec{u}}\,\frac{\partial \tilde{\Psi}_G}{\partial s_G}$$

$$= i\frac{\partial}{\partial s_G}(\vec{G}.\vec{u}) \cdot 2\,i\,K\,\frac{\partial \tilde{\Psi}_0}{\partial s_0} + v_{-G}\,e^{\,i\,\vec{G}.\vec{u}} \cdot \frac{v_{-G}}{2iK}\,e^{-\,i\,\vec{G}.\vec{u}}\,\tilde{\Psi}_0,$$

where we have substituted using eqs. (4.8a) and (4.8b). By simplifying, we will get

$$\frac{\partial^2 \tilde{\Psi}_0}{\partial s_0 \partial s_G} - i\frac{\partial}{\partial s_G}(\vec{G}.\vec{u})\,\frac{\partial \tilde{\Psi}_0}{\partial s_0} + \frac{v_G v_{-G}}{4K^2}\,\tilde{\Psi}_0 = 0. \hspace{2cm} (4.9a)$$

Similarly we will also get

$$\frac{\partial^2 \tilde{\Psi}_G}{\partial s_0 \partial s_G} + i\frac{\partial}{\partial s_0}(\vec{G}.\vec{u})\,\frac{\partial \tilde{\Psi}_G}{\partial s_G} + \frac{v_G v_{-G}}{4K^2}\,\tilde{\Psi}_G = 0. \hspace{2cm} (4.9b)$$

According to the Riemann method [27], the solutions of the differential equation (4.9b) with the known boundary conditions along the crystal surface RQ (see Fig. 4.1), will take the following form,

$$\tilde{\Psi}_G(P) = \tilde{\Psi}_G(Q) + \int_{QR} \left\{ \frac{\partial R_G}{\partial s_0} - 4\,i\,B\,s_G\,R_G \right\} \tilde{\Psi}_G(r)\,ds_0$$

$$+ \int_{QR} R_G\,\frac{\partial \tilde{\Psi}_G(r)}{\partial s_G}\,ds_G\,, \hspace{1.5cm} (4.10)$$
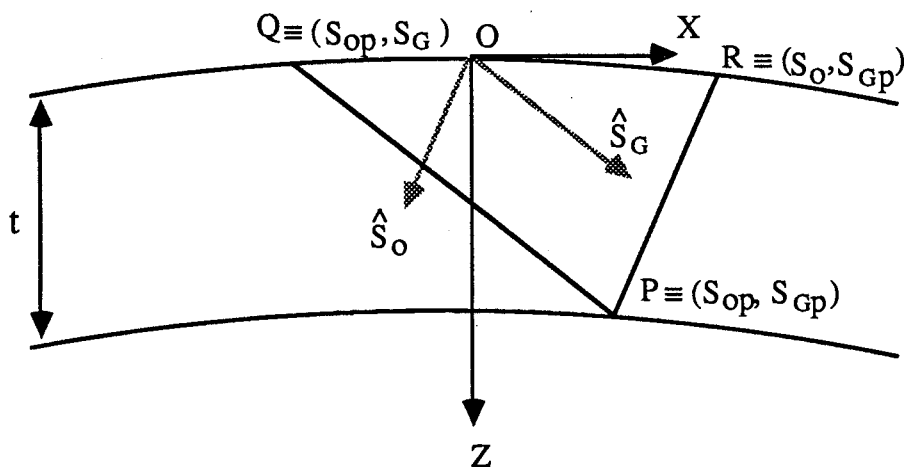
Figure 4.1: Representation of the Borrmann triangle PRQ which determines the waves at an observation point P on the lower surface of the crystal. The points Q and R lie on the upper surface; QP and RP are parallel to the directions of $\hat{S}_G$ and $\hat{S}_O$ respectively.

where $R_G(s_0, s_G)$ is the Riemann function which is given by the homogeneous conjugate equation, i.e.

$$\frac{\partial^2 R_G}{\partial s_0 \partial s_G} - 4iB\frac{\partial}{\partial s_G}(s_G R_G) + \frac{v_G v_{-G}}{4K^2} R_G = 0 .$$ (4.11a)

Furthermore, R_G should satisfy the following necessary conditions as well:

$$[R_G]_{s_0 = s_{op}} = 1$$ (4.11b)

and

$$[R_G]_{s_G = s_{Gp}} = e^{4iBs_{Gp}(s_0 - s_{op})}$$ (4.11c)

(see appendix 6 for more detail) Here P is an observation point inside or on the lower surface and the points Q and R lie on the upper surface as shown in Fig. 4.1. In the pure Laue case the points Q and R are the end points of the inverse Borrmann triangle corresponding to the observation point P. Similarly one could write an expression for the amplitude of the internal wave in the transmitted direction.

In order to solve the problem one has to find the Riemann function R_G. This function was first obtained by Chukhovskii and Petrashen [11] in the case of a homogeneously bent crystal and is given by

$$R_G = \exp[-4iBs_G(s_{op} - s_0)] \cdot {}_1F_1\left[-\frac{i\sigma^2}{4B}, 1; -4iB(s_{op} - s_0)(s_{Gp} - s_G)\right],$$ (4.12a)

$$\text{where} \quad \sigma^2 = \frac{v_G v_{-G}}{4K^2}$$ (4.12b)

and ${}_1F_1$ is the confluent hypergeometric function (see again appendix 6 for more detail).

In the expression (4.12a), (s_{op}, s_{Gp}) determines the observation point while (s_o, s_G) defines the source point.

By substituting eqs. (4.7) into eq. (4.10), we get

$$\Psi_G(P) = e^{-i\left(2As_{op}^2 + Ds_{op} + \frac{F}{2}\right)} \left\{ \left[\Psi_G(r) \, e^{i\left(2As_o^2 + Ds_o + \frac{F}{2}\right)} \right]_Q + \right.$$

$$\int_{Q(P)}^{R(P)} \left(\frac{\partial R_G}{\partial s_o} - 4iB \, s_G \, R_G \right) \Psi_G(r) \, e^{i\left(2As_o^2 + Ds_o + \frac{F}{2}\right)} ds_o +$$

$$\left. \int_{Q(P)}^{R(P)} R_G \, \frac{v_{-G} \, e^{i\vec{G}.\vec{u}}}{2iK} \Psi_o(r) \, e^{-i\left(2Cs_G^2 + E \, s_G + \frac{F}{2}\right)} ds_G \right\}.$$

Note that $\frac{\partial \tilde{\Psi}_G}{\partial s_G}$ is replaced by $\dfrac{v_{-G} \, e^{i\vec{G}.\vec{u}}}{2iK} \tilde{\Psi}_o$ using eq. (4.8b) in the third term of the above expression. Note that the integral path (QR) in the above expression is along the upper surface of the crystal where we know a great deal about the amplitudes of the internal wave function. Substituting eqs. (4.12) into the above expression with an allowance for the boundary conditions on the upper surface QR, we obtain the general solution of the amplitude of the internal wave function in the diffracted direction.

In the case of the non extreme asymmetric Laue transmission geometry, the boundary conditions at the upper surface (z=0) yield

$$\Phi_o \, e^{ik_{ox} x} = \Psi_o(\vec{r}) \, e^{iK_{ox} x} + \Psi_G(\vec{r}) \, e^{i(K_{ox} + G_x) x},$$

i.e. $\qquad \Psi_0(\vec{r}) = \Phi_0 \, e^{i \, (k_{ox} - K_{ox}) \, x} \, , \quad \Psi_G(\vec{r}) = 0.$

Next, the above expression (with the boundary conditions at the upper surface) is reduced to

$$\Psi_G(P) = e^{- i \left(2As_{op}^2 + Ds_{op} + \frac{F}{2} \right)}$$

$$\int_Q^R R_G \, \frac{v_{-G} \, e^{i \, \vec{G} \cdot \vec{u}}}{2iK} \Psi_o(r) \, e^{- i \left(2Cs_G^2 + E \, s_G + \frac{F}{2} \right)} ds_G$$

$$= \int_Q^R \frac{v_{-G} \, \Phi_0 \, e^{i \, (k_{ox} - K_{ox}) \, x}}{2iK} \, e^{-i \left\{ Ds_{op} + Es_G + F \right\}}$$

$$\left\{ R_G \, e^{-i \left[4Bs_o s_G + 2Cs_G^2 + 2As_{op}^2 \right]} \right\} ds_G, \qquad (4.13)$$

where we have used eq. (4.8c). By substituting R_G from eq. (4.12a) into eq. (4.13) we get

$$\Psi_G(P) = \int_Q^R \frac{v_{-G} \, \Phi_0 \, e^{i \, (k_{ox} - K_{ox}) \, x}}{2iK} \cdot e^{i \left\{ \varphi_G - (\vec{G} \cdot \vec{u})_P - \frac{B\rho^2}{2} \right\}}$$

$$\cdot {}_1F_1 \left[1 + \frac{i\sigma^2}{4B}, 1; iB\rho^2 \right] ds_G \quad (4.14a)$$

where $\qquad \rho^2 \equiv 4 \, (s_{op} - s_o)(s_{Gp} - s_G),$ $\qquad\qquad\qquad (4.14b)$

$$(\vec{G}\cdot\vec{u})_P \equiv 2 \{A\, s_{op}^2 + 2B\, s_{op}\, s_{Gp} + C\, s_{Gp}^2\} + D\, s_{op} + E\, s_{Gp} + F \qquad (4.14c)$$

and

$$\varphi_G \equiv 2B(\, s_{op} + s_o\,)(\, s_{Gp} - s_G\,) + 2C(\, s_{Gp}^2 - s_G^2\,) + E(\, s_{Gp} - s_G\,) \qquad (4.14d)$$

Here we have used the Kummer transformation for the confluent hypergeometric function

$$_1F_1\Big[-\frac{i\sigma^2}{4B}, 1; -iB\rho^2\Big] = e^{-iB\rho^2}\ _1F_1\Big[1 + \frac{i\sigma^2}{4B}, 1; iB\rho^2\Big].$$

Similarly one find an expression for the amplitude of the internal wave in the transmitted direction. We now have the solutions for the amplitudes of the internal waves at any point P in terms of integrals of known functions. The limits of integration are determined by the inverse Borrmann triangle associated with the observation point. Therefore only the strain field in the Borrmann triangle matters in calculating the amplitudes of the internal waves. The strain fields outside the Borrmann triangle won't affect the amplitudes of the internal waves. Further progress requires numerical methods.

4.3 Calculation of the diffracted beam intensity

In this section, as a particular case of the above, we consider bending as elaborated by Penning and Polder (1961) [25]. The geometry of the bending is shown in Fig. 4.2. The origin of the usual coordinate system for diffraction theory lies at the upper surface of the crystal, while in elasticity theory the origin is generally chosen to be at the middle of the slab. The components of the displacement vector (u',v',w') parallel to the x', y' and z' axes are given by [25]

$$u' = -\frac{v x' z'}{R} \ ; \quad v' = \frac{y' z'}{R}; \quad w' = -\frac{(y'^2 - v x'^2 + v z'^2)}{2R} \qquad (4.15)$$
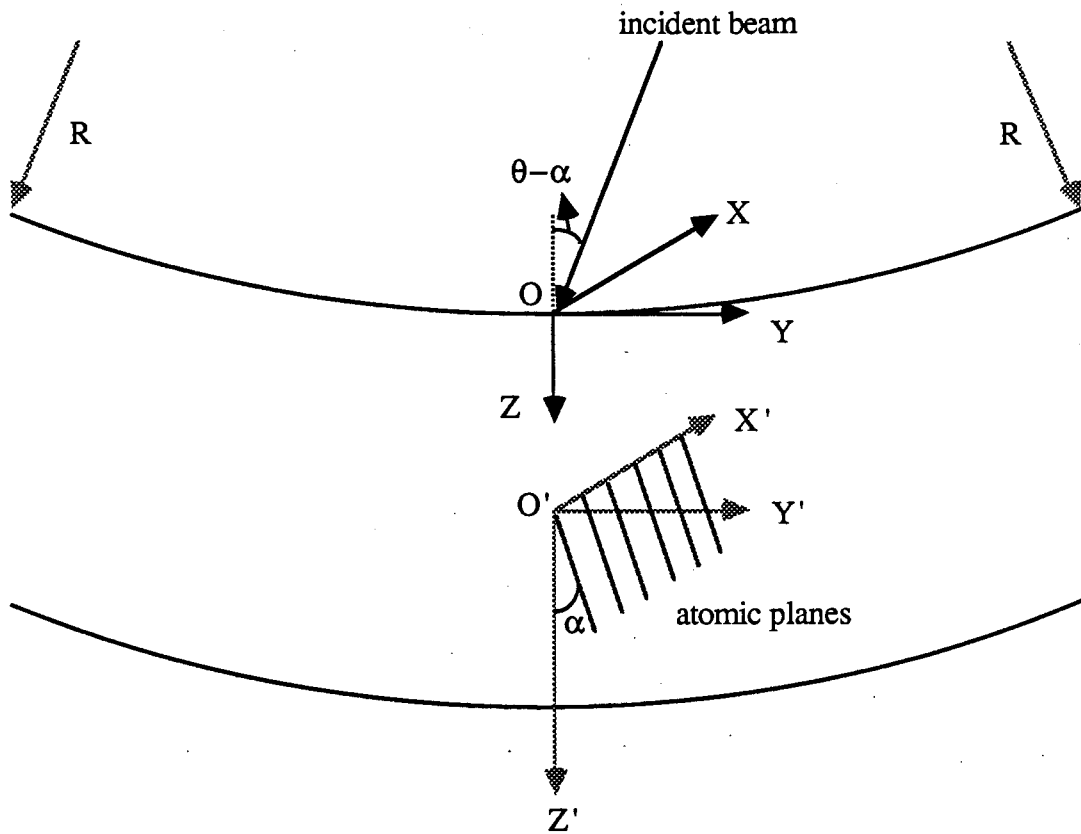
Figure 4.2: The geometry of the crystal experiencing homogeneous bending which was elaborated by Penning and Polder [25]. As drawn, both R and α are positive. O is the origin of the coordinate system for diffraction theory and O' is the origin of the coordinate system for the elasticity theory. Out of the plane of the paper the isotropic media bends with the opposite curvature producing a saddle shape (see Fig. 4.3).

respectively, where R is the radius of curvature and v is Poisson's ratio. Note that the local radii of curvature of the mid-surface in planes parallel to yz and xz, R and $-R/_v$, are constant and independent of position. These results are obtained for a prismatic beam which is bent in one of its principal planes by two equal and opposite couples [28]. In deriving these displacement components, they ignore the fact that the crystal is a crystal and treat the crystalline media as an isotropic medium with Poisson's ratio v. We need the components of the displacement vector (u,v,w) parallel to the x, y and z axes of the coordinate system with origin at O in order to calculate the coefficients A, B, C, D, E and F. These components are given by

$$u = -\frac{vx\left\{z - \frac{t}{2}\right\}}{R}; \quad v = \frac{y\left\{z - \frac{t}{2}\right\}}{R}; \quad w = -\frac{\left[y^2 - vx^2 + v\left\{z - \frac{t}{2}\right\}^2\right]}{2R} \qquad (4.16)$$

Note that the relations between the two coordinate systems are x'=x, y'=y and $z'=\left\{z - \frac{t}{2}\right\}$, where t is the thickness of the crystal. The mid-surface displacement calculated using the above equation (4.16) is saddle shaped as shown in Fig 4.3.

We consider the reflection corresponding to the lattice planes whose scattering vector is in the xz plane at y = 0, where the bending takes place as the result of an enforced bend in the yz plane. The reciprocal lattice vector $\vec{G}$ associated with these reflecting planes make an angle α with the crystal surface. Then,

$$\vec{G}.\vec{u} = G\cos\alpha\ u - G\sin\alpha\ w$$

$$= -G\cos\alpha\ \frac{vx\left\{z - \frac{t}{2}\right\}}{R} + G\sin\alpha\ \frac{\left[-vx^2 + v\left\{z - \frac{t}{2}\right\}^2\right]}{2R} \qquad (4.17)$$
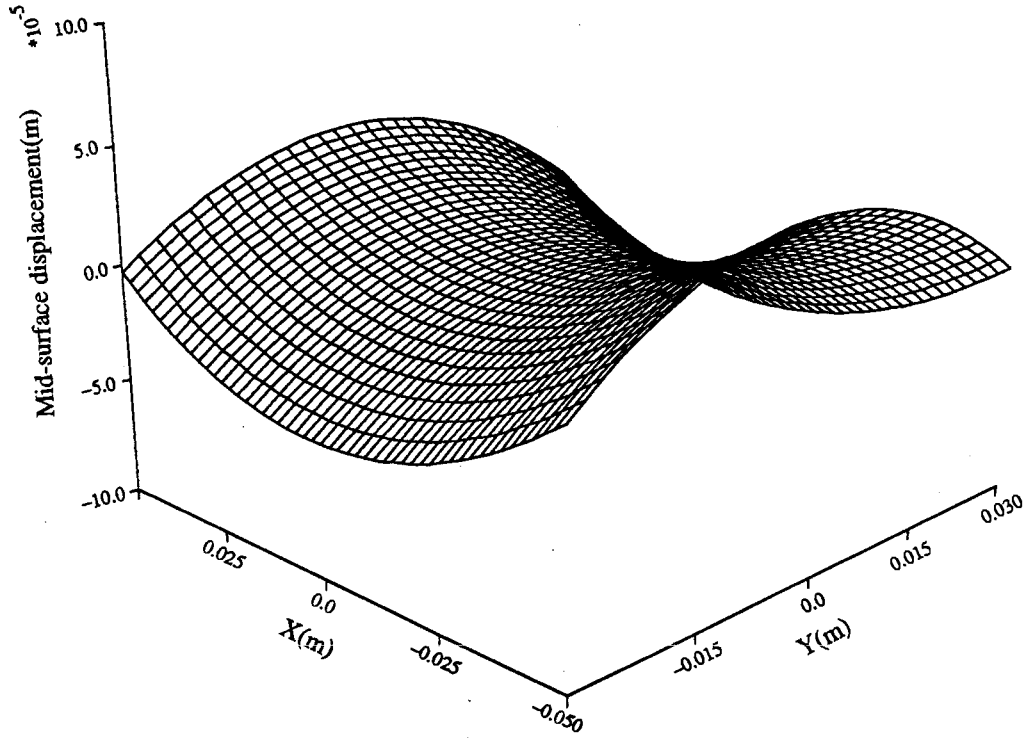
Figure 4.3: The mid-surface displacement of a homogeneously bent crystal elaborated by Penning and Polder ; $v = \frac{1}{3}$; R = 10m.

By comparing the eq. (4.17) with the eq. (4.6), the coefficients A, B, C, D, E and F can be determined. They are given by the following relations (see appendix 7):

$$A = \frac{1}{4}\frac{\partial^2}{\partial s_O^2}(\vec{G}.\vec{u}) = \frac{v\,G\,\sin(2\theta_B^* - \alpha)}{4\,R} \qquad (4.18a)$$

$$B = \frac{1}{4}\frac{\partial^2}{\partial s_O \partial s_G}(\vec{G}.\vec{u}) = -\frac{v\,G\,\sin\alpha}{4\,R} \qquad (4.18b)$$

$$C = \frac{1}{4}\frac{\partial^2}{\partial s_G^2}(\vec{G}.\vec{u}) = -\frac{v\,G\,\sin(2\theta_B^* + \alpha)}{4\,R} \qquad (4.18c)$$

$$D = \text{constant term of}\left[\frac{\partial}{\partial s_O}(\vec{G}.\vec{u})\right] = -\frac{v\,G\,t\,\sin\theta_B^*}{2\,R} \qquad (4.18d)$$

$$E = \text{constant term of}\left[\frac{\partial}{\partial s_G}(\vec{G}.\vec{u})\right] = \frac{v\,G\,t\,\sin\theta_B^*}{2\,R} \qquad (4.18e)$$

$$F = \text{constant term of}\,(\vec{G}.\vec{u}) = \frac{v\,G\,t^2\,\sin\alpha}{8\,R} \qquad (4.18f)$$

In order to calculate the internal wave amplitudes, one should know how to handle the confluent hypergeometric function. The mathematical treatment of this function is very complicated. However, one can expand the confluent hypergeometric function in an ascending series of Chebyshev polynomials [28], i.e.

$$_1F_1(a, c; z) = \sum_{n=0}^{\infty} C_n(w)\, T_n^*\left(\frac{z}{w}\right) \qquad 0 \le \frac{z}{w} \le 1, \qquad (4.19a)$$

where $T_n^*\left(x \equiv \frac{z}{w}\right) = T_n(2x - 1) = \cos\{n\cos^{-1}(2x - 1)\}$ $\qquad (4.19b)$

is the shifted Chebyshev polynomials of the first kind and w is the preselected scale factor

such that $0 \le \frac{z}{w} \le 1$.

The coefficients of the above expansion $C_n(w)$ satisfy the following recurrence formula.

$$\frac{2\,C_n(w)}{\varepsilon_n} = \frac{(n+1)}{(n+2)(n+a)}\left\{\frac{4(n+c)(n+2)}{w} - (n+3-a)\right\}C_{n+1}(w) +$$

$$\left\{1 + \frac{4(n+1)(n+3-c)}{(n+a)(n+w)}\right\}C_{n+2}(w) + \frac{(n+1)(n+3-a)}{(n+2)(n+a)}C_{n+3}(w) \quad (4.20)$$

where $\varepsilon_0 = 1$ and $\varepsilon_n = 2$ for $n > 0$.

The coefficients $C_n(w)$'s can be found by using the above recursion formula {eq. (4.20)}

in the backward direction, together with the following normalization relation

$$\sum_{n=0}^{\infty}(-1)^n\,C_n(w) = 1. \quad (4.21)$$

This means if we work with $(n+1)$ terms, we take $C_{n+2} = 0$, $C_{n+3} = 0$ and $C_{n+1} = C$

(constant) and calculate C_n using the above recursion relation {eq. (4.20)} and finally

scale the coefficients dividing by $\sum_{n=0}^{\infty}(-1)^n\,C_n(w)$.

Now we can calculate the diffracted wave amplitude (the approximate value depends

on the value of n) numerically using the expansion of confluent hypergeometric function in

terms of Chebyshev polynomials. The diffraction profiles are calculated as a function of

misset angle for different values of curvature with $v = \frac{1}{3}$. The calculations are made for the

(400) Si reflection {(111) cut crystal} in which the crystal surface is parallel to $(4\bar{2}\bar{2})$.

Because of the Pendellösung fringes in the Laue geometry, the diffraction profiles depend

strongly on the thickness of the crystal. However, we fixed the crystal thickness (75 μm)

to study the dependence of the diffraction profile on the curvature of the bending. The

results are shown in Fig 4.4. The rocking curves retain the box-like shape characteristics,
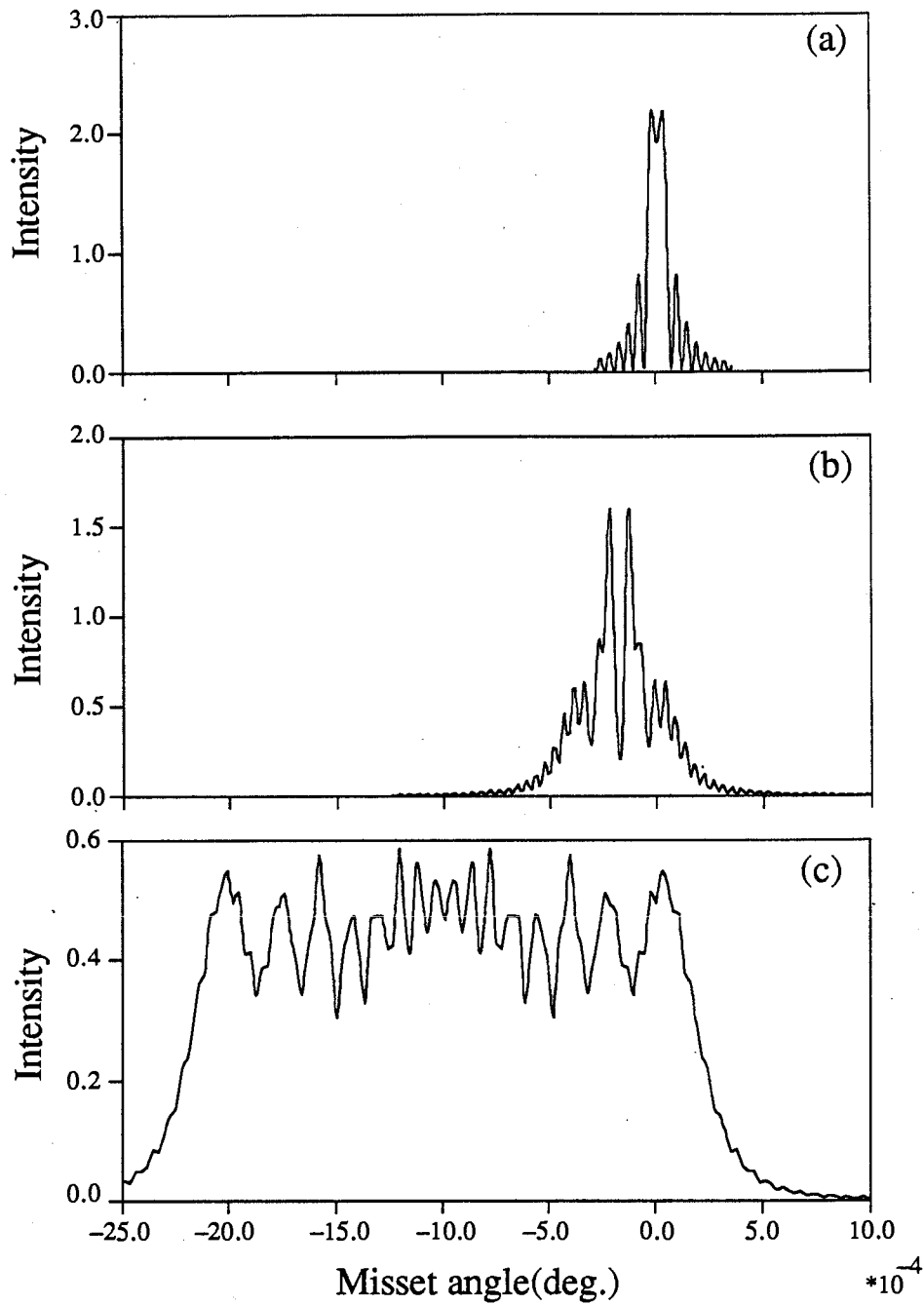
Figure 4.4: Bent crystal rocking curves for (a) R=100m (b) R=10m (c) R=2m. The calculations are made for the (400) Si reflection in which the crystal surface is parallel to $(4\,\bar{2}\,\bar{2})$; $\nu = \frac{1}{3}$; $t = 75\mu m$. The incident beam is assumed to have only one energy but a range of angles. In an actual experiment the fine structures would be averaged over.

i.e. FWHM increases with increasing curvature. In addition, the peak intensity drops at greater deformations.

In Fig. 4.5, the intensity integrated over angle for constant k_0 is displayed as a function of curvature. The integrated intensity was calculated from rocking curves, example of which are shown in Fig. 4.4. It is necessary to note that the range of angles contributing to the intensity changes with curvature. In this calculation we have fixed the crystal thickness. The kink in Fig. 4.5 is not so noticeable at some other values of crystal thickness. This can be explained using the fact that the period of thickness oscillation contracts with increasing curvature of the bending. To show this we calculate the integrated intensity as a function of thickness of the crystal for different values of curvature and display the results in Fig. 4.6. It is evident that the period of the oscillations depends on curvature and the value of the integrated intensity increases with increasing curvature. The integrated intensity for the unbent crystal ($R = \infty$) oscillates about a constant value. For the bent crystal, the integrated intensity oscillates about a value that linearly increases with thickness. Note that the rate of increase is larger for larger values of curvature. This suggest that the integrated intensity of a bent crystal consists of oscillating and non oscillating components. From Fig. 4.6, it can be seen that at fixed thickness, the kink in intensity versus curvature appears because of the shift in period with curvature. The experiments on the effect of bending on pendellösung oscillations are qualitatively like the calculated behaviour.

4.4   Conventional bending theory of thin crystal plates

The above diffraction theory was constructed for a deformed crystal in which a displacement field is expressed only in terms of a second order polynomial of coordinates of the position. This fits well to the Penning and Polder case, but in general the curvatures change with positions. In order to compare theory with experiment, one has to know the
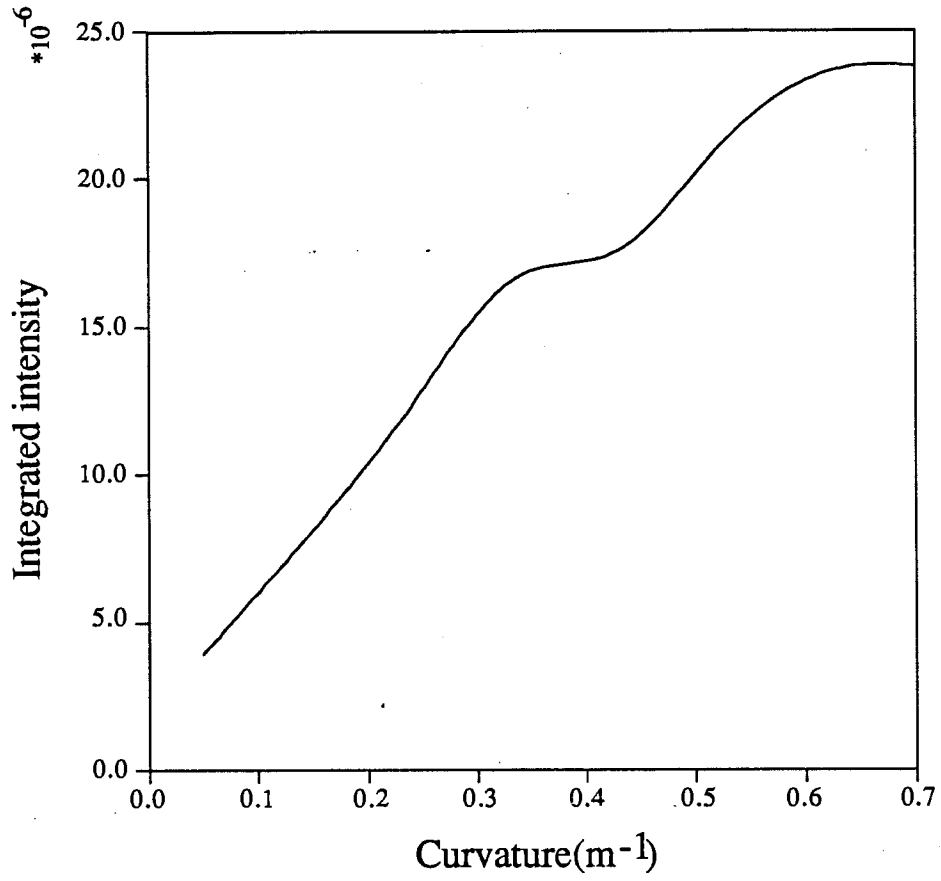
Figure 4.5: Integrated intensity as a function of curvature of the bending.
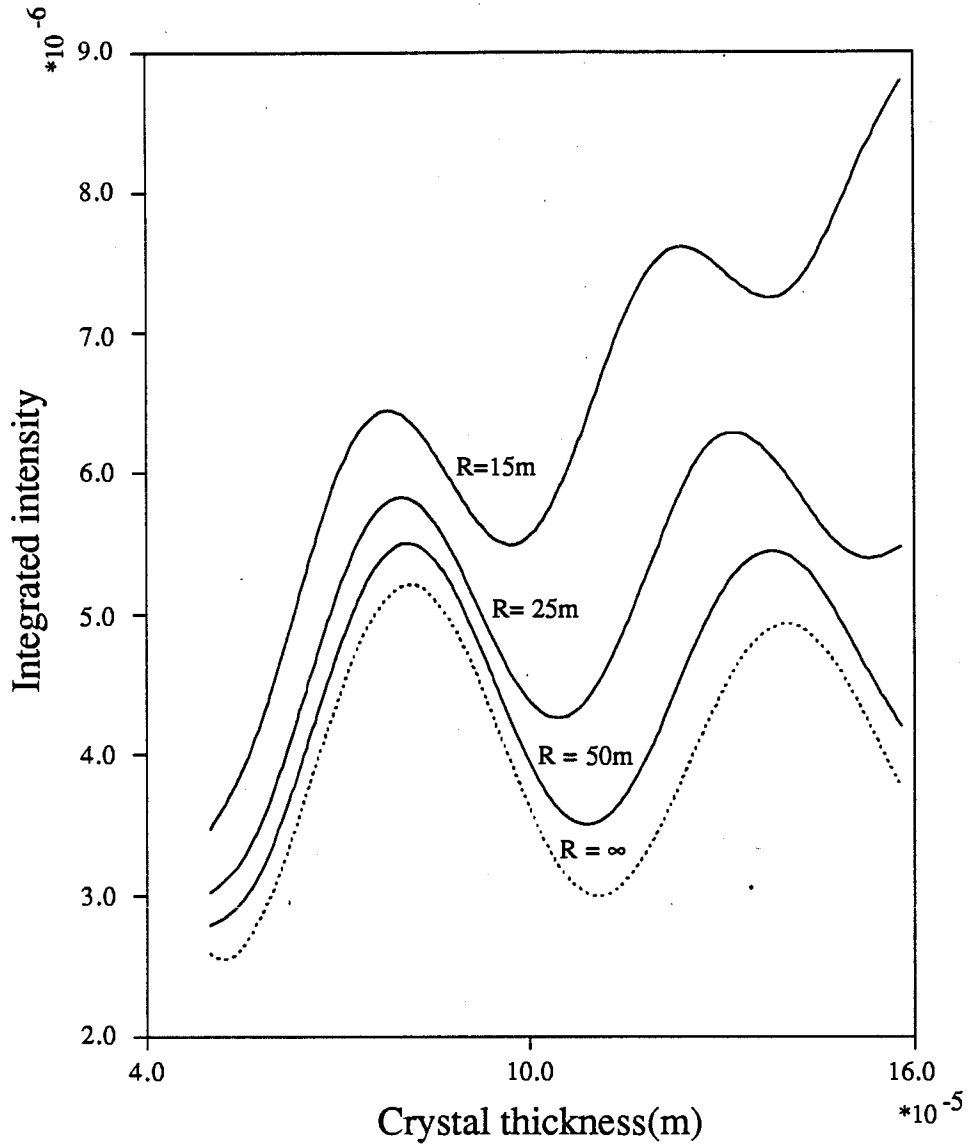
Figure 4.6: Integrated intensity as a function of thickness of the crystal for different values of radius of curvature.

displacement fields corresponding to the type of bending created during the experiment. This can be obtained by applying the conventional elasticity theory with boundary conditions suitable for the experimental situation. In most situations, the displacement field cannot be expressed accurately in terms of a second order polynomial of coordinates, i.e. higher order polynomials are necessary to specify the displacement field adequately.

We now consider the following type of bending as an example. The method of bending is to apply forces which determine the positions and slopes of the surfaces at two opposite edges, leaving two edges free. For this purpose we used four aluminium rods in pairs to create couples near each of the two edges. This bending device is illustrated in Fig. 4.7a. Under these conditions, the boundary conditions in the xyz coordinate system (see Fig. 4.7b) are given by

$$w = 0 \text{ at } y = \pm b \tag{4.22a}$$

and

$$\frac{dw}{dy} = \mp m \text{ at } y = \pm b, \tag{4.22b}$$

where w is the z component of the mid-surface displacement vector and m is the slope of the mid-surface at the fixed edges. Note that 2a, 2b and t are the dimensions of the crystal plate.

In conventional elasticity theory we use the calculus of variations to produce differential equations from the elastic energy. For simplicity, we choose Si crystals (cubic crystal) as our model to calculate this energy. The coordinate axes are parallel to the cubic edges which are also parallel to the edges of the crystal. Taking the elastic symmetry into account, one can write the elastic energy per unit volume as

Top view   Side elevation

crystal

Front elavation

(a)

X

2a

O

Y

Z

2b
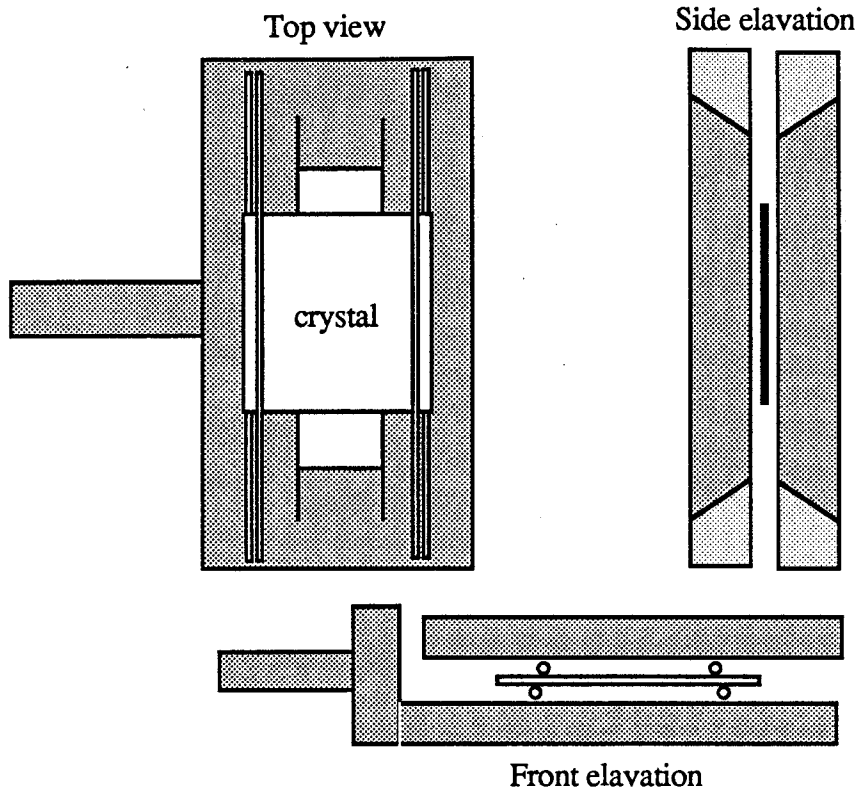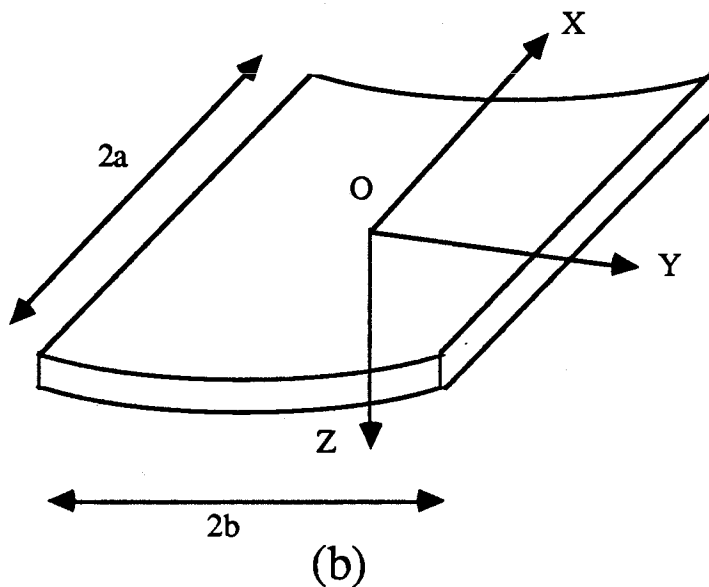
(b)

Figure 4.7: (a) Scheme of the bending system.

(b) The coordinate system of the bent crystal.

$$U = \frac{1}{2} C_{11} \left\{ e_{xx}^2 + e_{yy}^2 + e_{zz}^2 \right\} + C_{12} \left\{ e_{yy} e_{zz} + e_{zz} e_{xx} + e_{xx} e_{yy} \right\}$$

$$+ \frac{1}{2} C_{44} \left\{ e_{yz}^2 + e_{zx}^2 + e_{xy}^2 \right\} \qquad (4.23)$$

where C_{11}, C_{12} and C_{44} are the elastic stiffness constants of a cubic crystal; e_{ij}, $i = x, y, z$

and $j = x, y, z$, are the strain components.

In applying the elasticity theory for a thin crystal plate, we make the following

assumptions.

– the deflection of the mid-surface is small compared to thickness of the crystal and

the slope of the deflected surface is much smaller than unity.

– straight sections, which in the undeformed state of the crystal are normal to mid-

surface, remain straight and normal to the bent mid-surface during the bending, i.e.

e_{yz} and e_{zx} are negligible.

– the deflection of the crystal is mainly associated with bending strains and the normal

strain e_{zz} may be neglected.

– normal stress in the cross sections parallel to mid-surface is small compared to

the stresses in the transverse cross sections.

– no mid-surface straining or so called in-plane straining, stretching or contracting

occurs as a result of bending.

With these assumptions, the above expression for the energy per unit volume is reduced to

(intermediate steps are omitted)

$$U = \frac{1}{2} C_{11} z^2 \left\{ \left(\frac{\partial^2 w}{\partial x^2} \right)^2 + \left(\frac{\partial^2 w}{\partial y^2} \right)^2 \right\} + C_{12} z^2 \left\{ \frac{\partial^2 w}{\partial x^2} \frac{\partial^2 w}{\partial y^2} \right\} + 2 C_{44} z^2 \left\{ \frac{\partial^2 w}{\partial x \partial y} \right\}^2 \qquad (4.24)$$

Then, the total potential energy is given by

$$E = \int_{-a}^{a} \int_{-b}^{b} \int_{\frac{-t}{2}}^{\frac{t}{2}} U \, dx \, dy \, dz$$

Suppose now that an arbitrary incremental displacement occurs, termed a virtual displacement, i.e. $w \to w + \delta w$. For a stable equilibrium, the total potential energy has to be a minimum, i.e. $E(w + \delta w) - E(w) = 0$ or $\delta E = 0$. The principle of minimum potential energy thus leads to the following equations:

$$\frac{\partial^4 w}{\partial x^4} + \frac{2(C_{12} + 2\, C_{44})}{C_{11}} \frac{\partial^4 w}{\partial x^2 \partial y^2} + \frac{\partial^4 w}{\partial y^4} = 0 \qquad (4.25a)$$

$$\frac{\partial^2 w}{\partial x^2} + \frac{C_{12}}{C_{11}} \frac{\partial^2 w}{\partial y^2} = 0 \qquad \text{at} \quad x = \pm a \qquad (4.25b)$$

$$\frac{\partial^3 w}{\partial x^3} + \frac{(C_{12} + 4\, C_{44})}{C_{11}} \frac{\partial^3 w}{\partial x \partial y^2} = 0 \qquad \text{at} \quad x = \pm a \qquad (4.25c)$$

(For details see appendix 8.). The first equation is the basic differential equation of a thin crystal plate theory. The second and the third equations are the boundary conditions at the free edges.

Determination of $w(x,y)$ relies upon the integration of eq. (4.25a) with the constants of integration dependent upon the boundary conditions at the free edges {eqs. (4.25b & c)} and the fixed edges [eqs. (4.22a & b)]. There are no exact solutions for $w(x,y)$. But one can try a polynomial form of solutions for $w(x,y)$. This will give an approximate solution of $w(x,y)$. We try a solution of the polynomial form

$$w(x,y) = \frac{m}{2b} \left\{ (b^2 - y^2) + (y^2 - b^2)^2 (A_0 + A_1 x^2 + A_2 x^4) \right\} \qquad (4.26)$$

Note that the boundary conditions at the fixed edges are already built in the above solution. Because of symmetry in our bending system, there are no odd order terms of coordinates in the above solution. By substituting the above solution of w into the eqs. (4.25), and then equating the constant terms on both sides, we can calculate the constants A_0, A_1 and A_2. The mid-surface displacement, calculated using the above expression {eq. (4.26)} of w(x,y), is shown in Fig. 4.8a.

In the case of the isotropic thick beam considered above, the curvature of mid-surface due to the opposite bending was constant ($= \frac{v}{R}$). In our type of bending, we see from Fig. 4.8a that a similar kind of opposite bending occurs, but it is much less and is concentrated only close to the free edges of the crystal. If we drop the term $A_2 x^4$ in the above solution of w, the solutions will give the opposite sign to A_1 and look more like the thick beam case. The crystals that we have used in our experiments are quite good mirrors. On bending, the reflection from the light sources can be used to see how uniform is the displacement along the x-axis. In the experiments, the bending was obtained by tightening five screws on each side of the crystal. The natural tendency of the crystal not to bend uniformly was partially compensated by the experimenters. The tendency of this bending not to be perfectly cylindrical is qualitatively explained by the higher order polynomial solutions using the conventional elasticity theory, as for example eq. (4.26).

In the above described bending theory, we have neglected the strain in the z direction. To explain the increase in intensity on bending, the strain field in the z direction has to be taken into account in diffraction theory. We include the strain field in the z direction to the first order as $\xi(x,y)z$. The displacement in the z direction becomes

$$w(x,y,z) = w(x,y,0) \ + \ \xi(x,y)\frac{z^2}{2} \ . \qquad (4.27)$$

Again by minimizing the total energy (similar to that shown in appendix 8) we get

$$\xi(x,y) = \frac{C_{12}}{C_{11}} \left\{ \frac{\partial^2 w(x,y,0)}{\partial x^2} + \frac{\partial^2 w(x,y,0)}{\partial y^2} \right\} \qquad (4.28)$$

and

$$\frac{\partial^4 w}{\partial x^4} + 2 \left\{ \frac{C_{11}C_{12} + 2\,C_{11}C_{44} - C_{12}^2}{C_{11}^2 - C_{12}^2} \right\} \frac{\partial^4 w}{\partial x^2 \partial y^2} + \frac{\partial^4 w}{\partial y^4} = 0 \qquad (4.29a)$$

$$\frac{\partial^2 w}{\partial x^2} + \left\{ \frac{C_{12}}{C_{11} + C_{12}} \right\} \frac{\partial^2 w}{\partial y^2} = 0 \qquad \text{at } x = \pm a \qquad (4.29b)$$

$$\frac{\partial^3 w}{\partial x^3} + \left\{ \frac{C_{11}C_{12} + 4\,C_{11}C_{44} - C_{12}^2}{C_{11}^2 - C_{12}^2} \right\} \frac{\partial^3 w}{\partial x \partial y^2} = 0 \qquad \text{at } x = \pm a. \qquad (4.29c)$$

In deriving the above expressions we have neglected the higher order terms (z^4 and z^6) which are small compared to z^2 term. The differential equations (4.29), which determine $w(x,y,0)$, are similar to eqs. (4.25) except the coefficients are slightly different, as $C_{11} \approx 3\ C_{12}$. Again we try a polynomial solution for $w(x,y,0)$ in the form given by eq. (4.26) and thereby the coefficients A_0, A_1 and A_2 are calculated. The mid-surface displacement $w(x,y,0)$, calculated using these coefficients, is shown in Fig. 4.8b. The mid-surface displacements, calculated with and without strain in the z direction, show little difference. The strain field in the z direction which is important in the diffraction theory, can be calculated from eq. (4.28) with $w(x,y,0)$ found from either eqs. (4.29) or (4.25), or from experimental measurements of $w(x,y,t/2)$. Of course, it is no more work to use the more accurate form, that is eq. (4.29).

In some experimental situations, the axes of the coordinate system are not parallel to the cubic edges. The elastic stiffness constants which enter into equations depend on the direction of the axes of the coordinate system. If the direction of the axes is changed, then
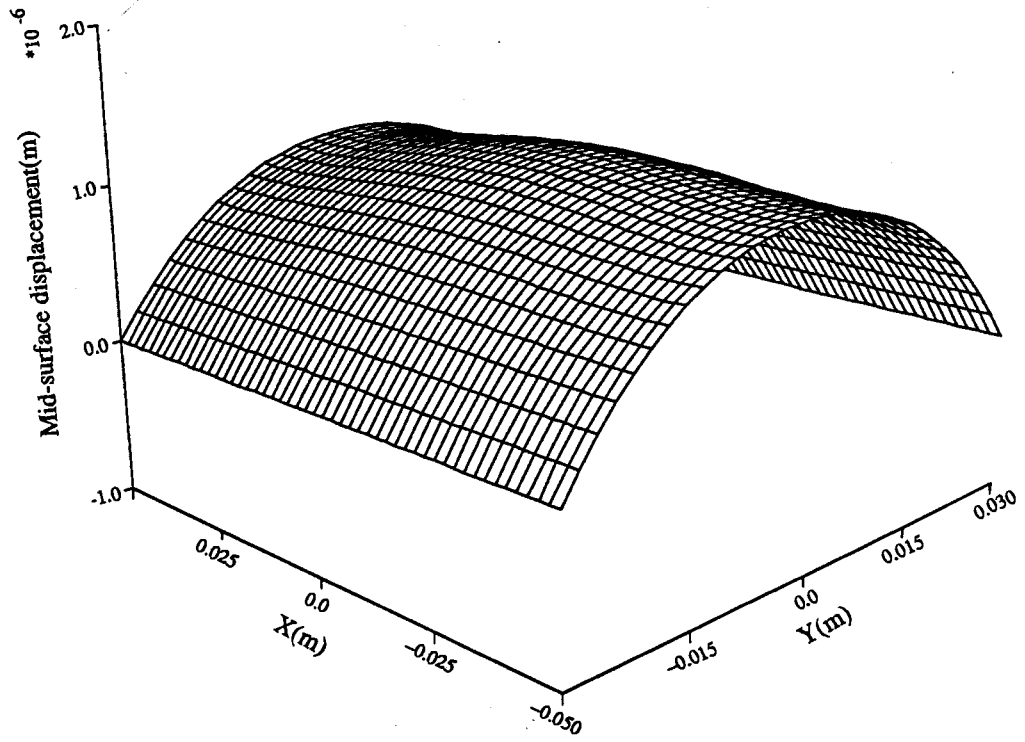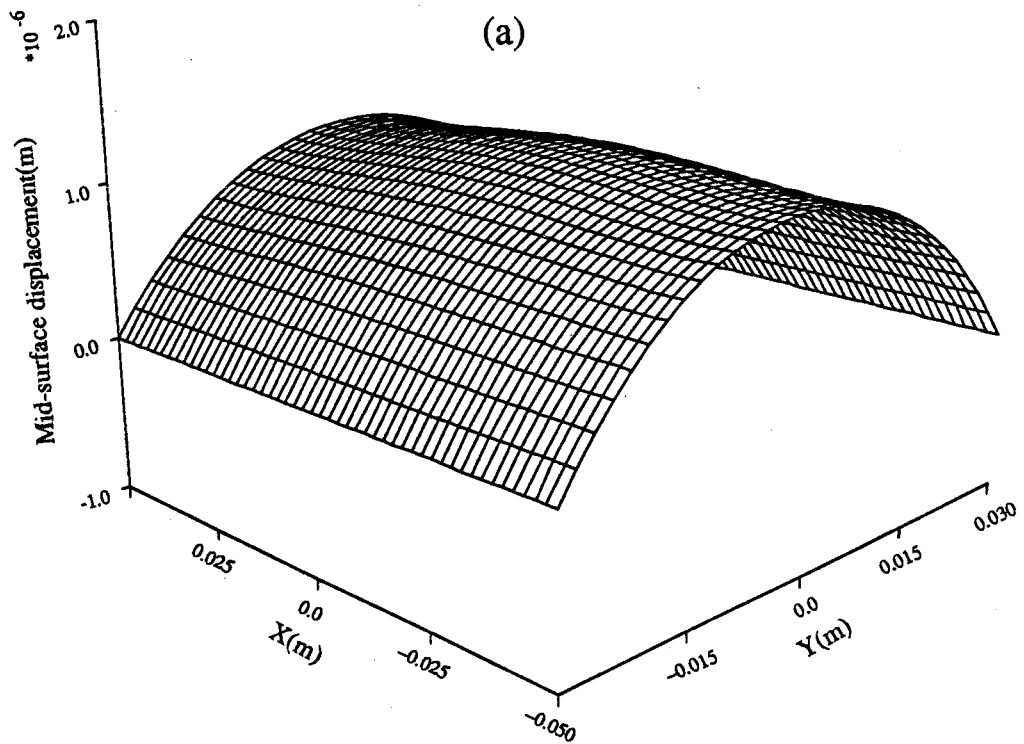
Figure 4.8: The mid-surface displacement of a bent crystal in our experimental set up (a) without the strain in the z direction and (b) with the strain $\xi(x,y)z$ in the z direction.

the elastic constants must be recalculated. One can determine the elastic constants

corresponding to the new coordinate system in terms of known elastic constants associated

with the simple coordinate system, that we have mentioned above, by finding a proper

transformation. This transformation tensor can be found using the expressions of the

elastic potential and the equations of the generalized Hooke's law with the elastic symmetry

[30]. The different sets of elastic constants are necessary to study the different types of Si

crystals {(111) and (100) cut wafers}.

4.5   Application of uniform strain gradient solutions to the experimental situation

The bending created in our experimental arrangements can be modeled by

conventional bending theory as explained in section 4.4. The mid-surface displacement

contains higher order terms (> second order). The local radii of curvature of the mid-

surface, R_x, R_y and R_{xy}, which are given by

$$\frac{1}{R_x} = \frac{\partial^2 w(x,y,o)}{\partial x^2}, \quad \frac{1}{R_y} = \frac{\partial^2 w(x,y,o)}{\partial y^2} \quad \text{and} \quad \frac{1}{R_{xy}} = \frac{\partial^2 w(x,y,o)}{\partial x \partial y}, \qquad (4.30)$$

vary position to position.

Calculating the intensity of the diffracted beam at an arbitrary point involves only the

strains in the inverse Borrmann triangle associated with that observation point. The

thickness of crystals that we used in our experiments is small compared to other

dimensions, so the width of the Borrmann triangle is small as well. Therefore we can

assume that the strain gradient in the Borrmann triangle is uniform. This uniform strain

gradient is determined by the local radii of curvature at the center of the Borrmann triangle.

The value of uniform strain gradient varies slowly from one Borrmann triangle to other.

The details are given below.

Let $(x_0, y_0, 0)$ be the center position of the Borrmann triangle. Using Taylor expansion, we write the mid-surface displacement at any point $(x_0+x, y_0+y, 0)$ as

$$w(x_0+x, y_0+y, 0) \approx w(x_0, y_0, 0) + \left(\frac{\partial w}{\partial x}\right)_{x_0, y_0} x + \left(\frac{\partial w}{\partial y}\right)_{x_0, y_0} y + \frac{1}{2}\left(\frac{\partial^2 w}{\partial x^2}\right)_{x_0, y_0} x^2$$

$$+ \frac{1}{2}\left(\frac{\partial^2 w}{\partial y^2}\right)_{x_0, y_0} y^2 + \left(\frac{\partial^2 w}{\partial x \partial y}\right)_{x_0, y_0} xy,$$

where higher order terms (>second order) are neglected. From eq. (4.27) with eq. (4.28), the displacement in the z direction becomes

$$w(x_0+x, y_0+y, z) \approx w(x_0, y_0, 0) + \left(\frac{\partial w}{\partial x}\right)_{x_0, y_0} x + \left(\frac{\partial w}{\partial y}\right)_{x_0, y_0} y + \left(\frac{\partial^2 w}{\partial x \partial y}\right)_{x_0, y_0} xy$$

$$+ \frac{1}{2}\left(\frac{\partial^2 w}{\partial x^2}\right)_{x_0, y_0}\left\{x^2 + \frac{C_{11}}{C_{12}} z^2\right\} + \frac{1}{2}\left(\frac{\partial^2 w}{\partial y^2}\right)_{x_0, y_0}\left\{y^2 + \frac{C_{11}}{C_{12}} z^2\right\}. \qquad (4.31a)$$

The coefficients of the second order terms, which are important in diffraction theory, are determined by the local radii of curvature {eq. (4.30)} at $(x_0, y_0, 0)$. The displacements in the x and y directions are given by

$$u(x_0+x, y_0+y, z) \approx -z\frac{\partial w}{\partial x} = -\left(\frac{\partial w}{\partial x}\right)_{x_0, y_0} z - \left(\frac{\partial^2 w}{\partial x^2}\right)_{x_0, y_0} xz$$

$$- \left(\frac{\partial^2 w}{\partial x \partial y}\right)_{x_0, y_0} yz \qquad (4.31b)$$

$$v(x_0+x, y_0+y, z) \approx -z\frac{\partial w}{\partial y} = -\left(\frac{\partial w}{\partial y}\right)_{x_0, y_0} z - \left(\frac{\partial^2 w}{\partial y^2}\right)_{x_0, y_0} yz$$

$$- \left(\frac{\partial^2 w}{\partial x \partial y}\right)_{x_o, y_o} xz, \qquad (4.31c)$$

where again we have neglected higher order terms. Now we know the displacement components (u,v,w) associated with any point in the Borrmann triangle. Since these displacements have been expressed only in terms of a second order polynomial they represent a uniform strain gradient which varies from one Borrmann triangle to other. We can use the solutions for uniform strain gradients and the intensity of the diffracted beam can be calculated at any point.

4.6 Bending theory of crystal plates with large deflections

In most of our experiments we have exceeded the limits in which the above described conventional bending theory can be applied, that is the deflections exceed the thickness of the crystal. Under this situation, the bending system is subjected to forces acting in the mid-surface (in-plane forces). The problem of plate bending with in-plane forces is considerably more complicated than the above simple bending theory. The deflection and the stress function are determined by a system of two nonlinear equations. In the case of bending which we used in our experiments, the following two non linear fourth order differential equations together with boundary conditions will determine the displacement field (see appendix 9 for details including nomenclature):

$$a_{11}\frac{\partial^4 F}{\partial x^4} + (2a_{12} + a_{44}) \frac{\partial^4 F}{\partial x^2 \partial y^2} + a_{11}\frac{\partial^4 F}{\partial y^4} = \left(\frac{\partial^2 w}{\partial x \partial y}\right)^2 - \frac{\partial^2 w}{\partial x^2} \cdot \frac{\partial^2 w}{\partial y^2}. \qquad (4.32a)$$

$$D_{11} \frac{\partial^4 w}{\partial x^4} + 2 (D_{12} + 2D_{44}) \frac{\partial^4 w}{\partial x^2 \partial y^2} + D_{11} \frac{\partial^4 w}{\partial y^4} =$$

$$t\left(\frac{\partial^2 F}{\partial y^2} \cdot \frac{\partial^2 w}{\partial x^2} - 2\frac{\partial^2 F}{\partial x \partial y} \cdot \frac{\partial^2 w}{\partial x \partial y} + \frac{\partial^2 F}{\partial x^2} \cdot \frac{\partial^2 w}{\partial y^2}\right) \qquad (4.32b)$$

$$D_{11}\frac{\partial^2 w}{\partial x^2} + D_{12}\frac{\partial^2 w}{\partial y^2} = 0 \ \text{ at } x = \pm a \qquad (4.32c)$$

$$(D_{12} + 4D_{44})\frac{\partial^3 w}{\partial x \partial y^2} + D_{11}\frac{\partial^3 w}{\partial x^3} = 0 \text{ at } x = \pm a \qquad (4.32d)$$

Note that the boundary conditions at the fixed edges are given by eqs. (4.22). The exact solutions is unknown for even a simple case of bending. Numerical methods can be applied. However, the solutions of this difficult bending theory are absolutely necessary to explain some of our experimental results. Solving these coupled fourth order differential equations lie just outside the scope of this thesis. The next stage in our work would encompass this.

CHAPTER 5

SUMMARY

The dynamical theory of neutron diffraction is studied for parallel-sided perfect crystals using the eikonal approach and the spatially dependent amplitude approach. In the eikonal approach a given incident plane wave generates four pairs of internal waves. The wave vectors of these waves are found by expressing the dispersion relation in terms of four convenient parameters K_{oz}^{*A}, K_{oz}^{*B}, K_{oz}^{*C} and K_{oz}^{*D}. Boundary conditions at the surfaces of the crystal determine all the unknown internal and external wave amplitudes. The spatially dependent amplitude approach was developed because of its utility in an approximate form called the T-T method. The spatially dependent amplitude approach yields the same results as the eikonal method but is less convenient because of the oblique coordinate system used in deriving the coupled differential equations. This is particularly so for extreme cases where wave vectors are nearly parallel to surfaces.

In studying the non extreme cases some approximations are useful in both approaches. In the eikonal approach, two pairs of internal waves suffice to describe the propagation of neutrons in the crystal. In the T-T approach, the second derivatives of the wave amplitudes are neglected in the coupled differential equations, using the fact that they are slowly varying. These two approaches lead to almost the same results in most cases. An analytical expression was obtained for the intensity of the diffracted beam in the Laue geometry. Integrated intensity was calculated by taking the wavelength spread and the angular spread of the incoming beam into account. By defining new dimensionless variables, normalized thickness and normalized intensity, we have obtained a universal curve representing intensity as a function of thickness from which one can calculate the period of oscillation in all possible cases of Laue transmission geometries. The experimentally measured diffracted beam intensity as a function of thickness of Si wafers

shows good agreement with the theory.

In the extreme cases, it has been shown that three pairs of internal waves are sufficient to describe adequately the propagation of neutrons inside the crystal. The dynamical diffraction theory for perfect crystals given in this thesis is unique in the fullness of the approach and its direct application to a simple and actual experimental geometry.

Using the T-T method, the solutions of the dynamical problem in the case of homogeneously bent crystals have been expressed previously in terms of confluent hypergeometric functions . Mathematical obscurities have been eliminated here by expressing the confluent hypergeometric functions in terms of Chebyshev polynomials. Calculating the amplitudes of the internal waves at an arbitrary point involves only the strain field in the inverse Borrmann triangle associated with the observation point. In our experiments the crystals are bent almost to a cylindrical form. The deviations are qualitatively explained by the solutions of the conventional elasticity theory. The results show that the strain gradient varies from position to position. However, the strain gradient can be treated as uniform in each Borrmann triangle for the Si wafers that we used in our experiments. The local strain gradients are determined by the local radii of curvature at the center point of the Borrmann triangles. The local radii of curvature, which vary from one Borrmann triangle to other, either can be calculated from the mid-surface displacement obtained using the conventional elasticity theory or measured experimentally. By knowing the value of uniform strain gradient in the Borrmann triangle, we can calculate the internal wave amplitudes at any point.

In some experiments we have exceeded the limits in which the conventional elasticity theory can be applied. In this situation, two coupled non linear fourth order differential equations determine the mid-surface displacement.

APPENDICES

Appendix 1

Typical values of some useful parameters for silicon crystals

Parameter	Symbol	Typical value
Lattice constant	a	5.4309 A° at 25°C
Scattering length	b	4.1534 x 10^{-15} m *
Fourier components of reduced periodic neutron-nuclear interaction potential	v_O	2.607 x 10^{15} m^{-2}
	v_G (odd reflections)	1.843 x 10^{15} m^{-2}
	v_G (even reflections)	2.607 x 10^{15} m^{-2}
Elastic stiffness constants	C_{11}	16.57 x 10^{10} Nm^{-2}
	C_{12}	6.39 x 10^{10} Nm^{-2}
	C_{44}	7.956 x 10^{10} Nm^{-2}

Properties of our monochromating system

The neutrons from the TNF facility is monochromated by 90° scattering from the (422) reflection from stacks of silicon wafers.

Wavelength of incoming neutrons from the monochromator $\lambda \approx 1.57$ A°

Magnitude of the wavevector $k_O \approx 4.0 \times 10^{10}$ m^{-1}

Index of refraction $n = \dfrac{K}{k_O} = \dfrac{\sqrt{k_O^2 - v_O}}{k_O} = 1 - 0.815 \times 10^{-6}$

Critical angle of the total external reflection = 9.334 x 10$^{-5\circ}$

Typical values of energy (ε) and pendellösung period for different reflections

$$\varepsilon = \frac{v_G \, v_{-G}}{(K_{Oz}^{*A} - K_{Oz}^{*B})(K_{Oz}^{*C} - K_{Oz}^{*D})}$$

where $(K_{OZ}^{*A} - K_{OZ}^{*B}) = 2\sqrt{k_{OZ}^2 - v_O} = 2\sqrt{k_O^2\cos^2(\theta-\alpha) - v_O}$

$$\approx 2\sqrt{k_O^2\cos^2(\theta_B-\alpha) - v_O}$$

and

$$(K_{OZ}^{*C} - K_{OZ}^{*D}) = 2\sqrt{k_{OZ}^2 - v_O - \Delta}$$

$$= 2\sqrt{k_O^2\cos^2(\theta-\alpha) - v_O - G^2\cos^2\alpha + 2k_OG\sin(\theta-\alpha)\cos\alpha}$$

$$\approx 2\sqrt{k_O^2\cos^2(\theta_B-\alpha) - v_O - G^2\cos^2\alpha + 2k_OG\sin(\theta_B-\alpha)\cos\alpha}\ .$$

ε is an energy in reduced units that sets the length scale for diffraction phenomena. In usual diffraction experiments, ε is essentially a constant for a given reflection.

$$\text{Pendellösung period} = \frac{\pi}{\sqrt{\varepsilon}}$$

Reflecting planes	Bragg angle [θ_B(deg.)]	Angle between the atomic planes and the surface normal [α (deg.)]	Energy in reduced units [ε (m^{-2})]	Pendellösung period (μm)
(400) (004 cut)	35.34	0.0	1.41×10^9	87.7
($4\bar{2}\bar{2}$) (111 cut)	45.11	0.0	1.77×10^9	85.0
($3\bar{1}\bar{1}$) (111 cut)	28.66	10.02	6.59×10^8	122.4
($1\bar{1}\bar{1}$) (111 cut)	14.51	19.47	6.445×10^8	123.75
(400) (111 cut)	35.34	35.26	2.82×10^9	59.1

This table is made for our experimental set up. Here we have included the Debye waller

temperature factor (W) in our calculations. Debye waller factor is given by

$$W = \frac{6h^2T}{m_A k\Theta^2} \cdot \frac{\sin^2\theta}{\lambda^2} \left[\Phi(x) + \frac{x}{4}\right]$$

where h - Planck's constant ; m_A - mass of the vibrating atom ; k - Boltzmann's constant ; Θ - Debye temperature of the crystal ; $x = \frac{\Theta}{T}$; T - absolute temperature ; $\Phi(x)$ is a function of x defined by $\Phi(x) = \frac{1}{x} \int\limits_{0}^{x} \frac{\xi \, d\xi}{e^\xi - 1}$.

In neutron diffraction experiments

$$W = K \frac{\sin^2\theta}{\lambda^2} = K \left\{\frac{h^2+k^2+l^2}{4 \, a^2}\right\}$$

$$= 0.00388251 \times (h^2+k^2+l^2) \quad *$$

* C. G. Shull, J. Appl. Cryst. 6, 257 (1973).

Appendix 2

Mathematical details involved in the calculation of diffracted beam intensity (eq. 2.22)

$$k_{oz}^2 - v_o = K_{oz}^{*A\,2}$$

$$(k_{oz}^2 - v_o - K_{oz}^{A\,2})(k_{oz}^2 - v_o - K_{oz}^{C\,2}) = (K_{oz}^{*A\,2} - K_{oz}^{A\,2})(K_{oz}^{*A\,2} - K_{oz}^{C\,2})$$

$$= K_{oz}^{*A\,4} - K_{oz}^{*A\,2}(K_{oz}^{A\,2} + K_{oz}^{C\,2}) + K_{oz}^{A\,2}K_{oz}^{C\,2}$$

$$= K_{oz}^{*A\,4} - K_{oz}^{*A\,2}\left[(K_{oz}^A + K_{oz}^C)^2 - 2\,K_{oz}^A K_{oz}^C\right] + K_{oz}^{A\,2}K_{oz}^{C\,2}$$

$$= K_{oz}^{*A\,4} - K_{oz}^{*A\,2}\left[(K_{oz}^{*A} + K_{oz}^{*C})^2 - 2(K_{oz}^{*A} K_{oz}^{*C} - \varepsilon)\right] + (K_{oz}^{*A} K_{oz}^{*C} - \varepsilon)^2$$

Note that $K_{oz}^A + K_{oz}^C = K_{oz}^{*A} + K_{oz}^{*C}$ and $K_{oz}^A K_{oz}^C = K_{oz}^{*A} K_{oz}^{*C} - \varepsilon$ (From eq. 2.1)

$$= -2\,\varepsilon\,K_{oz}^{*A}(K_{oz}^{*A} + K_{oz}^{*C}) + \varepsilon^2$$

$$\approx -2\,\varepsilon\,K_{oz}^{*A}(K_{oz}^{*A} + K_{oz}^{*C})$$

The second term ε^2 is very small compared to the first term $-2\,\varepsilon\,K_{oz}^{*A}(K_{oz}^{*A} + K_{oz}^{*C})$ and can be neglected.

$$K_{oz}^{A\,2} - K_{oz}^{C\,2} = (K_{oz}^A + K_{oz}^C)(K_{oz}^A - K_{oz}^C)$$

$$= (K_{oz}^{*A} + K_{oz}^{*C})\sqrt{(K_{oz}^A + K_{oz}^C)^2 - 4\,K_{oz}^A K_{oz}^C}$$

$$= (K_{oz}^{*A} + K_{oz}^{*C}) \sqrt{(K_{oz}^{*A} - K_{oz}^{*C})^2 + 4\,\varepsilon}$$

From eq. (2.10a)

$$\Psi_G^A = \frac{(k_{oz}^2 - v_o - K_{oz}^{A\,2})(k_{oz}^2 - v_o - K_{oz}^{C\,2})}{(K_{oz}^{A\,2} - K_{oz}^{C\,2})} \Phi_o$$

$$= \frac{-2\,\varepsilon\,K_{oz}^{*A}(K_{oz}^{*A} + K_{oz}^{*C})}{(K_{oz}^{*A} + K_{oz}^{*C})\sqrt{(K_{oz}^{*A} - K_{oz}^{*C})^2 + 4\,\varepsilon}} \Phi_o$$

$$= \frac{-2\,\varepsilon\,K_{oz}^{*A}}{\sqrt{(K_{oz}^{*A} - K_{oz}^{*C})^2 + 4\,\varepsilon}} \Phi_o$$

Note:- $K_{Gz}^A - K_{Gz}^C = K_{oz}^A - K_{oz}^C = \sqrt{(K_{oz}^{*A} - K_{oz}^{*C})^2 + 4\,\varepsilon}$

$$I_d = 4\,\Psi_G^{A\,2} \sin^2 \frac{(K_{Gz}^A - K_{Gz}^C)\,t}{2}$$

$$= \frac{16\,\varepsilon^2\,K_{oz}^{*A\,2}\,\Phi_o^2}{v_{-G}^2\,\{(K_{oz}^{*A} - K_{oz}^{*C})^2 + 4\,\varepsilon\}} \sin^2 \left\{ \frac{\sqrt{(K_{oz}^{*A} - K_{oz}^{*C})^2 + 4\,\varepsilon}}{2}\,t \right\}$$

$$(2.22)$$

Appendix 3

Derivation of the variable $(K_{oz}^{*A} - K_{oz}^{*C})$ as a function of ΔK and Δq

$$K_{oz}^{*A} = \sqrt{k_{oz}^2 - v_o} = k_{oz} - \frac{v_o}{2k_{oz}}$$

$$= (k_o + \Delta K) \cos(\theta_B - \alpha + \Delta\theta) - \frac{v_o}{2(k_o + \Delta K) \cos(\theta_B - \alpha + \Delta\theta)}$$

where ΔK and $\Delta\theta$ are the aribitary values of the magnitude of the wave vector spread and of the angular spread of the incoming neutron source.

Here we have replaced k_o by $(k_o + \Delta K)$ and $(\theta - \alpha)$ by $(\theta_B - \alpha + \Delta\theta)$.

$$\approx (k_o + \Delta K) \{\cos(\theta_B - \alpha) - \sin(\theta_B - \alpha)\, \Delta\theta\} - \frac{v_o}{2\, k_o \cos(\theta_B - \alpha)}$$

$$\approx k_o\cos(\theta_B - \alpha) + \Delta K \cos(\theta_B - \alpha) - k_o\sin(\theta_B - \alpha)\, \Delta\theta - \frac{v_o}{2\, k_o \cos(\theta_B - \alpha)}$$

$$K_{oz}^{*C} = -G_z + \sqrt{k_{oz}^2 - v_o - G_x^2 - 2\, k_{ox}\, G_x}$$

$$= -G_z + \sqrt{k_o^2 - (k_{ox} + G_x)^2 - v_o}$$

$$k_o^2 - (k_{ox} + G_x)^2 = (k_o + \Delta K)^2 - \{-(k_o + \Delta K) \sin(\theta_B - \alpha + \Delta\theta) + 2\, k_o \sin\theta_B \cos\alpha\}^2$$

Note that, the value of $G\ (= 2\, k_o \sin\theta_B)$ is fixed.

$$\approx (k_o + \Delta K)^2 - \{-k_o \sin(\theta_B - \alpha) - \Delta K \sin(\theta_B - \alpha) - k_o \cos(\theta_B - \alpha)\Delta\theta + 2\, k_o \sin\theta_B \cos\alpha\}^2$$

$$\approx k_O^2 + 2 k_O \, \Delta K - \{ k_O \sin (\theta_B+\alpha) - \Delta K \sin (\theta_B-\alpha) - k_O \cos (\theta_B-\alpha)\Delta\theta \}^2$$

$$\approx k_O^2 + 2 k_O \, \Delta K - k_O^2 \sin^2 (\theta_B+\alpha) + 2 k_O \, \Delta K \sin (\theta_B-\alpha) \sin (\theta_B+\alpha)$$
$$+ 2k_O^2 \, \cos (\theta_B-\alpha) \, \sin (\theta_B+\alpha) \, \Delta\theta$$

$$= k_O^2 \cos^2 (\theta_B+\alpha) + 2k_O^2 \, \cos (\theta_B-\alpha) \, \sin (\theta_B+\alpha) \, \Delta\theta$$
$$+ 2 k_O \, \Delta K \, \{1 + \sin (\theta_B-\alpha) \sin (\theta_B+\alpha)\}$$

$$\sqrt{k_O^2 - (k_{ox} + G_x)^2} \approx k_O \cos (\theta_B+\alpha) + \frac{k_O \cos (\theta_B-\alpha) \, \sin (\theta_B+\alpha)}{\cos (\theta_B+\alpha)} \, \Delta\theta$$

$$+ \frac{\Delta K \, \{1 + \sin (\theta_B-\alpha) \sin (\theta_B+\alpha)\}}{\cos (\theta_B+\alpha)}$$

$$K_{oz}^{*}C \approx 2 k_O \sin \theta_B \sin \alpha + k_O \cos (\theta_B+\alpha) + \frac{k_O \cos (\theta_B-\alpha) \, \sin (\theta_B+\alpha)}{\cos (\theta_B+\alpha)} \, \Delta\theta$$

$$+ \frac{\Delta K \, \{1 + \sin (\theta_B-\alpha) \sin (\theta_B+\alpha)\}}{\cos (\theta_B+\alpha)} - \frac{v_o}{2 k_O \cos (\theta_B+\alpha)}$$

$$K_{oz}^{*}A - K_{oz}^{*}C = - \frac{k_O \sin 2\theta}{\cos (\theta_B+\alpha)} \, \Delta\theta - \frac{(\cos 2\theta_B - 1)}{\cos (\theta_B+\alpha)} \Delta K - \frac{v_o}{2 k_O \cos (\theta_B-\alpha)}$$

$$+ \frac{v_o}{2 k_O \cos (\theta_B+\alpha)}$$

Appendix 4

Calculation of Jacobian $J (K_{oz}^{*A} - K_{oz}^{*C}, K_{oz}^{*A})$

$$J (K_{oz}^{*A} - K_{oz}^{*C}, K_{oz}^{*A}) = \frac{\partial k_{ox}}{\partial (K_{oz}^{*A} - K_{oz}^{*C})} \cdot \frac{\partial k_{oz}}{\partial K_{oz}^{*A}} - \frac{\partial k_{ox}}{\partial K_{oz}^{*A}} \cdot \frac{\partial k_{oz}}{\partial (K_{oz}^{*A} - K_{oz}^{*C})}$$

$$K_{oz}^{*A} = \sqrt{k_{oz}^2 - v_o} \quad \Rightarrow \quad k_{oz} = \sqrt{K_{oz}^{*A\,2} + v_o}$$

$$\frac{\partial k_{oz}}{\partial (K_{oz}^{*A} - K_{oz}^{*C})} = 0, \quad \frac{\partial k_{oz}}{\partial K_{oz}^{*A}} = \frac{K_{oz}^{*A}}{\sqrt{K_{oz}^{*A\,2} + v_o}}$$

$$(K_{oz}^{*A} - K_{oz}^{*C}) = K_{oz}^{*A} + G_z - \sqrt{k_{oz}^2 - v_o - G_x^2 - 2 k_{ox} G_x}$$

$$k_{oz}^2 - v_o - G_x^2 - 2 k_{ox} G_x = \{ K_{oz}^{*A} + G_z - (K_{oz}^{*A} - K_{oz}^{*C}) \}^2$$

$$2 k_{ox} G_x = -(K_{oz}^{*A} - K_{oz}^{*C})^2 - G^2 + 2 G_z (K_{oz}^{*A} - K_{oz}^{*C}) + 2 K_{oz}^{*A} (K_{oz}^{*A} - K_{oz}^{*C})$$
$$- 2 G_z K_{oz}^{*A}$$

$$2 G_x \frac{\partial k_{ox}}{\partial (K_{oz}^{*A} - K_{oz}^{*C})} = -2 (K_{oz}^{*A} - K_{oz}^{*C}) + 2 G_z + 2 K_{oz}^{*A} = 2 (K_{oz}^{*C} + G_z)$$

$$2 G_x \frac{\partial k_{ox}}{\partial K_{oz}^{*A}} = 2 (K_{oz}^{*A} - K_{oz}^{*C}) - 2 G_z$$

$$J (K_{oz}^{*A} - K_{oz}^{*C}, K_{oz}^{*A}) = \frac{(K_{oz}^{*C} + G_z)}{G_x} \cdot \frac{K_{oz}^{*A}}{\sqrt{K_{oz}^{*A\,2} + v_o}}$$

$$\approx \frac{k_o \cos (\theta_B + \alpha)}{2 k_o \sin \theta_B \sin \alpha} = \frac{\cos (\theta_B + \alpha)}{2 \sin \theta_B \sin \alpha}$$

Appendix 5

Modification of Rustichelli's expressions for the deviation from the Bragg law and FWHM of the envelope of the diffraction pattern for the extreme asymmetric Laue case.
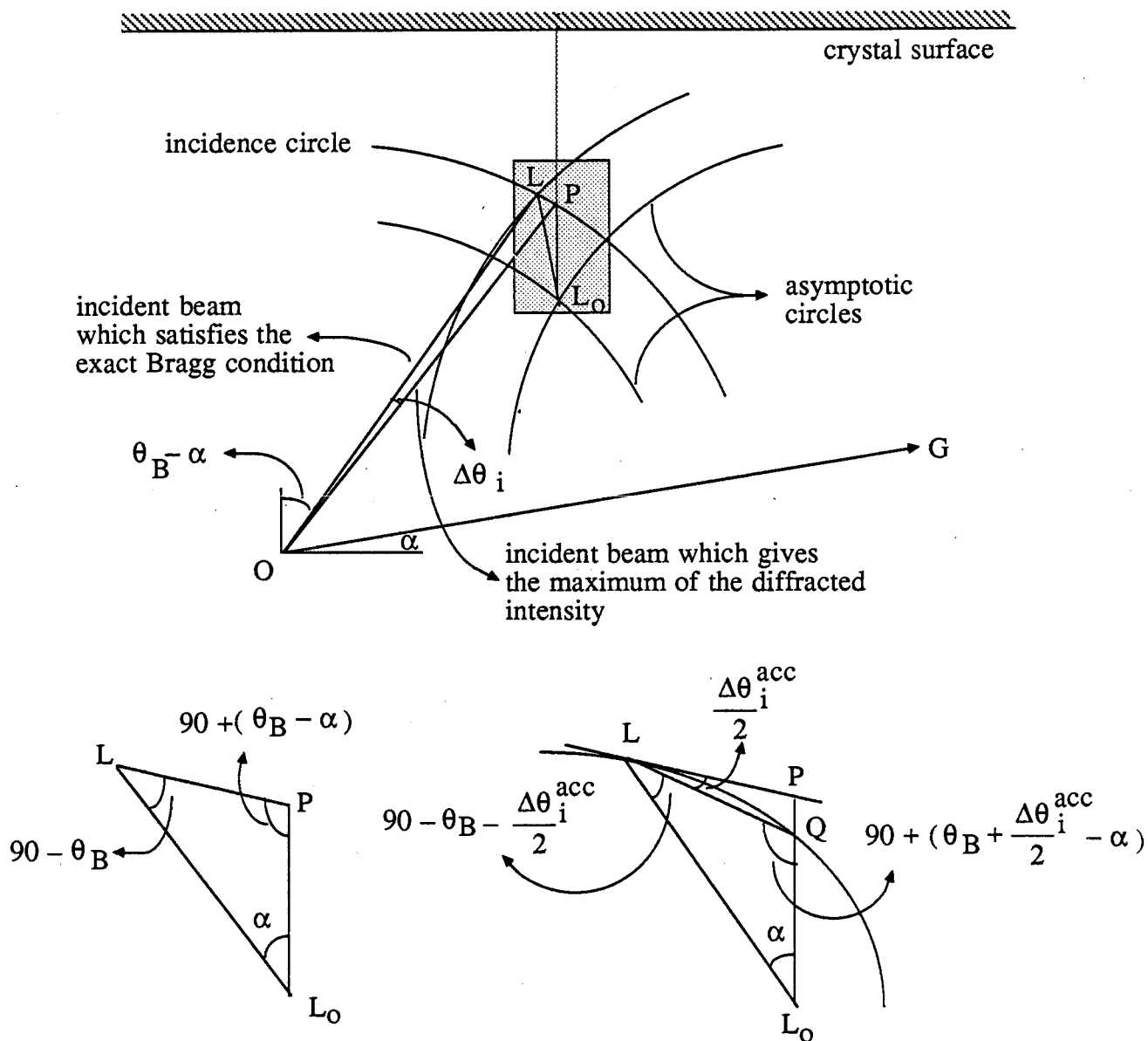
Representation of the deviation from the exact Bragg condition

In the conventional treatment, the incidence circle is approximated by the tangent to it at the Laue point L.

$$\Delta\theta_i^c = \frac{LP}{k_o}$$

$$\frac{LP}{\sin \alpha} = \frac{LL_o}{\sin (90 + \theta_B - \alpha)} = \frac{LL_o}{\cos (\theta_B - \alpha)}$$

$$LL_o = k_o \cos \theta_B - K \cos \theta_B^*$$

We know that $k_o \sin \theta_B = K \sin \theta_B^*$

Let $\theta_B^* = \theta_B + \Delta\theta_B$

$$k_o \sin \theta_B = \sqrt{k_o^2 - v_o} \, \sin \theta_B^*$$

$$k_o \sin (\theta_B^* - \Delta\theta_B) = \left(k_o - \frac{v_o}{2 k_o} \right) \sin \theta_B^*$$

$$k_o \sin \theta_B^* - k_o \cos \theta_B^* \, \Delta\theta_B = k_o \sin \theta_B^* - \frac{v_o}{2 k_o} \, \sin \theta_B^*$$

$$\Delta\theta_B = \frac{v_o}{2 k_o^2} \, \tan \theta_B^*$$

$$LL_o = k_o \cos (\theta_B^* - \Delta\theta_B) - K \cos \theta_B^*$$

$$= k_o \cos \theta_B^* + k_o \sin \theta_B^* \, \Delta\theta_B - \left(k_o - \frac{v_o}{2 k_o} \right) \cos \theta_B^*$$

$$= k_O \sin \theta_B^* \; \frac{v_O}{2 \, k_O^2} \; \tan \theta_B^* + \frac{v_O}{2 \, k_O} \; \cos \theta_B^*$$

$$= \frac{v_O}{2 \, k_O \cos \theta_B^*} \approx \frac{v_O}{2 \, k_O \cos \theta_B}$$

$$LP = LL_O \frac{\sin \alpha}{\cos (\theta_B - \alpha)}$$

$$\approx \frac{v_O}{2 \, k_O \cos \theta_B} \; \frac{\sin \alpha}{\cos (\theta_B - \alpha)}$$

$$= \frac{v_O}{2 \, k_O \sin 2\theta_B} \left\{ \frac{\cos (\theta_B - \alpha) - \cos (\theta_B + \alpha)}{\cos (\theta_B - \alpha)} \right\}$$

$$= \frac{v_O}{2 \, k_O \sin 2\theta_B} \left\{ 1 - \frac{\cos (\theta_B + \alpha)}{\cos (\theta_B - \alpha)} \right\}$$

$$\Delta\theta_i^c = \frac{v_O}{2 \, k_O^2 \sin 2\theta_B} \left\{ 1 - \frac{\cos (\theta_B + \alpha)}{\cos (\theta_B - \alpha)} \right\} \qquad *$$

This expression can be obtained also in the process of making $(K_{OZ}^{*A} - K_{OZ}^{*C}) = 0$ with $\Delta K = 0$. Note that $\Delta\theta_i^c$ diverges as $(\theta_B - \alpha) \to 90°$.

Rustichelli derived the more correct expression for the deviation from the Bragg law $(\Delta\theta_i^{acc})$ with the assumption that the asymptotic forms of the dispersion surface and the incidence cicle are actually circles.

i.e. Here we assume LQ is a arc of the incidence circle.

$$\Delta\theta_i^{acc} = \frac{\text{arc } LQ}{k_o}$$

$$LQ \text{ (chord)} = 2 k_o \sin\left(\frac{\Delta\theta_i^{acc}}{2}\right)$$

$$\frac{LLo}{\sin\left(90 + \left[\theta_B + \dfrac{\Delta\theta_i^{acc}}{2} - \alpha\right]\right)} = \frac{LQ}{\sin \alpha}$$

$$\frac{v_o}{2 k_o \cos\theta_B \cos\left(\theta_B + \dfrac{\Delta\theta_i^{acc}}{2} - \alpha\right)} = \frac{2 k_o \sin\left(\dfrac{\Delta\theta_i^{acc}}{2}\right)}{\sin \alpha}$$

$$\frac{v_o}{2 k_o \cos\theta_B \left\{\cos(\theta_B - \alpha) - \sin(\theta_B - \alpha)\dfrac{\Delta\theta_i^{acc}}{2}\right\}} = \frac{2 k_o \left(\dfrac{\Delta\theta_i^{acc}}{2}\right)}{\sin \alpha}$$

$$\sin(\theta_B - \alpha)\left(\frac{\Delta\theta_i^{acc}}{2}\right)^2 - \cos(\theta_B - \alpha)\left(\frac{\Delta\theta_i^{acc}}{2}\right) + \frac{v_o \sin\alpha}{4 k_o^2 \cos\theta_B} = 0$$

$$\Delta\theta_i^{acc} = \frac{1}{\sin(\theta_B - \alpha)}\left\{\cos(\theta_B - \alpha) \pm \sqrt{\cos^2(\theta_B - \alpha) - \frac{v_o \sin(\theta_B - \alpha)}{k_o^2 \sin 2\theta_B}\left[\cos(\theta_B - \alpha) - \cos(\theta_B + \alpha)\right]}\ \right\}$$

$$\Delta\theta_i^{acc} = \frac{\gamma_1 \pm \sqrt{\gamma_1^2 - \dfrac{v_o}{k_o^2 \sin 2\theta_B}\sqrt{1 - \gamma_1^2}\ \gamma_1\left(1 - \dfrac{\gamma_2}{\gamma_1}\right)}}{\sqrt{1 - \gamma_1^2}}$$

where $\gamma_1 = \cos(\theta_B - \alpha)$ and $\gamma_2 = \cos(\theta_B + \alpha)$

$$\Delta\theta_i^{acc} = \frac{\gamma_1 - \sqrt{\gamma_1^2 - \dfrac{v_o}{k_o^2 \sin 2\theta_B} \sqrt{1 - \gamma_1^2}\, \gamma_1 \left(1 - \dfrac{\gamma_2}{\gamma_1}\right)}}{\sqrt{1 - \gamma_1^2}} \qquad *$$

This final expression is obtained by eliminating one of the two solutions by physical considerations. Note $\Delta\theta_i^{acc} \to -\sqrt{\dfrac{v_o}{k_o^2}}$ as $\gamma_1 \to 0$.

Full width at half maximum of the Lorentzian envelope:-

In the conventional treatment, the incidence circle and the asymptotic form of the dispersion surface is approximated by straight lines. From the analytical expression of the Lorentzian envelope, the intensity falls to half of its maximum when $(K_{oz}^{*A} - K_{oz}^{*C}) = \pm 2\sqrt{\varepsilon}$

$$\Delta\theta_w^c = \frac{AB}{k_o}$$

$$AB = CD, \quad CL_O = DL_O = \frac{1}{2} CD$$

$$\frac{ED}{\sin 2\theta_B} = \frac{L_OD}{\sin [90 - (\theta_B + \alpha)]} = \frac{L_OD}{\cos (\theta_B + \alpha)}$$

$$ED = 2\sqrt{\epsilon} \approx \frac{v_G}{k_O \sqrt{\cos (\theta_B - \alpha) \, \cos (\theta_B + \alpha)}}$$

$$L_OD = \frac{v_G \cos (\theta_B + \alpha)}{k_O \sqrt{\cos (\theta_B - \alpha) \, \cos (\theta_B + \alpha)}} \frac{1}{\sin 2\theta_B}$$

$$= \frac{v_G}{k_O \sin 2\theta_B} \sqrt{\frac{\cos (\theta_B + \alpha)}{\cos (\theta_B - \alpha)}}$$

$$\Delta\theta_w^c = \frac{2 \, v_G}{k_O^2 \sin 2\theta_B} \sqrt{\frac{\cos (\theta_B + \alpha)}{\cos (\theta_B - \alpha)}} \qquad *$$

This expression can be obtained also from the condition $(K_{oz}^{*A} - K_{oz}^{*C})^2 = 4 \, \epsilon$ with $\Delta K = 0$.

$$\Delta\theta_w^c = \frac{\partial(\Delta\theta_i^c)}{\partial(LP)} \cdot AB$$

For AB<< ko, it is also valid to a good approximation that

$$\Delta\theta_w^{acc} = \frac{\partial(\Delta\theta_i^{acc})}{\partial(LP)} \cdot AB$$

$$\frac{\Delta\theta_w^{acc}}{\Delta\theta_w^c} = \frac{\partial(\Delta\theta_i^{acc})}{\partial(LP)} \Big/ \frac{\partial(\Delta\theta_i^c)}{\partial(LP)}$$

$$LP = \quad = \frac{v_o}{2\,k_o\,\sin 2\theta_B}\left\{1 - \frac{\gamma_2}{\gamma_1}\right\}$$

$$\frac{\partial(\Delta\theta_i^c)}{\partial(LP)} = \frac{1}{k_o}$$

$$\Delta\theta_i^{acc} = \frac{\gamma_1 - \sqrt{\gamma_1^2 - \frac{2\,LP}{k_o}\,\gamma_1\,\sqrt{1-\gamma_1^2}}}{\sqrt{1-\gamma_1^2}}$$

$$\frac{\partial(\Delta\theta_i^{acc})}{\partial(LP)} = \frac{\gamma_1}{k_o\sqrt{\gamma_1^2 - \frac{2\,LP}{k_o}\,\gamma_1\,\sqrt{1-\gamma_1^2}}}$$

$$\frac{\Delta\theta_w^{acc}}{\Delta\theta_w^c} = \frac{\gamma_1}{\sqrt{\gamma_1^2 - \frac{v_o}{k_o^2\,\sin 2\theta_B}\,\gamma_1\,(1-\frac{\gamma_2}{\gamma_1})\sqrt{1-\gamma_1^2}}}$$

$$\Delta\theta_w^{acc} = \frac{\gamma_1}{\sqrt{\gamma_1^2 - \frac{v_o}{k_o^2\,\sin 2\theta_B}\,\gamma_1\,(1-\frac{\gamma_2}{\gamma_1})\sqrt{1-\gamma_1^2}}} \; \frac{2\,v_G}{k_o^2\,\sin 2\theta_B}\sqrt{\frac{\gamma_2}{\gamma_1}}$$

Note that $\Delta\theta_w^{acc} \to 0$ as $\gamma_1 \to 0$.

Appendix 6

Solution to a partial differential equation using the Riemann's method.

Consider a partial differential equation of the form

$$\frac{\partial^2 U}{\partial x \partial y} + a(x,y)\frac{\partial U}{\partial x} + b(x,y)\frac{\partial U}{\partial y} + c(x,y)\, U = F(x,y)$$

We now introduce the differential operator which is adjoint to the above differential equation

$$MV = \frac{\partial^2 V}{\partial x \partial y} - \frac{\partial}{\partial x}(aV) - \frac{\partial}{\partial y}(bV) + cV$$
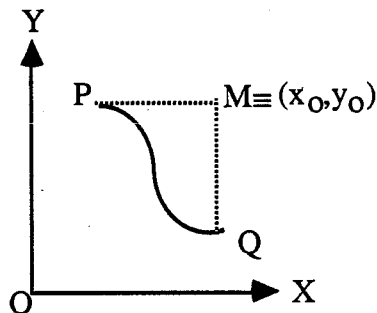
Let $V(x,y,x_0,y_0)$ be any function satisfying the following conditions.

$$MV = 0$$

$$[\,V\,]_{x=x_0} = \exp \int_{y_0}^{y} a(x_0,y)\, dy$$

$$[\,V\,]_{y=y_0} = \exp \int_{x_0}^{x} b(x,y_0)\, dx$$

Then, Riemann formula gives

$$U(x_o,y_o) = \frac{1}{2}[UV]_Q + \frac{1}{2}[UV]_R - \Phi + \iint_\Omega V\, F(x,y)\, dx\, dy$$

Where $\Phi = \int_Q^R \left\{ \left[\frac{1}{2}\left(U\frac{\partial V}{\partial x} - V\frac{\partial U}{\partial x}\right) - bUV \right] dx \right.$

$$\left. - \left[\frac{1}{2}\left(U\frac{\partial V}{\partial y} - V\frac{\partial U}{\partial y}\right) - aUV \right] dy) \right\}$$

Compare the above differential equation with the one that we intend to solve [eq. (4.9b)]

i.e. $\qquad \dfrac{\partial^2 \widetilde{\Psi}_G}{\partial s_o \partial s_G} + i\dfrac{\partial}{\partial s_o}(\vec{G}.\vec{u})\,\dfrac{\partial \widetilde{\Psi}_G}{\partial s_G} + \sigma^2\,\widetilde{\Psi}_G = 0$

where $\sigma^2 = \dfrac{v_G v_{-G}}{4K^2}$

$x \equiv s_o$, $y \equiv s_G$, $a(x,y) = 0$, $b(x,y) = i\dfrac{\partial}{\partial s_o}(\vec{G}.\vec{u}) = 4iBs_G$, $c(x,y) = \sigma^2$,

$U = \widetilde{\Psi}_G(s_o,s_G)$, $F(x,y) = 0$
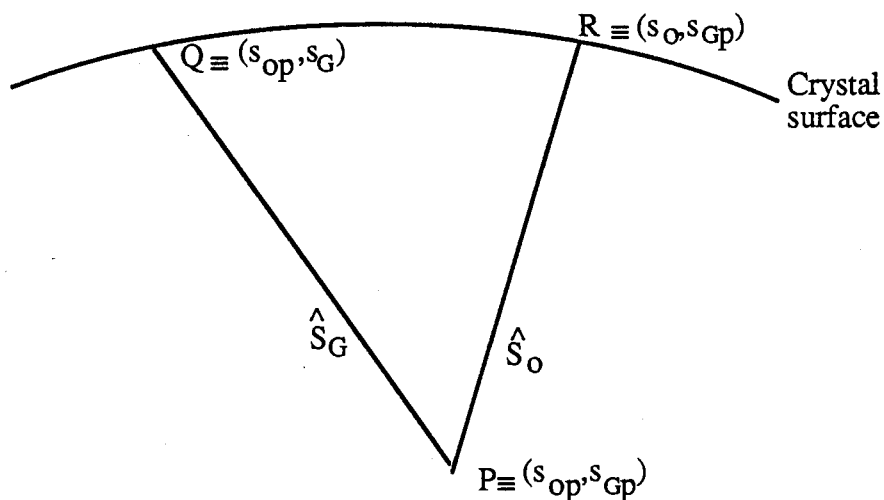
The adjoint operator will be of the form

$$MR_G = \frac{\partial^2 R_G}{\partial s_0 \partial s_G} - 4iB \frac{\partial}{\partial s_G}(s_G R_G) + \sigma^2 R_G$$

If R_G is satisfying the following three conditions,

$$\frac{\partial^2 R_G}{\partial s_0 \partial s_G} - 4iB \frac{\partial}{\partial s_G}(s_G R_G) + \sigma^2 R_G = 0 \qquad *$$

$$[R_G]_{s_0 = s_{op}} = \exp \int_{s_{Gp}}^{s_G} o . ds_G = e^0 = 1 \qquad *$$

$$[R_G]_{s_G = s_{Gp}} = \exp \int_{s_{op}}^{s_0} 4iBs_G . ds_0 = e^{4iBs_{Gp}(s_0 - s_{op})} \qquad *$$

One can write from the Riemann formula that

$$\tilde{\Psi}_G (p) = \frac{1}{2}[\tilde{\Psi}_G R_G]_Q + \frac{1}{2}[\tilde{\Psi}_G R_G]_R - \Phi + 0$$

$$\tilde{\Psi}_G (p) = \frac{1}{2}[\tilde{\Psi}_G R_G]_Q + \frac{1}{2}[\tilde{\Psi}_G R_G]_R + \int_R^Q \frac{1}{2}\left(\tilde{\Psi}_G \frac{\partial R_G}{\partial s_G} - R_G \frac{\partial \tilde{\Psi}_G}{\partial s_G}\right) ds_G$$

$$- \int_R^Q \left\{\frac{1}{2}\left(\tilde{\Psi}_G \frac{\partial R_G}{\partial s_0} - R_G \frac{\partial \tilde{\Psi}_G}{\partial s_0}\right) - 4iBs_G R_G \tilde{\Psi}_G \right\} ds_0$$

$$= \frac{1}{2}[\tilde{\Psi}_G R_G]_Q + \frac{1}{2}[\tilde{\Psi}_G R_G]_R + \int_R^Q \left\{\frac{1}{2}\frac{\partial}{\partial s_G}(R_G \tilde{\Psi}_G) - R_G \frac{\partial \tilde{\Psi}_G}{\partial s_G}\right\} ds_G$$

$$-\int_R^Q \left\{ -\frac{1}{2}\frac{\partial}{\partial s_o}(R_G \,\tilde{\Psi}_G) + \tilde{\Psi}_G \frac{\partial R_G}{\partial s_o} - 4iBs_G R_G \tilde{\Psi}_G \right\} ds_o$$

$$= \frac{1}{2}[\tilde{\Psi}_G \, R_G]_Q + \frac{1}{2}[\tilde{\Psi}_G \, R_G]_R - \frac{1}{2}[\tilde{\Psi}_G \, R_G]_Q^R +$$

$$\int_Q^R \left\{ \tilde{\Psi}_G \frac{\partial R_G}{\partial s_o} - 4iBs_G R_G \tilde{\Psi}_G \right\} ds_o + \int_Q^R R_G \frac{\partial \tilde{\Psi}_G}{\partial s_G} ds_G$$

$$= [\tilde{\Psi}_G \, R_G]_Q + \int_Q^R \left(\frac{\partial R_G}{\partial s_o} - 4iBs_G R_G \right) \tilde{\Psi}_G \, ds_o + \int_Q^R R_G \frac{\partial \tilde{\Psi}_G}{\partial s_G} ds_G$$

Note that $[R_G]_Q = [R_G]_{s_o=s_{op}} = 1$.

$$\tilde{\Psi}_G(p) = [\tilde{\Psi}_G]_Q + \int_Q^R \left(\frac{\partial R_G}{\partial s_o} - 4iBs_G R_G \right) \tilde{\Psi}_G \, ds_o + \int_Q^R R_G \frac{\partial \tilde{\Psi}_G}{\partial s_G} ds_G \qquad *$$

Solution of the homogeneous conjugate equation:-

$$\frac{\partial^2 R_G}{\partial s_o \partial s_G} - 4iB \frac{\partial}{\partial s_G}(s_G R_G) + \sigma^2 R_G = 0$$

Making use of the substitution $R_G = \tilde{R}_G \, e^{-4iB(s_{op}-s_o)s_G}$, the above conjugate equation will reduce to

$$\frac{\partial^2 \tilde{R}_G}{\partial s_o \partial s_G} - 4iB(s_{op}-s_o)\frac{\partial \tilde{R}_G}{\partial s_G} + \sigma^2 \tilde{R}_G = 0$$

The solution of this differential equation is a confluent hypergeometric function, i.e.

$$\tilde{R}_G = {}_1F_1\left[-\frac{i\sigma^2}{4B}, 1; -4iB(s_{op}-s_o)(s_{Gp}-s_G)\right]$$

$$R_G = \exp\left[-4iBs_G(s_{op}-s_o)\right] \cdot {}_1F_1\left[-\frac{i\sigma^2}{4B}, 1; -4iB(s_{op}-s_o)(s_{Gp}-s_G)\right]$$

Further more the solution R_G satisfies the necessary conditions.

$$[R_G]_{s_o=s_{op}} = 1 \qquad\qquad *$$

$$[R_G]_{s_G=s_{Gp}} = e^{\,4iBs_{Gp}(s_o-s_{op})} \qquad\qquad *$$

Appendix 7

Calculation of the coefficients A, B, C, D, E and F

$$\vec{G}.\vec{u} = 2\{ A s_0^2 + 2B s_0 s_G + C s_G^2 \} + D s_0 + E s_G + F$$

It follows that,

$$A = \frac{1}{4} \frac{\partial^2}{\partial s_0^2} (\vec{G}.\vec{u})$$

$$B = \frac{1}{4} \frac{\partial^2}{\partial s_0 \partial s_G} (\vec{G}.\vec{u})$$

$$C = \frac{1}{4} \frac{\partial^2}{\partial s_G^2} (\vec{G}.\vec{u})$$

$$D = \text{constant term of} \left[\frac{\partial}{\partial s_0} (\vec{G}.\vec{u}) \right]$$

$$E = \text{constant term of} \left[\frac{\partial}{\partial s_G} (\vec{G}.\vec{u}) \right]$$

$$F = \text{constant term of} (\vec{G}.\vec{u})$$

The relations between the rectangular coordinte system and the oblique coordinate system (see Fig. 1.) are

$$x = - s_0 \sin (\theta_B^* - \alpha) + s_G \sin (\theta_B^* + \alpha)$$

$$z = s_0 \cos (\theta_B^* - \alpha) + s_G \cos (\theta_B^* + \alpha)$$

$$\frac{\partial}{\partial s_0} = \frac{\partial x}{\partial s_0} \cdot \frac{\partial}{\partial x} + \frac{\partial z}{\partial s_0} \cdot \frac{\partial}{\partial z} = - \sin (\theta_B^* - \alpha) \frac{\partial}{\partial x} + \cos (\theta_B^* - \alpha) \frac{\partial}{\partial z}$$

$$\frac{\partial}{\partial s_G} = \frac{\partial x}{\partial s_G} \cdot \frac{\partial}{\partial x} + \frac{\partial z}{\partial s_G} \cdot \frac{\partial}{\partial z} = \sin (\theta_B^* + \alpha) \frac{\partial}{\partial x} + \cos (\theta_B^* + \alpha) \frac{\partial}{\partial z}$$

$$\frac{\partial^2}{\partial s_0^2} = \sin^2 (\theta_B^* - \alpha) \frac{\partial^2}{\partial x^2} + \cos^2 (\theta_B^* - \alpha) \frac{\partial^2}{\partial z^2} - 2 \sin (\theta_B^* - \alpha) \cos (\theta_B^* - \alpha) \frac{\partial^2}{\partial x \partial z}$$

$$\frac{\partial^2}{\partial s_G^2} = \sin^2(\theta_B^* + \alpha)\frac{\partial^2}{\partial x^2} + \cos^2(\theta_B^* + \alpha)\frac{\partial^2}{\partial z^2} + 2\sin(\theta_B^* + \alpha)\cos(\theta_B^* + \alpha)\frac{\partial^2}{\partial x \partial z}$$

$$\frac{\partial^2}{\partial s_0 \partial s_G} = -\sin(\theta_B^* - \alpha)\sin(\theta_B^* + \alpha)\frac{\partial^2}{\partial x^2} + \cos(\theta_B^* - \alpha)\cos(\theta_B^* + \alpha)\frac{\partial^2}{\partial z^2} + \sin 2\alpha \frac{\partial^2}{\partial x \partial z}$$

In the case of a homogeneously bent crystal elaborated by Penning and Polder,

$$\vec{G}.\vec{u} = -G\cos\alpha \frac{vx\left\{z - \frac{t}{2}\right\}}{R} + G\sin\alpha \frac{\left[-vx^2 + v\left\{z - \frac{t}{2}\right\}^2\right]}{2R}$$

Note that here we are considering the bending of XZ plane at $y = 0$.

$$\frac{\partial^2(\vec{G}.\vec{u})}{\partial x^2} = \frac{-vG\sin\alpha}{R} \quad ; \qquad \frac{\partial^2(\vec{G}.\vec{u})}{\partial z^2} = \frac{vG\sin\alpha}{R} \quad ;$$

$$\frac{\partial^2(\vec{G}.\vec{u})}{\partial x \partial z} = \frac{-vG\cos\alpha}{R} \quad ; \quad \text{Constant term of}\left[\frac{\partial}{\partial x}(\vec{G}.\vec{u})\right] = \frac{vG\cos\alpha\, t}{2R} \quad ;$$

$$\text{Constant term of}\left[\frac{\partial}{\partial z}(\vec{G}.\vec{u})\right] = \frac{-vG\sin\alpha\, t}{2R} .$$

$$A = \frac{1}{4}\Big\{\sin^2(\theta_B^* - \alpha)\frac{-vG\sin\alpha}{R} + \cos^2(\theta_B^* - \alpha)\frac{vG\sin\alpha}{R}$$
$$+ 2\sin(\theta_B^* - \alpha)\cos(\theta_B^* - \alpha)\frac{vG\cos\alpha}{R}\Big\}$$

$$= \frac{vG\sin(2\theta_B^* - \alpha)}{4R} \qquad\qquad *$$

$$B = \frac{1}{4}\Big\{-\sin(\theta_B^* - \alpha)\sin(\theta_B^* + \alpha)\frac{-vG\sin\alpha}{R}$$

$$+ \cos(\theta_B^* - \alpha)\cos(\theta_B^* + \alpha)\frac{\nu\, G \sin \alpha}{R} + \sin 2\alpha \frac{\nu\, G \cos \alpha}{R} \Big\}$$

$$= -\frac{\nu\, G \sin \alpha}{4\, R} \qquad\qquad *$$

$$C = \frac{1}{4}\Big\{ \sin^2(\theta_B^* + \alpha)\frac{-\nu\, G \sin \alpha}{R} + \cos^2(\theta_B^* + \alpha)\frac{\nu\, G \sin \alpha}{R}$$

$$+ 2 \sin(\theta_B^* + \alpha)\cos(\theta_B^* + \alpha)\frac{-\nu\, G \cos \alpha}{R}\Big\}$$

$$= -\frac{\nu\, G \sin(2\theta_B^* + \alpha)}{4\, R} \qquad\qquad *$$

$$D = -\sin(\theta_B^* - \alpha)\frac{\nu\, G \cos \alpha\, t}{2R} + \cos(\theta_B^* - \alpha)\frac{-\nu\, G \sin \alpha\, t}{2R}$$

$$= -\frac{\nu\, G\, t \sin \theta_B^*}{2\, R} \qquad\qquad *$$

$$E = \sin(\theta_B^* + \alpha)\frac{\nu\, G \cos \alpha\, t}{2R} + \cos(\theta_B^* + \alpha)\frac{-\nu\, G \sin \alpha\, t}{2R}$$

$$= \frac{\nu\, G\, t \sin \theta_B^*}{2\, R} \qquad\qquad *$$

$$F = \text{constant term of } (\vec{G}.\vec{u}) = \frac{\nu\, G\, t^2 \sin \alpha}{8R} \qquad\qquad *$$

Appendix 8

Derivation of the basic differential equation of thin crystal plate theory and
the boundary conditions using the variational method.

Total potential energy = E = $\displaystyle\int_{-a}^{a} \int_{-b}^{b} \int_{-\frac{t}{2}}^{\frac{t}{2}} \left[\frac{1}{2} C_{11} \left\{ z^2 \left(\frac{\partial^2 w}{\partial x^2}\right)^2 + z^2 \left(\frac{\partial^2 w}{\partial y^2}\right)^2 \right\} \right.$

$$\left. + C_{12} z^2 \left\{\frac{\partial^2 w}{\partial x^2} \frac{\partial^2 w}{\partial y^2}\right\} + 2 C_{44} z^2 \left\{\frac{\partial^2 w}{\partial x \partial y}\right\}^2 \right] dx \, dy \, dz$$

where 2a, 2b and t are the dimensions of the crystal plate.

$$= \frac{1}{2} C_{11} \cdot \frac{t^3}{12} \int_{-a}^{a} \int_{-b}^{b} \left\{ \left(\frac{\partial^2 w}{\partial x^2}\right)^2 + \left(\frac{\partial^2 w}{\partial y^2}\right)^2 \right\} dx \, dy$$

$$+ C_{12} \cdot \frac{t^3}{12} \int_{-a}^{a} \int_{-b}^{b} \left\{\frac{\partial^2 w}{\partial x^2} \frac{\partial^2 w}{\partial y^2}\right\} dx \, dy + 2 C_{44} \cdot \frac{t^3}{12} \int_{-a}^{a} \int_{-b}^{b} \left\{\frac{\partial^2 w}{\partial x \partial y}\right\}^2 dx \, dy$$

Consider the change due to a virtual displacement δw in the term $\left(\frac{\partial^2 w}{\partial x^2}\right)^2$

$$\int_{-a}^{a} \int_{-b}^{b} \left[\left(\frac{\partial^2 (w+\delta w)}{\partial x^2}\right)^2 - \left(\frac{\partial^2 w}{\partial x^2}\right)^2 \right] dx \, dy$$

$$\approx \int_{-a}^{a} \int_{-b}^{b} 2 \frac{\partial^2 w}{\partial x^2} \frac{\partial^2 (\delta w)}{\partial x^2} dx \, dy = \int_{-b}^{b} 2 \left[\frac{\partial^2 w}{\partial x^2} \frac{\partial (\delta w)}{\partial x} \right]_{x=-a}^{a} dy$$

$$- \int_{-a}^{a} \int_{-b}^{b} 2 \frac{\partial^3 w}{\partial x^3} \frac{\partial (\delta w)}{\partial x} dx \, dy$$

$$= \int_{-b}^{b} 2\left[\frac{\partial^2 w}{\partial x^2}\frac{\partial(\delta w)}{\partial x}\right]_{x=-a}^{a} dy - \int_{-b}^{b} 2\left[\frac{\partial^3 w}{\partial x^3}\delta w\right]_{x=-a}^{a} dy + \int_{-a}^{a}\int_{-b}^{b} 2\frac{\partial^4 w}{\partial x^4}\delta w\, dx\, dy \qquad *$$

Similarly one can write the change in $\left(\dfrac{\partial^2 w}{\partial y^2}\right)^2$

$$= \int_{-a}^{a} 2\left[\frac{\partial^2 w}{\partial y^2}\frac{\partial(\delta w)}{\partial y}\right]_{y=-b}^{b} dx - \int_{-a}^{a} 2\left[\frac{\partial^3 w}{\partial y^3}\delta w\right]_{y=-b}^{b} dx + \int_{-a}^{a}\int_{-b}^{b} 2\frac{\partial^4 w}{\partial y^4}\delta w\, dx\, dy \qquad *$$

Consider the change in the term $\dfrac{\partial^2 w}{\partial x^2}\cdot\dfrac{\partial^2 w}{\partial y^2}$ due to the virtual displacement δw

$$\int_{-a}^{a}\int_{-b}^{b}\left\{\frac{\partial^2(w+\delta w)}{\partial x^2}\frac{\partial^2(w+\delta w)}{\partial y^2} - \frac{\partial^2 w}{\partial x^2}\frac{\partial^2 w}{\partial y^2}\right\} dx\, dy$$

$$\approx \int_{-a}^{a}\int_{-b}^{b}\left\{\frac{\partial^2 w}{\partial x^2}\frac{\partial^2(\delta w)}{\partial y^2} + \frac{\partial^2 w}{\partial y^2}\frac{\partial^2(\delta w)}{\partial x^2}\right\} dx\, dy$$

$$= \int_{-a}^{a}\left[\frac{\partial^2 w}{\partial x^2}\frac{\partial(\delta w)}{\partial y}\right]_{y=-b}^{b} dx - \int_{-a}^{a}\left[\frac{\partial^3 w}{\partial x^2\partial y}\delta w\right]_{y=-b}^{b} dx + \int_{-a}^{a}\int_{-b}^{b}\frac{\partial^4 w}{\partial x^2\partial y^2}\delta w\, dx\, dy$$

$$+ \int_{-b}^{b}\left[\frac{\partial^2 w}{\partial y^2}\frac{\partial(\delta w)}{\partial x}\right]_{x=-a}^{a} dy - \int_{-b}^{b}\left[\frac{\partial^3 w}{\partial x\partial y^2}\delta w\right]_{x=-a}^{a} dy + \int_{-a}^{a}\int_{-b}^{b}\frac{\partial^4 w}{\partial x^2\partial y^2}\delta w\, dx\, dy \qquad *$$

Consider the change in the term $\left(\dfrac{\partial^2 w}{\partial x\partial y}\right)^2$

$$\int_{-a}^{a}\int_{-b}^{b}\left[\left(\frac{\partial^2(w+\delta w)}{\partial x\partial y}\right)^2 - \left(\frac{\partial^2 w}{\partial x\partial y}\right)^2\right] dx\, dy$$

$$\approx \int_{-a}^{a} \int_{-b}^{b} 2 \frac{\partial^2 w}{\partial x \partial y} \cdot \frac{\partial^2(\delta w)}{\partial x \partial y} dx \, dy = \int_{-a}^{a} 2 \left[\frac{\partial^2 w}{\partial x \partial y} \frac{\partial(\delta w)}{\partial x} \right]_{y=-b}^{b} dx$$

$$- \int_{-a}^{a} \int_{-b}^{b} 2 \frac{\partial^3 w}{\partial x \partial y^2} \frac{\partial(\delta w)}{\partial x} dx \, dy$$

$$= 2 \left[\left[\frac{\partial^2 w}{\partial x \partial y} \delta w \right]_{y=-b}^{b} \right]_{x=-a}^{a} - 2 \int_{-a}^{a} \left[\frac{\partial^3 w}{\partial x^2 \partial y} \delta w \right]_{y=-b}^{b} dx$$

$$- 2 \int_{-b}^{b} \left[\frac{\partial^3 w}{\partial x \partial y^2} \delta w \right]_{x=-a}^{a} dy + 2 \int_{-a}^{a} \int_{-b}^{b} \frac{\partial^4 w}{\partial x^2 \partial y^2} \cdot \delta w \, dx \, dy \qquad *$$

By combining the changes in each term of the total potential energy expression, and then equating the coefficients of dx, dy and dxdy to zero together with the boundary conditions at the fixed edges {eq. (4.22)}, we will get the following expressions.

$$\frac{\partial^4 w}{\partial x^4} + \frac{2(C_{12} + 2 C_{44})}{C_{11}} \frac{\partial^4 w}{\partial x^2 \partial y^2} + \frac{\partial^4 w}{\partial y^4} = 0$$

$$\frac{\partial^2 w}{\partial x^2} + \frac{C_{12}}{C_{11}} \frac{\partial^2 w}{\partial y^2} = 0 \qquad \text{at} \ \ x = \pm a$$

$$\frac{\partial^3 w}{\partial x^3} + \frac{(C_{12} + 4 C_{44})}{C_{11}} \frac{\partial^3 w}{\partial x \partial y^2} = 0 \qquad \text{at} \ \ x = \pm a$$

Note that, here the boundary conditions are $w = 0$, $\delta w = 0$ and $\frac{\partial(\delta w)}{\partial y} = 0$ at $y = \pm b$.

The first expression was obtained by equating the coefficient of dxdy to zero. This is the basic differential equation of thin crystal plate theory. The coefficient of dx goes to zero

automatically. The second and the third equations are the boundary conditions at the free edges which are obtained by equating the coefficient of dy to zero.

Appendix 9

Derivation of fundamental differential equations and boundary conditions in the case of bending of a thin crystal plate which is subjected to in-plane forces (plate with large deflections)

In studying the combined action of the bending and in-plane forces, we assume that the stress components are composed of two parts:

$$\sigma_x = \bar{\sigma}_x + \sigma_x' \; , \; \sigma_y = \bar{\sigma}_y + \sigma_y' \; , \; \tau_{xy} = \bar{\tau}_{xy} + \tau_{xy}' , \; \tau_{xz} = \tau_{xz}' , \; \tau_{yz} = \tau_{yz}'$$

Here $\bar{\sigma}_x$, $\bar{\sigma}_y$ and $\bar{\tau}_{xy}$ are the values of the mean stress through the thickness arising from in-plane forces only; σ_x', σ_y' and τ_{xy}' are the stresses associated with the pure bending. Furthermore, we assume that the strain components are also expressed in two parts:

$$\varepsilon_x = \bar{\varepsilon}_x + \varepsilon_x' \; , \; \varepsilon_y = \bar{\varepsilon}_y + \varepsilon_y' \; , \; \gamma_{xy} = \bar{\gamma}_{xy} + \gamma_{xy}' \; .$$

Calculation of stress components (σ_x', σ_y' and τ_{xy}'), strain components (ε_x', ε_y' and γ_{xy}') and corresponding moments and forces:-

In calculating these components we make following two assumptions for bending of thin plates.

- straight sections, which in the undeformed state of the plate are normal to its mid-surface, remain straight and normal to the bent mid-surface during the bending.

- normal stress σ_z' in cross sections parallel to the mid-surface is small compared with the stress in the tranverse cross sections, i.e. σ_x', σ_y' and τ_{xy}'.

It follows from the first assumption that

$$u = -z \frac{\partial w}{\partial x}, \quad v = -z \frac{\partial w}{\partial y};$$

$$\varepsilon_x' = -z \frac{\partial^2 w}{\partial x^2}, \quad \varepsilon_y' = -z \frac{\partial^2 w}{\partial y^2}, \quad \gamma_{xy}' = -2z \frac{\partial^2 w}{\partial x \partial y},$$

where u, v are the displacements of any point in the direction of X and Y axes; w(x,y) is the deflection of the mid-surface. We will consider a Si crystal plate (cubic crystal) in which the coordinate axes are chosen parallel to the cubic edges. Under this condition, the array of values of the elastic constants are given by the following matrix:

$$|a_{ij}| = \begin{pmatrix} a_{11} & a_{12} & a_{12} & 0 & 0 & 0 \\ a_{12} & a_{11} & a_{12} & 0 & 0 & 0 \\ a_{12} & a_{12} & a_{11} & 0 & 0 & 0 \\ 0 & 0 & 0 & a_{44} & 0 & 0 \\ 0 & 0 & 0 & 0 & a_{44} & 0 \\ 0 & 0 & 0 & 0 & 0 & a_{44} \end{pmatrix}$$

Assuming that the equations of the generalized Hooke's law are correct for the plate, we get

$$\varepsilon_x' = a_{11} \sigma_x' + a_{12} \sigma_y'; \quad \varepsilon_y' = a_{12} \sigma_x' + a_{11} \sigma_y'; \quad \gamma_{xy}' = a_{44} \tau_{xy}'$$

By solving these equations for the stress components we obtain

$$\sigma_x' = -z \left\{ B_{11} \frac{\partial^2 w}{\partial x^2} + B_{12} \frac{\partial^2 w}{\partial y^2} \right\}; \quad \sigma_y' = -z \left\{ B_{12} \frac{\partial^2 w}{\partial x^2} + B_{11} \frac{\partial^2 w}{\partial y^2} \right\};$$

$$\tau_{xy}' = -2 z B_{44} \frac{\partial^2 w}{\partial x \partial y},$$

where

$$B_{11} = \frac{a_{11}}{(a_{11}^2 - a_{12}^2)}, \quad B_{12} = \frac{-a_{12}}{(a_{11}^2 - a_{12}^2)}, \quad B_{44} = \frac{1}{a_{44}}.$$

The other stress components τ'_{zx} and τ'_{zy} will be determined from the equilibrium equations,

$$\frac{\partial \sigma'_x}{\partial x} + \frac{\partial \tau'_{xy}}{\partial y} + \frac{\partial \tau'_{zx}}{\partial z} = 0, \qquad \frac{\partial \tau'_{xy}}{\partial x} + \frac{\partial \sigma'_y}{\partial y} + \frac{\partial \tau'_{zy}}{\partial z} = 0 .$$

Considering that $z = \pm \frac{t}{2}$, $\tau'_{zx} = \tau'_{zy} = 0$ on the external surfaces, we obtain

$$\tau'_{zx} = \frac{1}{2}\left(z^2 - \frac{t^2}{4}\right)\left\{B_{11}\frac{\partial^3 w}{\partial x^3} + (B_{12} + 2B_{44})\frac{\partial^3 w}{\partial x \partial y^2}\right\},$$

$$\tau'_{zy} = \frac{1}{2}\left(z^2 - \frac{t^2}{4}\right)\left\{(B_{12} + 2B_{44})\frac{\partial^3 w}{\partial x^2 \partial y} + B_{11}\frac{\partial^3 w}{\partial y^3}\right\}.$$

When we cut this plate with certain surfaces parallel to the initial mid-surface with height equal to the plate thickness and with bases dx and dy, then stress components σ'_x, σ'_y, τ'_{xy} will be reduced to moments $M'_y dx$, $H'_{xy} dx$ and $M'_x dy$, $H'_{yx} dy$, and τ'_{zx}, τ'_{zy} will be reduced to forces $N'_x dy$, $N'_y dx$. Values of M'_x, M'_y are called the bending moments; H'_{xy}, H'_{yx}, the twisting moments, and N'_x, N'_y, the transverse shear forces (all of them per unit length in the mid-surface). Obviously,

$$M'_x = \int_{-t/2}^{t/2} \sigma'_x z \, dz \,, \quad M'_y = \int_{-t/2}^{t/2} \sigma'_y z \, dz \,, \quad H'_{xy} = H'_{yx} = \int_{-t/2}^{t/2} \tau'_{xy} z \, dz$$

$$N'_x = \int_{-t/2}^{t/2} \tau'_{zx} \, dz \,, \quad N'_y = \int_{-t/2}^{t/2} \tau'_{zy} \, dz$$

By substituting for σ'_x, σ'_y, τ'_{xy}, τ'_{zx} and τ'_{zy} in the above integrals, we get
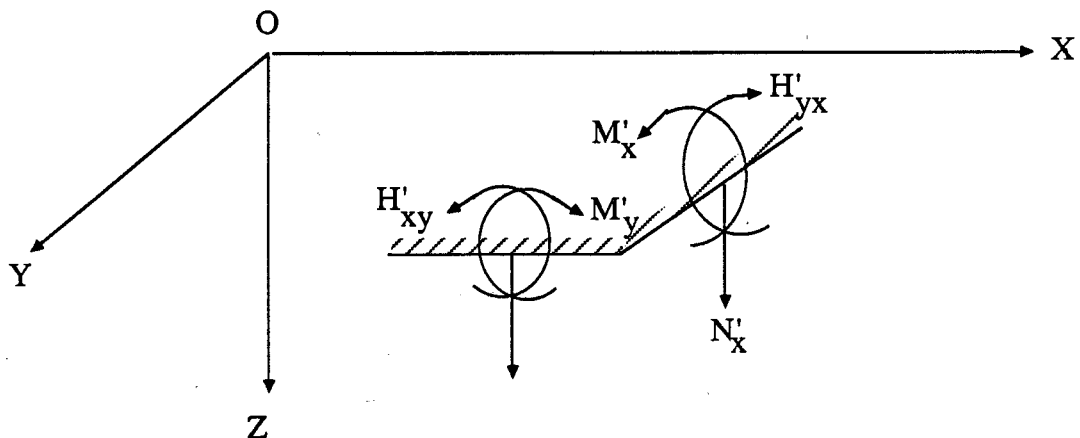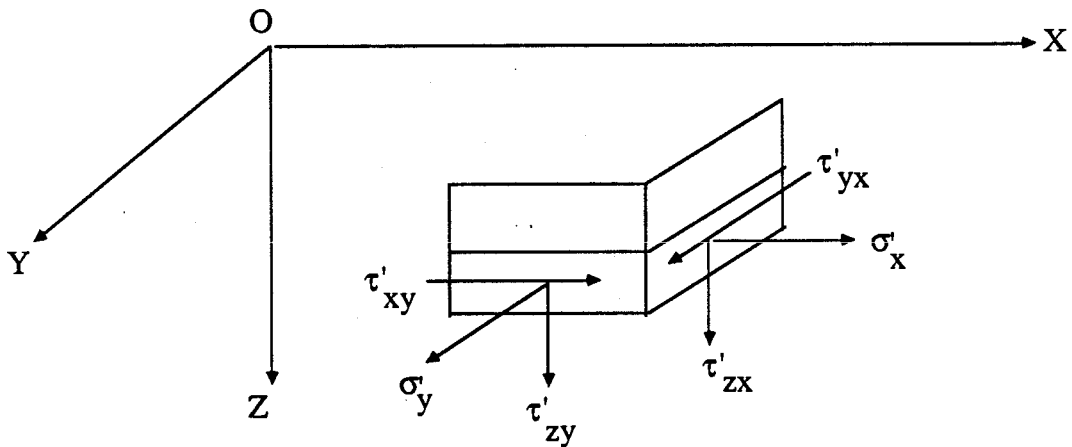
$$M_x' = - \left\{ D_{11} \frac{\partial^2 w}{\partial x^2} + D_{12} \frac{\partial^2 w}{\partial y^2} \right\}; \quad M_y' = - \left\{ D_{12} \frac{\partial^2 w}{\partial x^2} + D_{11} \frac{\partial^2 w}{\partial y^2} \right\};$$

$$H_{xy}' = - 2 D_{44} \frac{\partial^2 w}{\partial x \partial y};$$

$$N_x' = - \left\{ D_{11} \frac{\partial^3 w}{\partial x^3} + (D_{12} + 2 D_{44}) \frac{\partial^3 w}{\partial x \partial y^2} \right\};$$

$$N_y' = - \left\{ (D_{12} + 2 D_{44}) \frac{\partial^3 w}{\partial x^2 \partial y} + D_{11} \frac{\partial^3 w}{\partial y^3} \right\},$$

where constants D_{ij} are related to B_{ij} by $D_{ij} = B_{ij} \frac{t^3}{12}$.

Calculation of stress components ($\bar{\sigma}_x$, $\bar{\sigma}_y$ and $\bar{\tau}_{xy}$), strain components ($\bar{\varepsilon}_x$, $\bar{\varepsilon}_y$ and $\bar{\gamma}_{xy}$) and corresponding in-plane and tangential forces:-

Quantities $\bar{\varepsilon}_x$, $\bar{\varepsilon}_y$ and $\bar{\gamma}_{xy}$ depend not only on displacements u and v, but also on the deflection w. By expanding the general expression

$$\varepsilon_x = \sqrt{1 + 2\frac{\partial u}{\partial x} + \left(\frac{\partial u}{\partial x}\right)^2 + \left(\frac{\partial v}{\partial x}\right)^2 + \left(\frac{\partial w}{\partial x}\right)^2} - 1$$

into a power series and retaining only the first power of the derivatives of u and v and the secondary powers of the derivatives of w, we obtain

$$\bar{\varepsilon}_x = \frac{\partial u}{\partial x} + \frac{1}{2}\left(\frac{\partial w}{\partial x}\right)^2 .$$

Similarly we get

$$\bar{\varepsilon}_y = \frac{\partial v}{\partial y} + \frac{1}{2}\left(\frac{\partial w}{\partial y}\right)^2 \quad \text{and} \quad \bar{\gamma}_{xy} = \frac{\partial u}{\partial y} + \frac{\partial v}{\partial x} + \frac{\partial w}{\partial x} \cdot \frac{\partial w}{\partial y} .$$
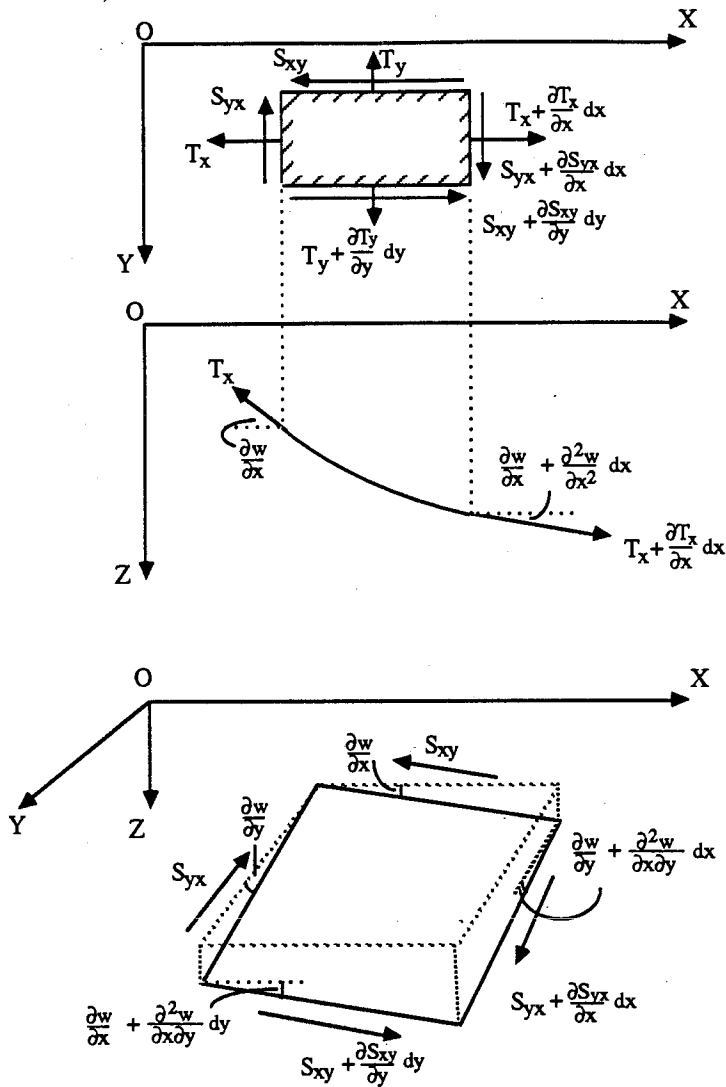
Elimination of u and v by means of differentiation results in

$$\frac{\partial^2 \bar{\varepsilon}_x}{\partial y^2} + \frac{\partial^2 \bar{\varepsilon}_y}{\partial x^2} - \frac{\partial^2 \bar{\gamma}_{xy}}{\partial x \partial y} = \left(\frac{\partial^2 w}{\partial x \partial y}\right)^2 - \frac{\partial^2 w}{\partial x^2} \cdot \frac{\partial^2 w}{\partial y^2} \tag{1}$$

Stresses $\bar{\sigma}_x$, $\bar{\sigma}_y$ and $\bar{\tau}_{xy}$ satisfy the equations of equilibrium:

$$\frac{\partial \bar{\sigma}_x}{\partial x} + \frac{\partial \bar{\tau}_{xy}}{\partial y} = 0 \ , \quad \frac{\partial \bar{\tau}_{xy}}{\partial x} + \frac{\partial \bar{\sigma}_y}{\partial y} = 0 \ ,$$

from which it follows that they are expressible in terms of a stress function F:

$$\bar{\sigma}_x = \frac{\partial^2 F}{\partial y^2}, \quad \bar{\sigma}_y = \frac{\partial^2 F}{\partial x^2}, \quad \bar{\tau}_{xy} = -\frac{\partial^2 F}{\partial x \partial y}.$$

Note that these stress components are again connected with the strain components by the generalized Hooke's law:

$$\bar{\varepsilon}_x = a_{11}\bar{\sigma}_x + a_{12}\bar{\sigma}_y, \quad \bar{\varepsilon}_y = a_{12}\bar{\sigma}_x + a_{11}\bar{\sigma}_y, \quad \bar{\gamma}_{xy} = a_{44}\bar{\tau}_{xy}$$

Now we introduce the quantities T_x, T_y, S_{xy}, S_{yx} as in-plane and tangential forces per unit length which can be defined as

$$T_x = \int_{-t/2}^{t/2} \sigma_x \, dz = t \, \bar{\sigma}_x \;, \; T_y = t \, \bar{\sigma}_y, \; S_{yx} = S_{xy} = t \, \bar{\tau}_{xy} \;.$$

In the absence of body forces, T_x, T_y and S_{xy} satisfy the following equations of equilibrium:

$$\frac{\partial T_x}{\partial x} + \frac{\partial S_{xy}}{\partial y} = 0 \;, \; \frac{\partial S_{yx}}{\partial x} + \frac{\partial T_y}{\partial y} = 0 \;.$$

Considering the curvature of the plate during deformation, the forces T_x, T_y and S_{xy} will not lie in the xy plane. We obtain the components of these forces in the the z-direction:

$$Z = \left(T_x \frac{\partial^2 w}{\partial x^2} + 2 \, S_{xy} \frac{\partial^2 w}{\partial x \partial y} + T_y \frac{\partial^2 w}{\partial y^2} \right) dx \, dy,$$

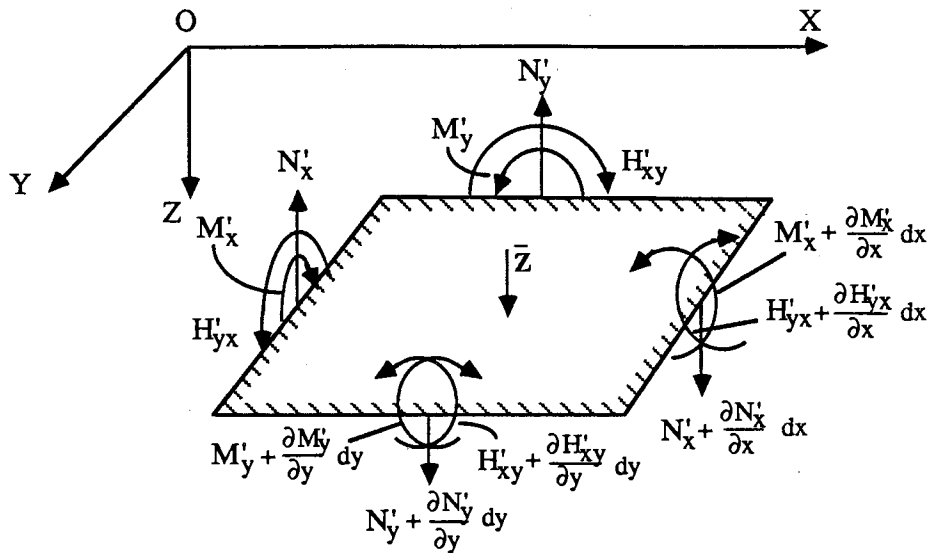or per unit area,

$$\bar{Z} = \left(T_x \frac{\partial^2 w}{\partial x^2} + 2 \, S_{xy} \frac{\partial^2 w}{\partial x \partial y} + T_y \frac{\partial^2 w}{\partial y^2} \right).$$

Here we have used the above equations of equilibrium. This force is similar to the load per unit area (q) in the usual bending problem. Therefore, this force should be added to the load q in studying the combined action.

The figure on the next page show all the forces and moments in the combined action of the bending and in-plane forces. From this figure, it is clear that the conditions of equilibrium of the element have the form:

$$\frac{\partial N'_x}{\partial x} + \frac{\partial N'_y}{\partial y} + \bar{Z} = 0,$$

i.e.
$$\frac{\partial N'_x}{\partial x} + \frac{\partial N'_y}{\partial y} + T_x \frac{\partial^2 w}{\partial x^2} + 2 S_{xy} \frac{\partial^2 w}{\partial x \partial y} + T_y \frac{\partial^2 w}{\partial y^2} = 0 \quad (2)$$

Notice that the load per unit area q = 0 in our bending system.

By substituting the components of stress (as a function of stress function F) together with the generalized Hooke's law into eq. (1), we will get,

$$a_{11}\frac{\partial^4 F}{\partial x^4} + (2a_{12} + a_{44}) \frac{\partial^4 F}{\partial x^2 \partial y^2} + a_{11}\frac{\partial^4 F}{\partial y^4} = \left(\frac{\partial^2 w}{\partial x \partial y}\right)^2 - \frac{\partial^2 w}{\partial x^2} \cdot \frac{\partial^2 w}{\partial y^2} . \qquad *$$

Similarly we will get

$$D_{11} \frac{\partial^4 w}{\partial x^4} + 2(D_{12} + 2D_{44}) \frac{\partial^4 w}{\partial x^2 \partial y^2} + D_{11} \frac{\partial^4 w}{\partial y^4} =$$

$$t\left(\frac{\partial^2 F}{\partial y^2} \cdot \frac{\partial^2 w}{\partial x^2} - 2\frac{\partial^2 F}{\partial x \partial y} \cdot \frac{\partial^2 w}{\partial x \partial y} + \frac{\partial^2 F}{\partial x^2} \cdot \frac{\partial^2 w}{\partial y^2}\right) \qquad *$$

from eq. (2). The solutions of these two coupled non-linear differential equations determine the deflection w and the stress function F.

Boundary conditions:-

At the supported edges $(y = \pm b)$ in our bending system,

$$w = 0, \frac{dw}{dy} = \mp m \qquad *$$

At the free edges $(x = \pm a)$, $M_x = 0$, where

$$M_x = \int_{-t/2}^{t/2} (\sigma'_x + \bar{\sigma}_x) z\,dz = M'_x + \int_{-t/2}^{t/2} \frac{\partial^2 F}{\partial x^2} z\,dz = M'_x + \frac{\partial^2 F}{\partial x^2} \left[\frac{z^2}{2}\right]_{-t/2}^{t/2}$$

$$= M'_x \, ,$$

i.e.
$$D_{11}\frac{\partial^2 w}{\partial x^2} + D_{12}\frac{\partial^2 w}{\partial y^2} = 0 \qquad *$$

Furthermore, $N'_x + \frac{\partial H_{yx}}{\partial y} = 0$ at the free edges, where

$$H_{yx} = \int_{-t/2}^{t/2} (\tau'_{yx} + \bar{\tau}_{yx}) z\,dz = H'_{yx} + \int_{-t/2}^{t/2} -\frac{\partial^2 F}{\partial x \partial y} z\,dz = H'_{yx} \, ,$$

i.e.
$$(D_{12} + 4D_{44})\frac{\partial^3 w}{\partial x \partial y^2} + D_{11}\frac{\partial^3 w}{\partial x^3} = 0 \qquad *$$

REFERENCES

[1]   W. H. Zachariasen, <u>Theory of X-ray Diffraction in Crystals</u>, John Wiley and Sons, London, 1945.

[2]   R. W. James, <u>The Optical Principles of the Diffraction of X-Rays</u>, Bell and Sons, London, 1950.

[3]   L. V. Azarov, R. Kaplow, N. Kato, R. J. Weiss, A. J. C. Wilson and R. A. Young, <u>X-Ray Diffraction</u>,   Chapters 3, 4 and 5, McGraw-Hill, London, 1974.

[4]   C. G. Shull, Phys. Rev. Lett. <u>21</u>, 1585 (1968).

[5]   V. F. Sears, Can. J. Phys. <u>56</u>, 1261 (1978).

[6]   H. Rauch and D. Pertaschek in <u>Neutron Diffraction</u>, ed. H. Dachs, Springer, Berlin (1978), pp. 303-351.

[7]   S. A. Werner, R. R. Berliner and M. Arif, Physica <u>137B</u>, 245 (1986).

[8]   S. Takagi, Acta Cryst. <u>15</u>, 1131 (1962); J. Phys. Soc. Japan <u>26</u>, 1239 (1969).

[9]   D. Taupin, Bull. Soc. Franc. Mineral Crist. <u>87</u>, 469 (1964).

[10] S. A. Werner, Phys. Rev. <u>B21</u>, 1774, (1980).

[11] F. N. Chukhovskii and P. V. Petrashen, Acta Cryst. <u>A33</u>, 311 (1977).

[12] S. G. Lekhnitskii, <u>Anisotropic plates</u>, (trans. S. W. Tsai & T. Cheron), Gordon and Breach Science Publishers, New York (1968), pp. 273-292.

[13] S. Slobodetskii and F. N. Chukhovskii, Sov. Phys. Cryst. <u>15</u>, 963 (1971); J. Arthur and M. A. Horne, Phys. Rev. <u>B32</u>, 5747 (1985); J. Arthur, C. G. Shull and A. Zelinger, Phys. Rev. <u>B32</u>, 5753 (1985).

[14] S. Kishino and K. Kohra, Japan J. app. Phys. <u>10</u>, 551 (1971).

[15] O. Brümmer, H. R. Höche and J. Nieber, Phys. Stat. Sol. <u>a33</u>, 587 (1976).

[16] O. Brümmer, H. R. Höche and J. Nieber, Phys. Stat. Sol. <u>a37</u>, 529 (1976).

[17] A. Zeilinger and T. J. Beatty. Phys. Rev. <u>B27</u>, 7239 (1983).

[18] S. Kishino , J. Phys. Soc. Japan <u>31</u>, 1168 (1971).

[19] T. Bedyńska, Phys. Stat. Sol. <u>a19</u>, 365 (1973).

[20] S. Kishino, A. Noda and K. Kohra, J. Phys. Soc. Japan <u>33</u>, 158 (1972).

[21] T. Bedyńska, Phys. Stat. Sol. <u>a25</u>, 405 (1974).

[22] J. Härtwig, Phys. Stat. Sol. <u>a37</u>, 417 (1976).

[23] J. Härtwig, Phys. Stat. Sol. <u>a42</u>, 495 (1977).

[24] F. Rustichelli, Phil. Mag. <u>31</u>, 1 (1975).

[25] P. Penning and D. Polder, Phylips. Res. <u>16</u>, 419 (1961).

[26] N. Kato, J. Phys. Soc. Japan <u>19</u>, 971 (1964).

[27] S. L. Sobolev, <u>Partial differential equations of Mathematical Physics</u>, pp. 58-71.

[28] Enrico Volterra and J. H. Gaines, <u>Advances Strength of Materials</u>, pp. 212-214.

[29] Y. L. Luke, <u>Algorithms for the computation of mathematical functions</u> (1977), pp. 70-76.

[30] S. G. Lekhnitskii, <u>Theory of elasticity of an inisotropic elastic body</u>, ed. J. Brandstatter (trans. P. Fern), Holden-Day, Inc., San Francisco (1963), pp. 32-40.